Geophysical Journal International

Geophys. J. Int. (2023) **233,** 2172–2206 https://doi.org/10.1093/gji/ggad060
Advance Access publication 2023 February 14
GJI Seismology

Fault-based probabilistic seismic hazard analysis in regions with low strain rates and a thick seismogenic layer: a case study from Malawi

J.N. Williams,[1,2,3] M.J. Werner,[1] K. Goda,[4] L.N.J. Wedmore,[1] R. De Risi,[5] J. Biggs,[1] H. Mdala,[6] Z. Dulanya,[7] Å. Fagereng,[2] F. Mphepo[6] and P. Chindandali[8]

[1]*School of Earth Sciences, University of Bristol, Bristol BS*8 1*RJ, UK. E-mail:* *jack.williams@otago.ac.nz*
[2]*School of Earth and Environmental Sciences, Cardiff University, Cardiff CF*10 3*AT, UK*
[3]*Department of Geology, University of Otago, Dunedin NZ* 9054*, New Zealand*
[4]*Department of Earth Sciences, Western University, Ontario N*6*A* 5*B*7*, Canada*
[5]*Department of Civil Engineering, University of Bristol, Bristol BS*8 1*TR, UK*
[6]*Malawi Geological Survey Department, P.O. Box* 9*, Mzuzu, Malawi*
[7]*Geography and Earth Sciences Department, University of Malawi, P.O Box* 280*, Zomba, Malawi*
[8]*Malawi Geological Survey Department, P.O. Box* 27*, Zomba, Malawi*

Accepted 2023 February 7. Received 2023 February 7; in original form 2022 May 30

SUMMARY

Historical and instrumental earthquake catalogs in low strain rate regions are not necessarily indicative of the long-term spatio-temporal distribution of seismicity. This implies that probabilistic seismic hazard analysis (PSHA) should also consider geologic and geodetic data through fault-based seismogenic sources. However, it is not always clear how on-fault magnitude-frequency distributions (MFDs) should be described and, if the seismogenic layer is especially thick, how fault sources should be extrapolated down-dip. We explore these issues in the context of a new PSHA for Malawi, where regional extensional rates are 0.5–2 mm yr^{-1}, the seismogenic layer is 30–40-km thick, the instrumental catalog is ∼60 yr long and fault-based sources were recently collated in the Malawi Seismogenic Source Model. Furthermore, Malawi is one of several countries along the East African Rift where exposure to seismic hazard is growing, but PSHA does not typically consider fault sources. We use stochastic event catalogs to explore different fault source down-dip extents and MFDs. Our PSHA indicates that hazard levels are highest for a Gutenberg–Richter on-fault MFD, even at low probabilities of exceedance (2 per cent in 50 yr), whilst seismic hazard levels are also sensitive to how relatively short (<50 km) fault sources are extrapolated down-dip. For sites close to fault sources (<40 km), seismic hazard levels are doubled compared to previous instrumental-seismicity based PSHA in Malawi. Cumulatively, these results highlight the need for careful fault source modelling in PSHA of low strain rate regions and the need for new fault-based PSHA elsewhere in the East Africa Rift.

Key words: Earthquake hazards; Statistical seismology; Continental tectonics: extensional.

1 INTRODUCTION

In low strain rate regions, long-term deformation rates may not be adequately captured by historical and instrumental earthquake catalogs (Lombardi & Marzocchi 2007; Clark *et al.* 2012; Stevens & Avouac 2021; Iturrieta *et al.* 2022). Therefore, probabilistic seismic hazard analysis (PSHA) that uses these catalogs to develop areal or smoothed-seismicity sources (e.g. Zahran *et al.* 2015; Goitom *et al.* 2017; Poggi *et al.* 2017) will be limited by the data available to constrain future earthquake rates. Incorporating geodetic and geologic data in PSHA through fault-based seismogenic sources can partly address this challenge. However, careful treatment of fault sources is required in low strain rate regions as estimated seismic hazard levels are highly sensitive to assumptions about their geometry and segmentation (Hodge *et al.* 2015; DuRoss *et al.* 2016; Gómez-Novell *et al.* 2020; Valentini *et al.* 2020; Visini *et al.* 2020; Goda & Sharipov 2021). A promising approach for representing fault segmentation in PSHA are inversion techniques that constrain the rate of all plausible ruptures in an interconnected fault system (Field *et al.* 2014, 2021; Geist & Parsons 2018; Chartier *et al.* 2019; Gerstenberger *et al.* 2022). However, various constraints on earthquake rates from geologic, geodetic and seismologic data must be satisfied to apply these techniques and this will be especially challenging in low strain rate regions where such data is scarce and earthquake rates may be non-stationary (Cox *et al.* 2012; Hodge *et al.* 2015; Vallage & Bollinger 2020; Stevens & Avouac 2021; Iturrieta *et al.* 2022).

The use of fault-based sources in PSHA also requires extrapolating geologic and geodetic constraints on fault deformation through the Earth's crust. In particular, assumptions about a fault's down-dip geometry and extent can influence its seismic moment rate, interaction with neighbouring faults and source-to-site distance in ground motion calculations. In most continental regions, the seismogenic layer is 10–20-km thick (e.g. Jackson *et al.* 2021) and so only a few studies have explicitly considered this uncertainty in PSHA (Wu *et al.* 2017; Ellis *et al.* 2021). However, assumptions for how faults are extrapolated down-dip in PSHA of regions where the seismogenic layer is much thicker (20–40 km), such as in the East African and Baikal rifts (Nyblade & Langston 1995; Déverchère *et al.* 2001; Lavayssière *et al.* 2019; Craig & Jackson 2021), have not been assessed.

In this study, we present a new fault-based PSHA for Malawi, which is located within the Western Branch of the East African Rift (EAR). The seismogenic layer in Malawi is estimated to be ∼30–40-km thick (Jackson & Blenkinsop 1993; Nyblade & Langston 1995; Ebinger *et al.* 2019; Stevens *et al.* 2021) and though geodetically derived EAR extension rates are low (0.5–2 mm yr^{-1}; Stamps *et al.* 2021; Wedmore *et al.* 2021), they are an order of magnitude higher than inferred from the last 50 yr of instrumentally recorded seismicity (Hodge *et al.* 2015; Ebinger *et al.* 2019). Hence, it provides an ideal case study to investigate PSHA in a low strain rate region with a thick seismogenic layer. Furthermore, constraints on the seismogenic potential of Malawi's active faults have improved with the collection of new geologic and geodetic data (Hodge *et al.* 2019; Scholz *et al.* 2020; Shillington *et al.* 2020; Wedmore *et al.* 2020a, b, 2021; Kolawole *et al.* 2021; Williams *et al.* 2022c), which have been synthesised into fault sources for PSHA in the Malawi Seismogenic Source Model (MSSM; Williams *et al.* 2022b).

Malawi is also one of several countries along the EAR where seismic risk is being exacerbated by population growth, rapid urbanisation and the development of seismically vulnerable building stock (Goda *et al.* 2016; Meghraoui *et al.* 2016; Poggi *et al.* 2017; World-Bank 2019; Kloukinas *et al.* 2020; Giordano *et al.* 2021). However, PSHA in the EAR still mainly considers the relatively short historical (150–600 yr) and instrumental (< 60 yr) record of seismicity alone (e.g. Midzi *et al.* 1999; Bwambale *et al.* 2016; Delvaux *et al.* 2017; Goitom *et al.* 2017; Poggi *et al.* 2017; Tuluka *et al.* 2020; Msabi & Ferdinand 2021). Here, we incorporate the MSSM into a PSHA for Malawi through stochastic event catalogs (Musson 1999; Atkinson & Goda 2013) to provide critical inputs for assessing Malawi's increasing seismic risk Goda *et al.* (2016, 2022) and to examine how uncertainty in the the down-dip extent and segmentation of fault sources influences PSHA in low strain rate regions.

2 BACKGROUND TO SEISMIC HAZARD ASSESSMENT IN MALAWI

2.1 The seismotectonic setting of Malawi

Malawi's national borders are closely aligned to a 900-km long section of the EAR's Western Branch, with earthquakes of moment magnitude (M_W) > 4.5 and active faults > 50-km long documented throughout (Fig. 1; Dixey 1926; Ebinger *et al.* 1987; Specht & Rosendahl 1989; Chapola & Kaphwiyo 1992; Poggi *et al.* 2017; Wedmore *et al.* 2020a; Williams *et al.* 2022c). In central and northern Malawi, the EAR has mostly been flooded by Lake Malawi, whilst in southern Malawi the rift is onshore and at its southern end has intersected and reactivated Karoo (i.e. Triassic-Jurassic) age faults (Dulanya 2017; Wedmore *et al.* 2020b; Kolawole *et al.* 2021; Williams *et al.* 2021a; Dulanya *et al.* 2022). Only negligible amounts of melt have been inferred from geophysical observations of Malawi's crust (Njinju *et al.* 2019; Accardo *et al.* 2020; Hopper *et al.* 2020) and so rift extension is primarily accommodated by normal fault earthquakes (Biggs *et al.* 2010; Hodge *et al.* 2015; Ebinger *et al.* 2019; Williams *et al.* 2022b).

The most comprehensive instrumental record of earthquakes in Malawi is the Sub-Saharan Africa Global Earthquake Model (SSA-GEM) catalog (Fig. 1a; Poggi *et al.* 2017). This was mainly developed from the International Seismological Centre (ISC) catalog, which in Malawi is complete since 1965 for events $M_W > 4.5$ (Hodge *et al.* 2015). Within this record, two events stand out: the 1989 M_W 6.3 Salima Earthquake and the 2009 Karonga earthquake sequence. The former was assigned a VIII on the Modified Mercalli Intensity Scale (MMI; Gupta & Malomo 1995) and its 32 ± 5 km focal depth is typical of Malawi's 30–40-km thick seismogenic layer (Jackson & Blenkinsop 1993; Nyblade & Langston 1995; Ebinger *et al.* 2019; Craig & Jackson 2021; Stevens *et al.* 2021). In contrast, the Karonga earthquake sequence primarily consisted of four shallow (focal depths 5–10 km) M_W 5.5–5.9 events over 13 d and resulted in a 9–18-km long surface rupture along the previously unrecognized St Mary Fault (Biggs *et al.* 2010; Hamiel *et al.* 2012; Macheyeki *et al.* 2015; Kolawole *et al.* 2018b). There are records of M 5–7 earthquakes in and around Malawi in the early 20th century; however, the lack of instrumentation in East Africa during this period mean the locations and magnitudes assigned to these events have large uncertainties (Ambraseys 1991; Poggi *et al.* 2017; Wedmore *et al.* 2022). Focal mechanism stress inversions indicate a normal fault stress state in Malawi with an ENE-WSW trending minimum principal compressive stress (Delvaux & Barth 2010; Ebinger *et al.* 2019; Williams *et al.* 2019).

2.2 Previous seismic hazard assessment in Malawi

In a PSHA for Malawi that considered areal sources developed from the SSA-GEM catalog, Poggi *et al.* (2017) found that for peak ground acceleration (PGA) there is a 10 per cent probability of exceeding (PoE) 0.10–0.15 g in 50 yr. Hazard levels were relatively uniform across Malawi in this study as it is largely covered by a single ∼380 000 km^2 areal source zone that extends from Mozambique to southern Tanzania. However, geodetic models indicate that EAR extension rates increase from south to north Malawi (Saria *et al.* 2014; Stamps *et al.* 2021; Wedmore *et al.* 2021) and there are also geologic observations of across-rift variations in fault activity (Accardo *et al.* 2018; Shillington *et al.* 2020; Wedmore *et al.* 2020a). These spatial variations in deformation were incorporated into a PSHA by Hodge *et al.* (2015), who developed seven fault-based seismogenic sources in Malawi using previously mapped rift-bounding faults (Flannery & Rosendahl 1990) and geodetically derived regional extension rates (Stamps *et al.* 2008). Inclusion of these sources into PSHA resulted in higher hazard levels adjacent to these faults [10 per cent PoE 0.15-0.25 g in 50 yr vs 10 per cent PoE 0.10–15 g in 50 yr in Poggi *et al.* (2017)], with these increases greatest for cases that inferred relatively frequent, moderate magnitude ruptures of short discrete fault segments, rather than rarer, larger magnitude earthquakes spanning entire faults.

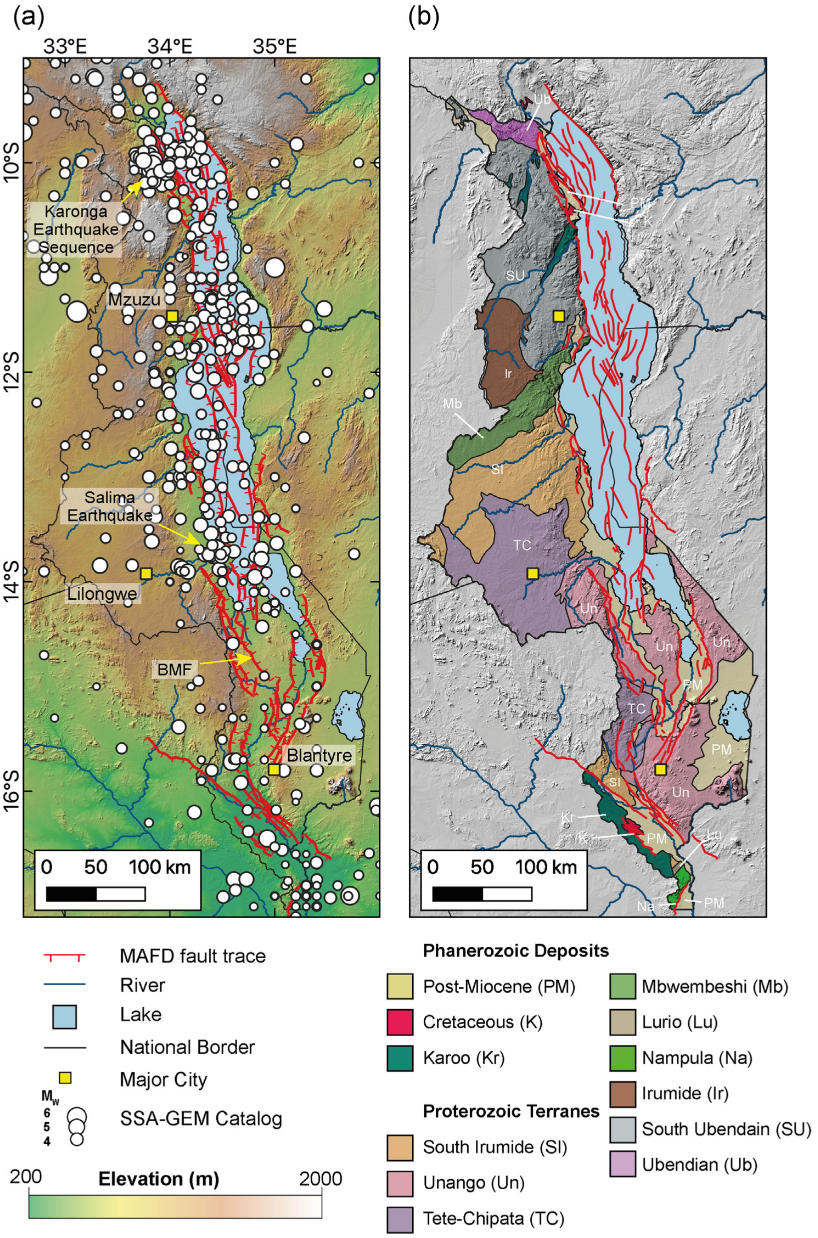

Figure 1. Map of Malawi in the context of (a) the Malawi Active Fault Database (MAFD; Williams *et al.* 2022c) and the Sub-Saharan Africa Global Earthquake Model (SSA-GEM) catalog Poggi *et al.* (2017) and (b) regional geological terranes Fullgraf *et al.* (2017). BMF; Bilila-Mtakataka Fault.

The PSHA presented by Hodge *et al.* (2015) was later incorporated into a quantitative seismic risk assessment (Goda *et al.* 2016), which highlighted that Malawi was at serious risk of building collapse during moderate-large magnitude earthquake (>10 000 buildings collapse for MMI > 6.5 shaking). The high exposure to moderate ground motions in Malawi is indicative of its seismically vulnerable building stock (Giordano *et al.* 2021; Novelli *et al.* 2021). Currently, no provisions are made for seismic loading in the official masonry construction code of practice in Malawi (MS791-1:2014; Malawi Bureau of Standards Board 2014). Earthquakes are qualitatively acknowledged for informal buildings through the Safer House Construction Guidelines (Cassani *et al.* 2016); however, considerable challenges exist in applying and enforcing these guidelines (Ngoma *et al.* 2019; Novelli *et al.* 2021).

Since 2015, high resolution digital elevation models (Hodge *et al.* 2019, 2020; Wedmore *et al.* 2020b, a), aeromagnetic and gravity data (Kolawole *et al.* 2018a, 2021; Chisenga *et al.* 2019) and a new generation of seismic reflection data in Lake Malawi (Shillington *et al.* 2016, 2020; Scholz *et al.* 2020) have led to significant advances in the identification and mapping of active faults in Malawi. These data sets were combined into the Malawi Active Fault Database (MAFD), a geospatial database for 113 faults that are inferred to be active in Malawi and neighbouring areas of Mozambique and Tanzania (Williams *et al.* 2021b, 2022c). In addition, new constraints on fault slip rates in Malawi have been provided from new geodetic data (Stamps *et al.* 2018; Wedmore *et al.* 2021) and the fault offsets of a 75 ka reflector in seismic reflection data in Lake Malawi (Shillington *et al.* 2020). These new data were combined into the MSSM, a database that provides slip rate, earthquake magnitudes and recurrence interval estimates of faults included in the MAFD (Williams *et al.* 2022a, b).

3 PSHA WORKFLOW

Here we combine the MSSM with previously defined EAR areal sources (Poggi *et al.* 2017) to develop a new PSHA for Malawi. We incorporate the MSSM (v1.2) by considering both the earthquake magnitude and recurrence interval assigned to each MSSM source (the 'Direct MSSM' approach) and a moment rate balancing approach that explicitly explores different hypotheses for the down-dip extent of the MSSM sources and whether they exhibit G–R or characteristic earthquake magnitude-frequency distributions (MFD; the 'Adapted MSSM' approach; Youngs & Coppersmith 1985; Convertito *et al.* 2006). These different MSSM interpretations are realised in five stochastic event catalogs, with off-fault events considered using an areal source based catalog. The PSHA is then formulated by evaluating these five catalogs using four ground motion models (GMMs; Atkinson & Adams 2013; Akkar *et al.* 2014; Boore *et al.* 2014; Chiou & Youngs 2014). Hence, for a given site, PoE and spectral period, we calculate 20 ground motion parameters. Following an ensemble approach, we use the mean and distribution of these values to describe seismic hazard and its uncertainty (Marzocchi *et al.* 2015; Meletti *et al.* 2021).

Our analysis is performed for a rectangular region that bounds Malawi with a grid spacing of 0.2° (Fig. 1). For each grid point, we consider two values for the average shear wave velocity to 30 m depth (V_{S30}): (1) a reference site condition ($V_{S30} = 760\ \mathrm{m\,s^{-1}}$) and (2) the value derived from the USGS V_{S30} database (Wald & Allen 2007). In addition, we performed site specific PSHA for the three largest cities in Malawi: Lilongwe, Blantyre and Mzuzu (Fig. 1a). We describe the earthquake sources and stochastic event catalogs further in Section 4, the GMMs in Section 5.1 and seismic hazard calculations in Section 5.2. PSHA results are presented in Section 6. A summary of our PSHA workflow is shown in Fig. 2. Abbreviations and symbols are listed in Table 1.

4 SOURCE MODELS

4.1 The Direct approach to the MSSM

The MSSM (v1.2) is a geospatial database of 140 geometrically defined section sources, 108 fault sources and 27 multifault sources that were identified from the 113 faults contained within the MAFD (Fig. 3; Williams *et al.* 2021b, 2022c). The number of faults in the MAFD and fault sources in the MSSM are not the same due to the requirement that sources are ≥5-km long and that faults that splay in map view are considered to represent different sources. A full description of the MSSM is provided by Williams *et al.* (2022b) and so we only briefly summarise the parameters of interest for PSHA here. An earthquake magnitude (m_s) and single event displacement ($\bar{D}_s$) estimate is assigned to each MSSM source using the Leonard (2010) magnitude–area scaling relationships for interplate dip-slip faults. For these calculations, source width (W_s) is derived through

$$W_s = \begin{cases} c_1 L_s^{\frac{2}{3}}, & \text{if } c_1 L_s^{\frac{2}{3}} \text{ is} < \frac{z}{\sin\delta_s} \\ \frac{z}{\sin\delta_s}, & \text{if } c_1 L_s^{\frac{2}{3}} \text{ is} \geq \frac{z}{\sin\delta_s} \end{cases} \tag{1}$$

where c_1 is an empirically derived parameter and equals 17.5 metres$^{\frac{1}{3}}$ for interplate dip-slip faults (Leonard 2010), L_s and δ_s are source length and dip and z is the seismogenic layer thickness. Previous studies have estimated that z is 30-40 km in Malawi (Ebinger *et al.* 2019; Stevens *et al.* 2021) and we apply an intermediate estimate of 35 km here. If two sources intersect down-dip, the shorter source is assumed to be truncated by the longer one and its W_s accordingly revised (Scholz & Contreras 1998).

For some sources in Lake Malawi, slip rates (S_s) have been derived from offsets across a 75 ka reflector in seismic reflection surveys (Shillington *et al.* 2020). Elsewhere, S_s are estimated using a systems-based approach that incorporates geodetically derived regional extension rates (Wedmore *et al.* 2021; Williams *et al.* 2021a, 2022b). The recurrence interval (R_s) for a full source earthquake with magnitude m_s is then derived by combining the slip rate (S_s) and displacement ($\bar{D}_s$) through the relationship: $R_s = \bar{D}_s / S_s$ (Wallace 1970).

4.2 The Adapted approach to the MSSM

The discrete section, fault and multifault sources in the MSSM are not an exhaustive list of potential earthquake ruptures in Malawi; in reality earthquakes can 'float' within a larger fault network (Visini *et al.* 2020; Field *et al.* 2021). In addition, eq. (1) suggests that a source's down-dip extent is dependent on its length ('length-limited'); however, we cannot exclude the possibility that unless intersected by another source, all the MSSM sources propagate through Malawi's 35-km thick seismogenic layer ('layer-limited'). This uncertainty is raised further in Malawi by: (1) possible lateral variations in the lower crust's composition and strain rate that can locally modulate whether the down-dip extent of faults is seismic or aseismic (Fagereng 2013; Hellebrekers *et al.* 2019; Wedmore *et al.* 2020a) and (2) intrarift faults in Malawi may accommodate upper-crustal flexural extensional strains that are induced from bending in the hanging-wall of large displacement (>5 km) border faults (Turcotte & Schubert 1982; Billings & Kattenhorn 2005; Kolawole *et al.* 2018a; Shillington *et al.* 2020; Williams *et al.* 2022b). Another possibility is that large earthquakes propagate below the seismogenic layer ('dynamic overshoot'; Shaw 2013; Ellis *et al.* 2021). We do not explicitly consider dynamic overshoot in this PSHA, though its implications are discussed in Williams *et al.* (2022b).

We explore the uncertainty on length- or layer-limited source down-dip extents using an 'adapted' approach to the MSSM. We do this by calculating a source's seismic moment release rate ($\dot{M}_0$) through

$$\dot{M}_0 = \mu S_s A_s \tag{2}$$

where μ is crustal rigidity and is taken as 33 GPa for consistency with the Leonard (2010) scaling relationships and A_s is source area and is accordingly adjusted for length- and layer-limited width cases (Fig. A7). We then combine the source's $\dot{M}_0$ with a b-value to develop continuous recurrence models that follow a G–R or characteristic MFD and allow ruptures to float anywhere within the fault plane (Figs 4 and 5; Youngs & Coppersmith 1985; Convertito *et al.* 2006; Goda & Sharipov 2021). For each source, MFD and width case, nine recurrence models are generated to incorporate uncertainty in the b-value and the source's largest magnitude event (M_{Max}; Figs 2 and A1). The equations that allow us to balance the $\dot{M}_0$ through source-specific magnitude probability distribution functions and earthquake rates and that were derived by Youngs &

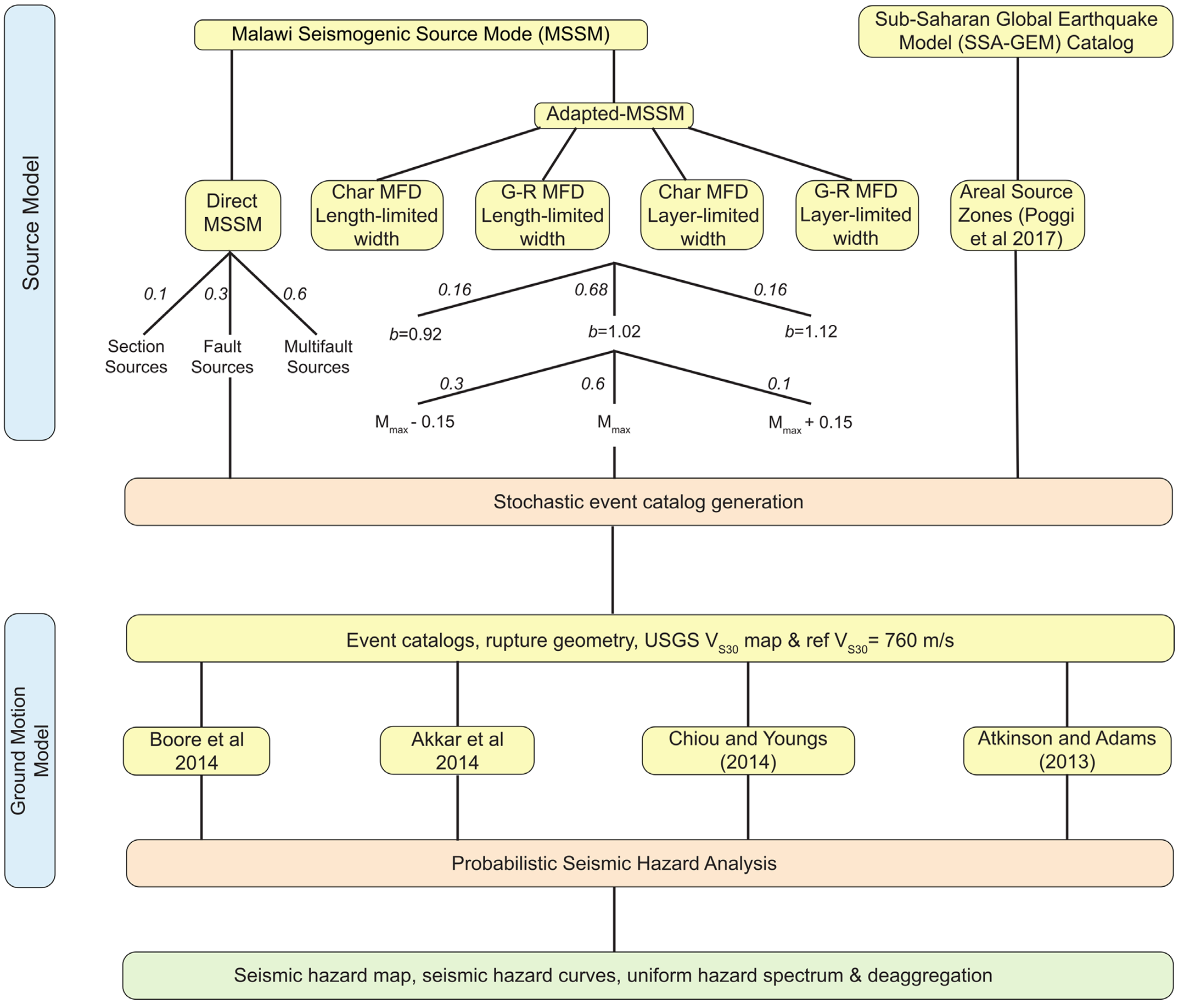

Figure 2. Flow chart for the PSHA conducted in this study. Branches are equally weighted unless otherwise stated. Weightings for the Adapted MSSM logic tree branches after Goda & Sharipov (2021).

Coppersmith (1985) and Convertito *et al.* (2006), are provided in Appendix A2.

Since the Adapted MSSM source models are continuous across a range of magnitudes, the division of the MSSM into discrete section, fault and multifault sources is not necessary. In other words, section source seismicity is already incorporated into the MFD of the larger fault or multifault source that they belong to (Fig. 4). Likewise, if a MSSM fault source is a constituent of a multifault source. In the Adapted MSSM approach we therefore only consider 79 sources; all multifault sources and fault sources that are not part of a mulitfault source.

4.3 Areal sources

We use the areal source zones developed for East Africa by Poggi *et al.* (2017) to incorporate: (1) earthquakes on unknown faults in Malawi, (2) earthquakes on faults included in the MAFD but not in the MSSM due to their short length (<5 km) and (3) earthquakes in regions adjacent (< 200 km) to Malawi, where no fault-based earthquake sources have been developed (Fig. 6). These areal source zones are defined by a truncated exponential G–R relationship that is fitted to the seismicity recorded in each area in the SSA-GEM catalog (Table 2; Poggi *et al.* 2017).

There are regions to the southwest and east of Malawi that are not covered by the Poggi *et al.* (2017) sources. However, since their seismic hazard is non-zero, we define areal sources for these regions by adjusting global rates of stable craton seismicity to their respective areas (Fig. 6, Table 2; Fenton *et al.* 2006). Strictly speaking these regions do not meet the criteria of 'stable cratons' set by Fenton *et al.* (2006) as they are within 200 km of passive margins and/or regions of Phanerozoic deformation. However, given the lack of recorded earthquakes in these regions, these estimates remain the best constraint on their seismicity.

Areal sources in this PSHA provide additional challenges. First, areal sources within Malawi require an upper magnitude bound (M_{Max}) that is indicative of the largest earthquake that could occur on an unmapped fault. Here, we set M_{Max} to 7.0, which is equivalent to a 40-km long fault for the Leonard (2010) scaling. This is guided by: (1) comparisons to other national-scale seismic hazard models where M_{Max} ranges between 6.5 and 7.5 (Stirling *et al.* 2012; Field *et al.* 2014; Woessner *et al.* 2015; Wang *et al.* 2016) and (2) the inference from its thick seismogenic layer and lack of chronostratigraphic data that there are relatively large unmapped active faults in Malawi (Williams *et al.* 2022c).

Secondly, high earthquake location uncertainties in Malawi (5–20 km; Jackson & Blenkinsop 1993; Gaherty *et al.* 2019) mean it is not possible to filter out 'on-fault' earthquakes from the

Table 1. List of acronyms and symbols used in this study.

Acronym/symbol	Definition
Acronyms	
CoV	Coefficient of Variation
EAR	East African Rift
G–R	Gutenberg–Richter
GMM	Ground Motion Model
GSRM	Global Strain Rate Model
MAFD	Malawi Active Fault Database
MMI	Modified Mercalli Intensity Scale
MPS19	Italian Seismic Hazard Model (Modello di Pericolosità Sismica)
MSSM	Malawi Seismogenic Source Model
MFD	Magnitude–frequency distribution
PGA	Peak ground acceleration
PoE	Probability of exceedance
PSHA	Probabilistic seismic hazard analysis
SA	Spectral Acceleration
SHIFT	Seismic hazard inferred from tectonics
SSA-GEM	Sub-Sahara African Global Earthquake Model catalog
SSA-GSRM	Sub-Saharan African Geodetic Strain Rate Model
V_{S30}	Average shear wave velocity to 30 m depth
Symbols	
α_C	Activity rate for a characteristic MFD
α_{NC}	Activity rate for the non-characteristic magnitude range in a characteristic MFD
α_{GR}	Activity rate for a G–R MFD
β	The product of the *b*-value and ln10
δ_s	Source dip
Δm_1	Magnitude range in characteristic MFD where recurrence rate is less than characteristic portion
Δm_2	Magnitude range for characteristic events
λ_s	Annual occurrence rate for source events
μ	Crustal rigidity
A_s	Source area
c_1 & c_2	Empirical constants from Leonard (2010)
$\bar{D}_s$	Source single event displacement
$f_M(m)$	Source probability density function for magnitude m
L_s	Source length
m	Earthquake magnitude
m_s	Source earthquake magnitude estimate
M_{Max}	Maximum expected earthquake magnitude
M_0^{Max}	Seismic moment for M_{Max}
M_{min}	Minimum earthquake magnitude considered for the PSHA
$\dot{M}_0$	Seismic moment release rate
M_W	Moment magnitude
N	Number of event catalog–GMM combinations
R_s	Source recurrence interval
S_s	Source slip rate
t_s	Time to source's next event in stochastic catalog
ν_{GM}	Rate of ground motion exceedance
W_s	Source width
z	Seismogenic layer thickness

SSA-GEM catalog when estimating the areal source's G–R parameters (with the exception of the 2009 Karonga earthquakes). An additive combination of the areal and MSSM sources could therefore lead to double-counting of seismicity across the magnitude range where these sources overlap (i.e. M_W 4.5–7.0). Combining these sources in this way, does not however, overestimate the moment release rate in Malawi (as constrained by geodesy) and nor does it imply an unusually high proportion of off-fault seismicity (Section 4.6.2, Appendix A4). We therefore retain this relatively simple approach for combining areal and MSSM sources and acknowledge that future PSHA in Malawi should more critically examine how these sources are incorporated (Section 7.2).

4.4 Stochastic event catalog generation

To perform the PSHA, we generated two million 1-yr long simulations for each of the five MSSM cases we wish to consider: the Direct-MSSM approach (Section 4.1) and four catalogs in the Adapted MSSM approach to cumulatively explore whether MSSM sources exhibit G–R or characteristic seismicity and if their

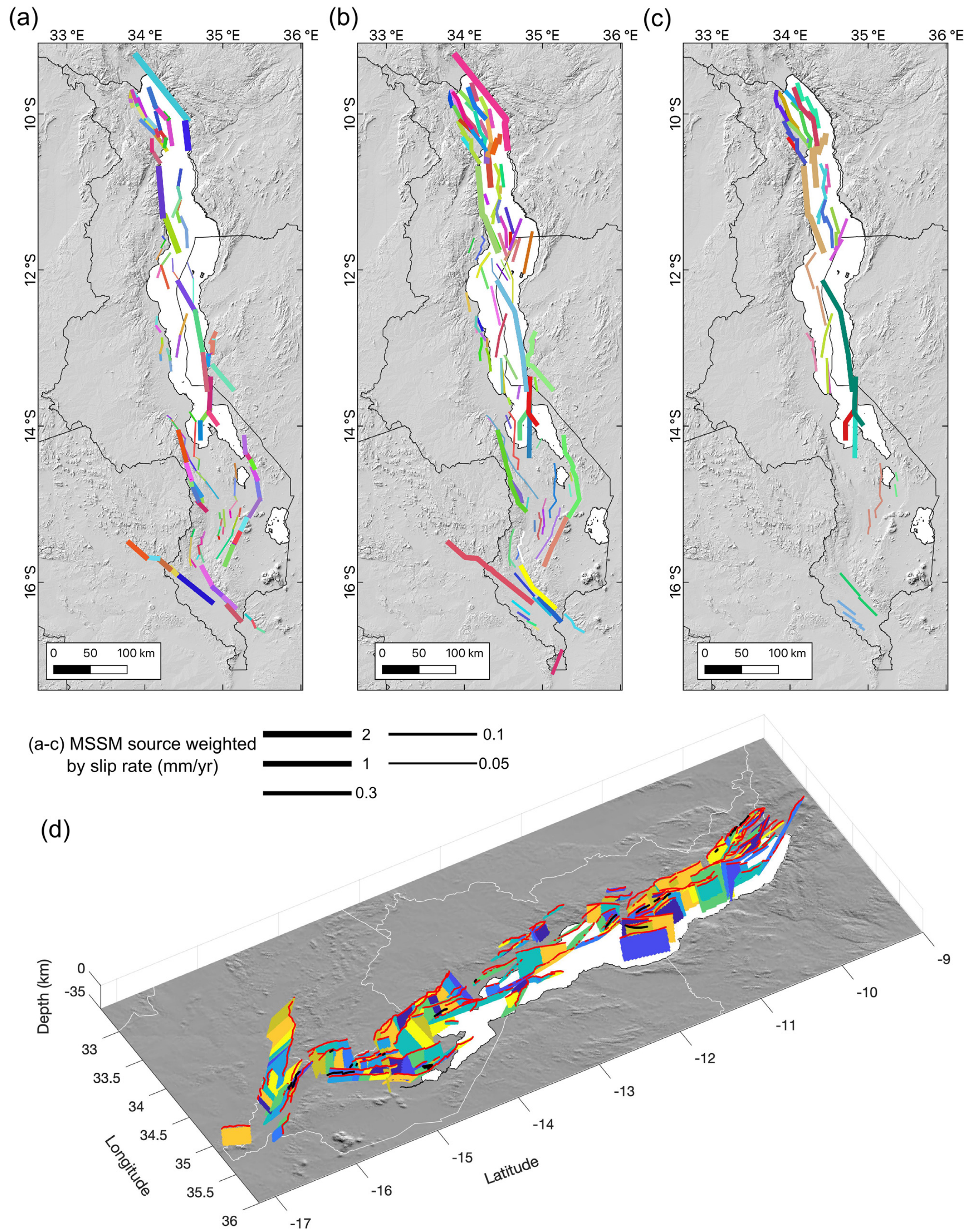

Figure 3. Maps showing extent of (a) section, (b) fault and (c) multifault sources in the MSSM, with lines weighted by the source's intermediate slip rate estimate. Each color represents a different source. (d) 3D model of MSSM sources used in the Direct MSSM and length-limited MSSM catalogs. The different colored planes represent either different MSSM faults, or multiple section sources along a single fault. Red lines are traces of the fault in the MAFD. Images underlain by SRTM DEM. Maps modified after (Williams *et al.* 2022b).

down-dip extrapolation is length- or layer-limited (Section 4.2, Figs 2, 4 and 7). To represent our additive combination of the MSSM and areal sources (Section 4.3), each MSSM-based catalog is combined with an equivalent length areal source catalog.

The identical length of each MSSM-based catalog is chosen to reflect that we have no constraints on what the 'true' source width or MFD is in Malawi and so we equally weight each hypothesis (Frankel *et al.* 2000; Goda & Sharipov 2021). Another interpretation is that these catalogs can be merged into one 'Combined Catalog' that consists of 10 million 1-yr catalog simulations of MSSM and areal source seismicity (Fig. 7). Compared to conventional PSHA, in which ground motions are derived from integrating over all sources, distances and magnitudes, these different stochastic catalogs provide an intuitive and flexible approach to explore alternative on-fault MFD and down-dip extents for a large number of sources (Musson 1999; Atkinson & Goda 2013).

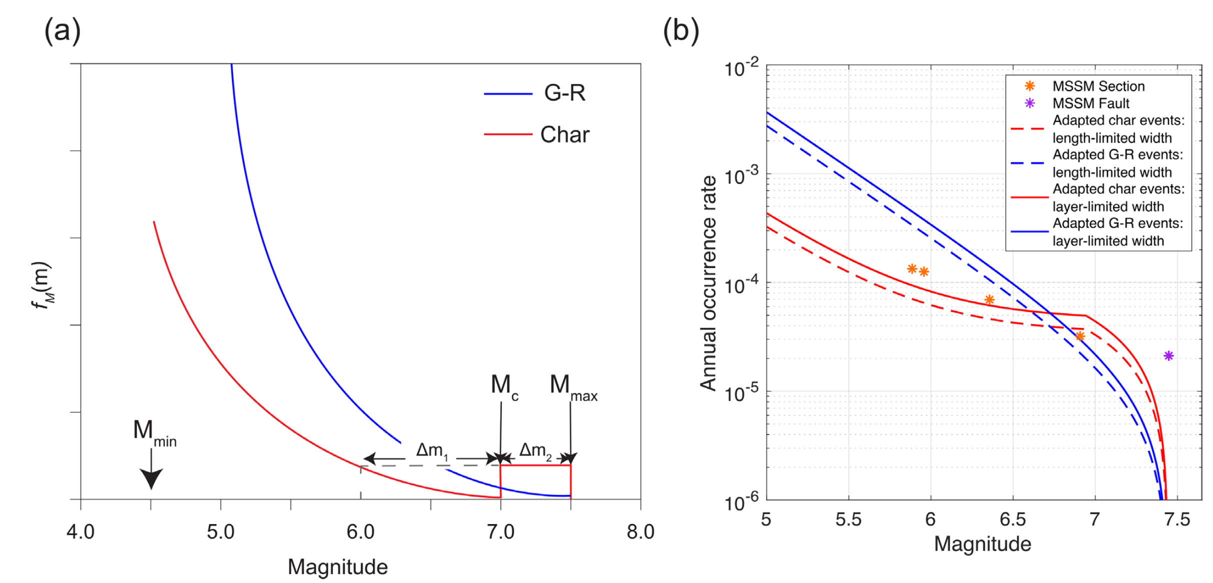

Figure 4. (a) Schematic representation of the probability density functions for magnitude (m) for a continuous G–R and characteristic (Char) recurrence model (modified after Convertito *et al.* 2006). (b) MFD curves for the Chingale Step Fault for the different cases of source width and recurrence models in the Adapted MSSM approach. Curves are for the median b-value and M_{Max} estimates. Also shown are the discrete points in magnitude–frequency space for the Chingale Step fault source and its constituent section sources in the Direct MSSM approach.

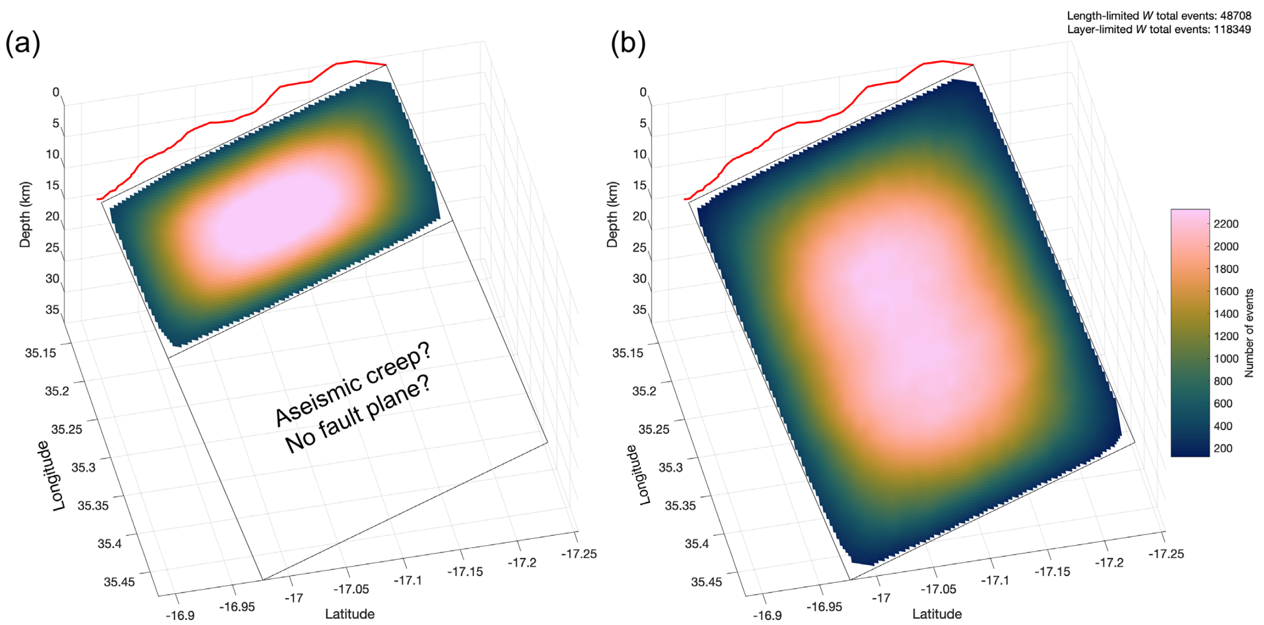

Figure 5. Exploration of length-limited and layer-limited source widths (W) in the Adapted MSSM approach for the Nsanje Fault source in the MSSM. In (a) W is assumed to be governed by its length through eq. (1), with the fault planes either not propagating through the full-width of the seismogenic crust or the crust down-dip of the fault being aseismic. In (b) the fault plane is interpreted to extend through the 35-km thick seismogenic layer. The fault surface is then contoured by the distribution of events in the Adapted MSSM stochastic event catalogs. Red line depicts the Nsanje Fault's trace in the MAFD.

Earthquake occurrence is modelled in the catalogs using a memory-less Poisson process and so each event is independent of time for a given source (e.g. Zhuang *et al.* 2012; Pace *et al.* 2016). In the Direct-MSSM catalog, a source's annual occurrence rate (λ_s) is taken from the inverse of its recurrence interval, so that the time to its next event (t_s) is

$$t_s = -\ln(1-u)/\lambda_s \quad (3)$$

where u is a sample from the standard uniform distribution. The event magnitude is then sampled from a random normal variable centred around the source's Leonard (2010) magnitude–area scaling with a standard deviation of 0.1 and truncated ±0.2 magnitude units.

Since section, fault and multifault source types are mutually exclusive, weightings must be assigned to describe their relative likelihood in the Direct-MSSM catalog. We therefore generated catalogs for all possible source type weighting combinations at intervals of 0.1 with the limitation that the weighting of any source type is ≥ 0.1 (Fig. 8a). We then combined each catalog with the areal source catalog and searched for the weighting combination that produced a catalog with the closest b-value to the regional estimate (1.02; Hodge *et al.* 2015; Poggi *et al.* 2017). From this test, we selected a weighting for section, fault and multifault sources of 0.1–0.3–0.6

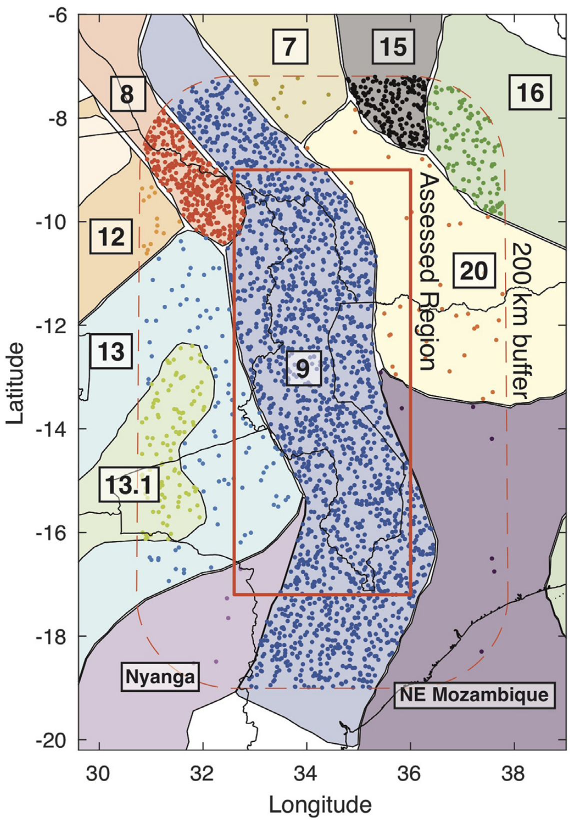

Figure 6. Areal sources previously developed for PSHA in East Africa (Poggi *et al.* 2017). Numeric code for each zone corresponds to the Source ID in Table 2. Source zones (Nyanga and NE Mozambique) that are characterised by global stable craton seismicity (Fenton & Bommer 2006) are also shown. Dots represent event locations from 1000 1-yr long stochastic event catalogs for each source. In these catalogs, events are randomly located within each source and those >200 km from the assessed region are removed during the PSHA.

(Fig. 8). Further details of this weighting procedure are given in Appendix A1.

Within each simulation cycle of the MSSM-Adapted catalogs, we randomly sample one of the nine recurrence models that is generated for each source width-MFD case (Fig. A1, Table A2) given the weightings in Fig. 2. Then from the catalogs with a G–R MFD, λ_s equals α_{GR} as defined in eq. (A4) and event magnitudes are taken from the probability density function in eq. (A1). For a characteristic MFD, λ_s is defined by α_C (eq. A5) and the magnitude of events is sampled from eq. (A2) (Appendix A2).

For the areal source catalog, λ_s and the magnitude distribution for each source is defined by its G–R relationship (Table 2). Events occur randomly anywhere within each source; however, events >200 km from the region assessed in the PSHA are subsequently removed (Fig. 6).

For the purposes of calculating ground motions, all events in the MSSM-based catalogs are presumed to be normal faulting earthquakes. This is consistent with their moderate fault dip, the regional stress state (Delvaux & Barth 2010; Ebinger *et al.* 2019; Williams *et al.* 2019), Late Quaternary fault slickensides (Wedmore *et al.* 2020a) and the offset of sediments under Lake Malawi (Accardo *et al.* 2018; Shillington *et al.* 2020). However, of the 63 focal mechanisms that were resolved during a 2-yr deployment of seismometers in northern Malawi, seven were strike-slip (Ebinger *et al.* 2019) and it has been proposed that some historical events elsewhere in the EAR were strike-slip (Ayele & Kulhanek 2000). To recognize this, 10 per cent of events in the Areal Source Catalog are randomly assigned to be strike-slip when applying the GMM (Section 5.1).

4.5 Rupture geometry

We define the rupture geometry of events in the MSSM-based catalogs using the MSSM geometric model (Fig. 3d; Williams *et al.* 2022b). This model consists of 2D planes in 3D space; however, for the purpose of source-to-site calculations, we convert it to a set of grid points at intervals of $1 \times 1 \times 0.6$ km in the $x \times y \times z$ direction respectively. In the Direct-MSSM catalog, the source geometry defines the lateral extent of their events. In addition, we allow the depth interval of smaller section or fault sources to randomly float within a larger fault or multifault plane.

In the length-limited Adapted-MSSM catalogs, we use the same geometric source model as the Direct-MSSM catalog. However, in the layer-limited catalogs, we revise this model so that all sources are extrapolated to a depth of 35 km unless intersected by another source. The length and width of each event in the Adapted-MSSM catalogs are calculated from the Leonard (2010) scaling relationships between source length, width and magnitude and then floating these dimensions randomly within the larger source plane (Fig. 5). In this approach, section boundaries or fault tips (for multifault sources) are not considered rupture barriers unlike in the Direct-MSSM Catalog.

In cases where MSSM sources intersect and it is not possible to fit a rupture onto the cut-off plane given the Leonard (2010) length-width scaling (eq. 1), an area that matches the event's magnitude is randomly fitted onto the plane instead. To save computational resources, events of M_W<5.4 in the Adapted-MSSM catalog are treated as point sources and are randomly located on the source plane. Areal source catalog events are also treated as point sources and their depth is randomly sampled from a normal distribution truncated between 5–35 km and with a mean and standard deviation of 20 and 5 km, respectively

4.6 Stochastic event catalog validation

We test the output of the stochastic event catalogs in two ways: (1) internal tests to investigate if the sources' moment rate ($\dot{M}_0$) and MFD shape match those from their input recurrence models and (2) external tests to determine if the total $\dot{M}_0$ of these catalogs is consistent with independent constraints for the $\dot{M}_0$ in Malawi from instrumental seismicity (Poggi *et al.* 2017) and geodesy (Kreemer *et al.* 2014; Stamps *et al.* 2018). Further details of these tests are provided in Appendix A.

4.6.1 Internal tests

For the Direct- and Adapted-MSSM internal tests, there is generally a good correlation between the $\dot{M}_0$ of MSSM source's calculated using their slip rate and area (eq. 2) and in the stochastic event catalogs (Fig. 9). We consider the Direct MSSM's catalog $\dot{M}_0$ (1.52×10^{18} Nm yr^{-1}) an acceptable fit to the target $\dot{M}_0$, as defined by weighting each source by rupture type and then summing up their $\dot{M}_0$ (1.48×10^{18} Nm yr^{-1}; Table A3).

For the MSSM adapted sources, the $\dot{M}_0$ of the entire catalog is 2–10 per cent lower than calculated from just combining the

Table 2. G–R and maximum magnitude (M_{Max}) parameters for areal source zones in Malawi and its surrounding (<200 km) region. Areal source zones taken from Poggi *et al.* (2017) or from adapting global rates of seismicity in stable cratons (Fenton *et al.* 2006). Extent of source zones shown in Fig. 6.

Source ID (Poggi *et al.* 2017)	Source Zone	*a*-value	*b*-value	M_{Max}
7	Lake Victoria	4	1.02	6.9
8	Tanganynika	4.84	1.02	7.9
9	Rukwa–Malawi	4.93	1.02	7.9*
12	Mweru South Katanga	4.05	0.99	6.9
13	Kariba-Okavango	4.08	0.99	6.9
13.1	Kariba-Okavango	3.99	0.99	6.9
15	Eastern Rift	5.31	1.17	7.4
16	Davie Rift	5.45	1.16	7.4
20	Rovuma Basin	3.31	1.02	6.9
N/A	Nyanga	1.73	0.8	7.0
N/A	Northeast Mozambique	1.93	0.8	7.0

M_{Max} revised to M_W 7.0 for events occurring within Malawi during PSHA

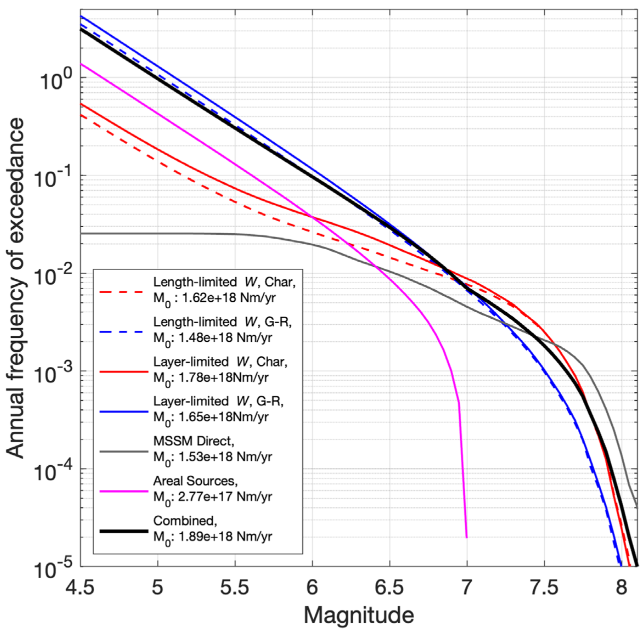

Figure 7. MFD and moment rate ($\dot{M}_0$) for the five MSSM-based simulated earthquake catalogs used in the PSHA. These catalogs are then each merged with the areal source catalog and then together into the 'Combined Catalog.' This plot only considers areal source catalog events that occur within the assessed region shown in Fig. 6.

$\dot{M}_0$ of all sources using eq. (2), with this discrepancy particularly high for the G–R catalogs (Table A3, Appendix A2). There are two causes for this discrepancy with the Youngs & Coppersmith (1985) $\dot{M}_0$ balancing approach: not incorporating events with M_W <4.5 in the catalogs and challenges replicating high magnitude events along low slip rate sources with a G–R MFD in the catalogs (Fig. A2b). A similar comparison for the areal source catalogs also indicate that their catalog MFD and $\dot{M}_0$ correspond to their given G–R relation, except for high magnitude events in the relatively low seismicity Nyanga and Northeast Mozambique source zones (Appendix A3).

In summary, the catalogs $\dot{M}_0$ and MFD shape correspond to the MSSM and areal sources' recurrence models, except for high magnitude low probability events (annual rates <0.0001; Appendices A2 and A3). In the context of PSHA, such infrequent events will only be a minor contributor to hazard levels. We therefore conclude that the MSSM and areal sources are sufficiently well represented in the stochastic event catalogs that we can used them to formulate our PSHA (Section 5.2) and hence they can replace the need to evaluate these sources using numerical integration instead (i.e. 'conventional' PSHA).

4.6.2 External tests

For the external tests, we first calculate the $\dot{M}_0$ of the areal sources developed in Malawi by Poggi *et al.* (2017) using their original M_{Max} estimate (7.9). This analysis is therefore representative of the $\dot{M}_0$ in Malawi from an extrapolated instrumental record (Appendix A3). From this approach we derive a $\dot{M}_0$ of ∼7.45 × 10^{17} Nm yr^{-1} (Table A4), which is just ∼40 per cent of the $\dot{M}_0$ from the Combined Catalog (∼1.89 × 10^{18} Nm yr^{-1}; Fig. 7).

Part of this discrepancy reflects differences in the M_{Max} estimates for Malawi between Poggi *et al.* (2017) and the MSSM-based Combined Catalog (M_W 7.9 vs 8.1). If the MSSM-based M_{Max} estimate is applied to the areal sources, the total $\dot{M}_0$ increases to 9.3 × 10^{17} Nm yr^{-1}. Increasing M_{Max} therefore reduces the $\dot{M}_0$ discrepancy, but cannot account for it alone. Instead, we consider three other possibilities: (1) the geodetic $\dot{M}_0$ from which the slip-rates in the MSSM are mainly derived from (Wedmore *et al.* 2021) is released aseismically, (2) the geodetic $\dot{M}_0$ is an overestimate, or (3) extrapolating the instrumental record underestimates long-term earthquake activity in Malawi.

With regards to the first scenario, the nucleation of earthquakes throughout Malawi's seismogenic layer (Ebinger *et al.* 2019; Stevens *et al.* 2021) and energetic slowly decaying aftershock sequences imply overall highly coupled faults (Ben-Zion 2008; Gaherty *et al.* 2019). Some degree of aseismic deformation in Malawi may still occur (Ebinger *et al.* 2019), with shallow (depths <5–10 km) aseismic afterslip observed following a M_W 5.2 earthquake near Karonga in 2014 (Zheng *et al.* 2020) and the 2006 M_W 7.0 Machaze earthquake in nearby Mozambique (Copley *et al.* 2012; Lloyd *et al.* 2019).

For the second scenario, we compare the Combined Catalog to independent estimates of the geodetic $\dot{M}_0$ in Malawi from: (1) the Global Strain Rate Model (GSRM v.2.1; Kreemer *et al.* 2014) and (2) the Sub-Saharan African Geodetic Strain Rate Model (SSA-GSRM v.1.0; Stamps *et al.* 2018). Following the approach used in the seismic hazard inferred from tectonics (SHIFT) model (Bird & Liu 2007; Bird & Kreemer 2015), the $\dot{M}_0$ of the GSRM v2.1 and SSA-GSRM v1.0 models are 9.5 × 10^{17} Nm yr^{-1} and

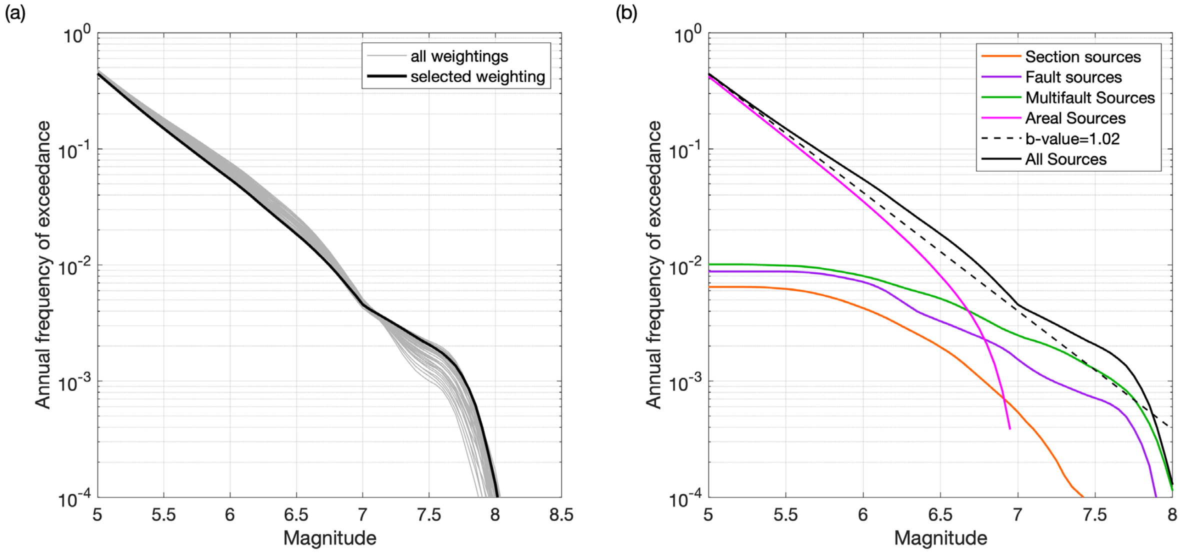

Figure 8. (a) MFD for the Direct MSSM-Areal combined Catalog in which 36 possible weighting combinations of section, fault and multifault ruptures are explored, with the MFD curve of the selected weighting combination highlighted. (b) MFD for the Direct MSSM-Area catalog for optimal set of rupture weightings, defined by a catalog with a *b*-value of 1.02. The MFD for individual source types is also shown.

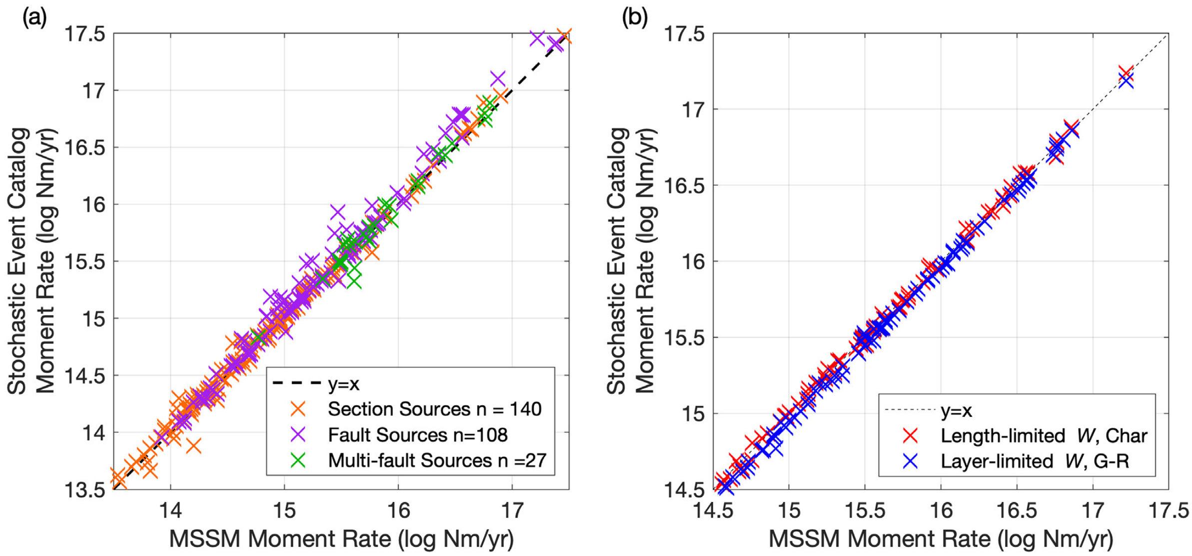

Figure 9. Comparison of the analytical moment rate ($\dot{M}_0$) of sources in the MSSM and their $\dot{M}_0$ in (a) the Direct MSSM catalog and (b) two of the Adapted MSSM simulated catalogs. In (a) the Direct MSSM source analytical $\dot{M}_0$ is weighted by source type as indicated in Section 4.4.

3.5×10^{18} Nm yr^{-1} (Appendix A5). The Combined Catalog $\dot{M}_0$ (1.89×10^{18} Nm yr^{-1}) is intermediate between these estimates and so suggests the Wedmore *et al.* (2021) geodetic model does not imply anomalously high extension rates in Malawi. Furthermore, the MSSM slip rates that are derived from the 75 ka seismic reflector offsets in Lake Malawi are consistent with geodetically derived regional extensional rates (Shillington *et al.* 2020; Williams *et al.* 2022b).

The Combined Catalog $\dot{M}_0$ is also not necessarily identical to the input geodetic $\dot{M}_0$ since: (1) it incorporates events that accommodate hanging-wall flexural extension along intrarift faults in northern and central Malawi and this deformation will not be captured by large-scale geodetic models (Muirhead *et al.* 2016; Shillington *et al.* 2020; Williams *et al.* 2022b), (2) areal source events are independent of the input geodetic $\dot{M}_0$ and (3) not all of the geodetic $\dot{M}_0$ is converted to seismic $\dot{M}_0$ due to the obliquity of MSSM sources to the regional extension direction (Williams *et al.* 2021a) and/or because they do not extend across the full width of the seismogenic layer (Section 4.2 and Fig. 5). We calculate that if all MSSM sources were optimally oriented to the regional extension direction and extended to the base of the seismogenic layer, the total $\dot{M}_0$ (1.88×10^{18} Nm yr^{-1}, Appendix A4) is nearly identical to the Combined Catalog (1.89×10^{18} Nm yr^{-1}). Therefore, a physical interpretation of the areal source source events is that they accommodate the deformation required to prevent space problems that would otherwise arise from normal fault obliquity and narrow fault widths in Malawi.

To investigate the third scenario that the SSA-GEM catalog underestimates long term earthquake activity in Malawi, we divided the Combined Catalog into 50-yr increments and compared these samples' $\dot{M}_0$ and MFD shape to the non-declustered 50-yr long (1965–2015) SSA-GEM catalog (Poggi *et al.* 2017). In this way, we can investigate how likely it is that the observed seismicity in Malawi would have been simulated in our event catalogs. We find that 12 per cent of the 50 yr Combined Catalog have a $\dot{M}_0$ equal to or less than the SSA-GEM catalog $\dot{M}_0$ (Fig. 10a). The MFD of this 50 yr period of instrumental seismicity is also within the variability of seismicity within the Combined Catalog 50 yr samples (Fig. 10b). Hence, if the Combined Catalog is representative of seismicity in Malawi, then the observed $\dot{M}_0$ between 1965 and 2015 is relatively, but not inconceivably, low.

We note too that the G–R stochastic catalog 50-yr samples cannot replicate the SSA-GEM $\dot{M}_0$ (Fig. 10). This result could be used to argue against applying G–R recurrence models to MSSM sources (Wesnousky *et al.* 1983; Ishibe & Shimazaki 2012). However, the event catalogs are generated using a time-independent Poisson approach (eq. 3) and it is plausible that clustered seismicity such as triggered events and/or long aftershock sequences, as occurred during the 2009 Karonga earthquakes, allow a MSSM source's MFD to align with a G–R relationship (Page & Felzer 2015; Stirling & Gerstenberger 2018; Wang *et al.* 2021). We suggest that if a non-Poission approach was used to generate the MSSM-catalogs, then more G–R catalog 50 yr samples would have a $\dot{M}_0$ that is comparable to the SSA-GEM catalog, even though the long-term deformation rates would not change.

In summary, there are many challenges in reconciling Malawi's observed seismic $\dot{M}_0$ and the MSSM-Areal Combined $\dot{M}_0$. We propose that this reflects an incomplete instrumental earthquake record, which in turn is indicative of the limited duration, poor instrumental coverage, clustered seismicity, low regional extension rates and locked faults (Ambraseys & Adams 1991; Biggs *et al.* 2010; Hodge *et al.* 2015; Stevens *et al.* 2021). This is further highlighted by the large uncertainty in how the catalog may be extrapolated to larger magnitudes (Fig. 10b; Tinti & Mulargia 1987). Our analysis does not consider uncertainty within the MSSM itself, or with applying the Leonard (2010) scaling relationships to faults in Malawi (Section 7.2). Nevertheless, the Combined Catalog satisfies constraints on the distribution of across-rift regional extensional strain (Shillington *et al.* 2020; Wedmore *et al.* 2020a), the regional *b*-value (Poggi *et al.* 2017) and the source specific $\dot{M}_0$ (Fig. 9). Furthermore, we have explored alternative hypotheses for uncertainty in on-fault MFDs and source down dip-extents. We therefore propose that it represents the best source model for PSHA currently available for Malawi.

5 SEISMIC HAZARD CALCULATIONS

5.1 Ground motion model

In the absence of strong ground motion data in East Africa (Midzi *et al.* 1999; Hodge *et al.* 2015; Poggi *et al.* 2017), we apply GMM from other similar tectonic terranes. In selecting the GMMs, we consider variations between 1D seismic velocity models in northern and southern Malawi in the crust's top 5 km (Fig. A8; Ebinger *et al.* 2019; Stevens *et al.* 2021) and that large magnitude earthquakes in Malawi have generated remarkably little fracturing in the surrounding crust (Wedmore *et al.* 2020b; Carpenter *et al.* 2022; Williams *et al.* 2022d). This led us to apply and equally weight three well-tested active crust GMMs (Akkar *et al.* 2014; Boore *et al.* 2014; Chiou & Youngs 2014) and one stable crust GMM (eastern crustal GMM from Atkinson & Adams 2013). Some of these GMMs were previously applied in East Africa by Poggi *et al.* (2017) and the ratio of active to stable crust GMMs is same as this study.

Cumulatively, these GMMs allow us to explore various source to site measurements: closest horizontal distance to rupture's surface projection (Joyner-Boore distance, R_{JB}), closest distance to rupture plane (R_{rup}), epicentral distance (R_{epi}) and hypocentral distance (R_{hypo}). In the instances that R_{epi} and R_{hypo} are applied to the MSSM fault-based events, distances are measured to a point randomly sampled within the simulated rupture's geometry. $R_{hypo} < 10$ km are not considered by the Atkinson & Adams (2013) GMM, so in these instances, ground motions are calculated with R_{hypo} fixed to 10 km.

To incorporate aleatory uncertainty, the respective sigma model for each GMM is applied to the calculated median ground motion. For the site-specific PSHA in the three largest cities in Malawi (Lilongwe, Blantryre and Mzuzu, Fig. 1), V_{S30} is set to reference values of 300 and 760 m s^{-1} s^{-1} and a range of spectral accelerations (SA) between 0-3 s are considered. For the PSHA maps, which are developed from 756 sites across Malawi in a 0.2° × 0.2° latitude and longitude grid, we consider PGA only and both a reference V_{S30} value (760 m s^{-1}) and the site-specific value derived from the USGS V_{S30} database (Fig. A6; Wald & Allen 2007). Ground motion calculations do not incorporate differences in lake floor elevation and substrata for the 59 sites in our grid under Lake Malawi. Because of this uncertainty, these sites are not explicitly shown in the hazard maps. However, to facilitate our understanding for how the MSSM sources influence hazard, they are retained in the hazard map comparisons.

5.2 Sensitivity analysis

We calculate the seismic hazard and its uncertainty by following the ensemble modelling framework used in the latest Italian seismic hazard model [Modello di Pericolosità Sismica (MPS19); Marzocchi *et al.* 2015; Meletti *et al.* 2021]. In this approach, N seismic hazard curves are generated for each site, where N is the number of source model-GMM combinations. For a given PoE and SA, N hazard values can therefore be sampled and fitted to a continuous distribution (i.e. 'horizontal dissections' of the curves), where the central value represents the seismic hazard estimate and the dispersion mimics the epistemic uncertainty (Marzocchi *et al.* 2015). In this study, $N = 20$ given that we consider four GMMs and five interpretations of the MSSM in the stochastic event catalogs (Figs 2 and 7). For each catalog–GMM combination, the annual probability (or rate) at which a specific ground motion intensity is exceeded ($\nu_{GM} \geq gm$) is calculated given the catalog's two million yr length (Section 4.4).

For the site-specific PSHA, the 20 ground motion intensity values at a given PoE and SA are described by a beta distribution, as this provides good fits to unimodal distributions bounded between 0 and 1 (Marzocchi *et al.* 2015). The spatial distribution of seismic hazard uncertainty is of greater interest for the PSHA maps and so is described by: (1) the interquartile range of the 20 seismic hazard values calculated at each site and (2) their Coefficient of Variation (CoV). The former describes the spatial distribution of the absolute uncertainty, whilst the latter is indicative of the uncertainty once normalized by the hazard level (Meletti *et al.* 2021). This analysis provides only a minimum bound on hazard uncertainty as we do not consider the uncertainty in the MSSM slip rate and recurrence interval estimates, the areal sources, or the nine recurrence models explored in the Adapted MSSM catalogs (Figs 2 and A1). Stochastic event catalog generation and seismic hazard calculations were performed using bespoke codes written in MATLAB and

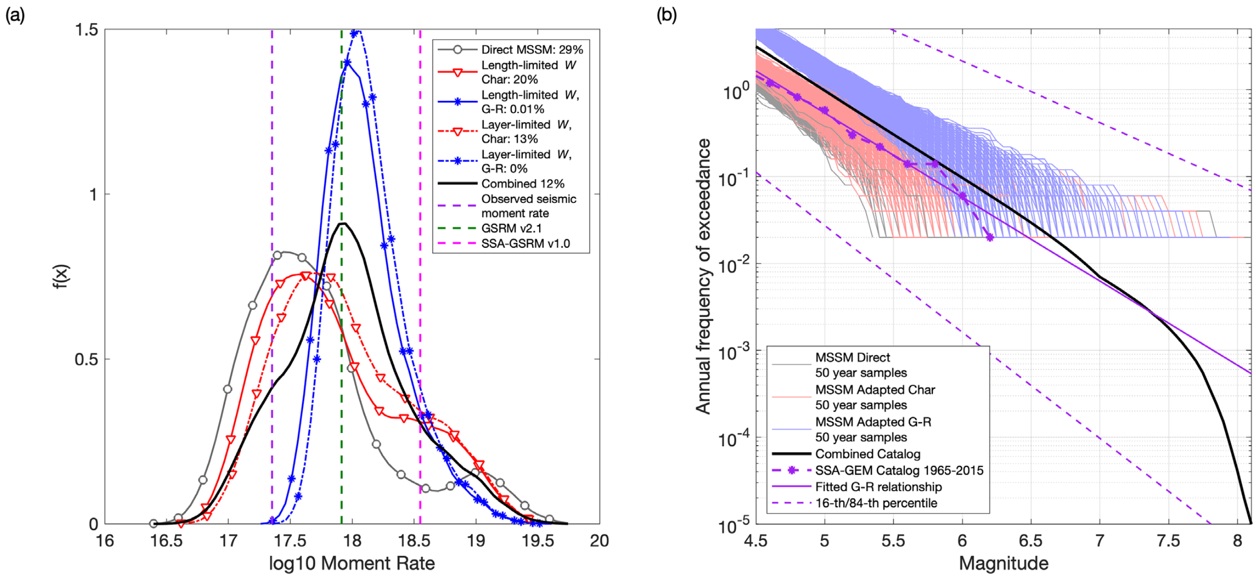

Figure 10. (a) Comparison of the moment rate ($\dot{M}_0$) in 50 yr samples of the stochastic event catalogs and the observed $\dot{M}_0$ from the SSA-GEM catalog between 1965-2015 for the assessed region shown in Fig. 6 (Poggi *et al.* 2017). Results for the Combined Catalog samples are shown as a kernel distribution (n = 200 000) and are also resolved into the five different interpretations of the MSSM (n = 40 000). The per cent by each catalog indicates the proportion of 50 yr samples that had a $\dot{M}_0 \leq$ SSA-GEM catalog. For context, the $\dot{M}_0$ over the assessed region from the the Global Strain Model (GSRM v.2.1; Kreemer *et al.* 2014) and Sub-Saharan African Geodetic Strain Model (SSA-GSRM v.1.0; Stamps *et al.* 2018) are also shown (see also Appendix A5). (b) Comparison of the Combined Catalog and SSA-GEM catalog MFD, with the MFD for 10 000 random 50 yr long samples of the Combined Catalog, colored by MSSM catalog also plotted. We also fit and extrapolate a G–R relationship and its associated uncertainties, to the 75 events in the SSA-GEM catalog in the assessed region with M_W >4.5 following Tinti & Mulargia (1987). The SSA-GEM catalog has not been declustered in this analysis.

available at https://github.com/jack-williams1/Malawi_PSHA and https://doi.org/10.5281/zenodo.7265780.

6 PSHA RESULTS

6.1 Site specific PSHA

The seismic hazard of the three selected sites (Lilongwe, Blantyre and Mzuzu; Fig. 1) shows considerable diversity. The mean hazard is lowest in Lilongwe (10 per cent PoE 0.11 g in 50 yr for PGA and V_{S30} of 760 m s^{-1}). Lilongwe is ∼55 km from the nearest MSSM source and so local (<40 km) M_W 5–6 events in the areal source model present the main source of hazard (Figs 11–13). The MSSM sources do, however, become important contributors to hazard in Lilongwe at low PoE and longer (>1 s) vibration periods (Fig. 12d). Hazard levels are higher in Blantyre and Mzuzu (10 per cent PoE 0.15–0.2 g in 50 yr). This reflects that both sites are < 20 km from MSSM sources, which dominate their hazard (Figs 11–13).

Since the hazard at high PoE and short vibration periods is dominated by areal source events in Lilongwe, seismic hazard uncertainty is mainly driven by the GMM selection (Fig. 11a). Conversely, in Blantyre and Mzuzu, both the source model (i.e. the event catalogs) and GMM selection contribute to uncertainty. In particular, high hazard levels are derived in Blantyre for the combinations that consider the Atkinson & Adams (2013) GMM and G–R on-fault MFD (Fig. 11e). However, in Mzuzu, the highest hazard levels are found for the Atkinson & Adams (2013) GMM regardless of the on-fault MFD (Fig. 11f). In all cases, the uncertainty in how the MSSM sources propagate through Malawi's 35-km thick seismogenic layer (i.e. length- or layer- limited width) do not significantly influence hazard estimates (Fig. 11).

6.2 Malawi seismic hazard maps

We first assess the relative contribution of areal and MSSM sources to seismic hazard in Malawi through maps that consider these sources separately. Figs 14(a) and (d) indicates that the hazard from areal sources is generally spatially uniform in Malawi, with a broad zone of relatively high hazard following the the relatively high $\dot{M}_0$ Rukwa–Malawi source zone (Tables 2 and A4, Figs 6 and A3; Poggi *et al.* 2017), which broadly corresponds to the EAR's trajectory through Malawi (Fig. 1).

By contrast, the fault-based MSSM sources imply a more complex spatial pattern of seismic hazard, with localized regions of relatively high hazard (10 per cent PoE ∼0.2–0.3 g in 50 yr) adjacent to rift-bounding 'border' faults (Fig. 14b and d). This reflects that border faults are thought to accommodate 50–90 per cent of extension in low strain magma-poor continental rifts such as in Malawi (Agostini *et al.* 2011; Accardo *et al.* 2018; Muirhead *et al.* 2019; Shillington *et al.* 2020; Wright *et al.* 2020; Wedmore *et al.* 2020a) and so these faults are assigned relatively high slip rates (0.5–2 mm yr^{-1}) in the MSSM. These maps indicate hazard levels are highest in regions surrounding the northern end of Lake Malawi, where rift extension rates are relatively high (Wedmore *et al.* 2021) and intrarift faults also accommodate local hanging-wall flexural extension (Shillington *et al.* 2020; Williams *et al.* 2022b).

As observed in the site-specific PSHA, G–R recurrence models imply higher hazard levels than the Direct MSSM or characteristic approach at high PoE (Fig. 15d and e). The effect on hazard levels for different source down-dip extents are smaller (<0.1 g for 10 per cent PoE in 50 yr hazard levels) and localized to regions with relatively short (<50 km) MSSM sources such as around Karonga and Malawi's southern tip (Fig. 15f). The uncertainty in the MSSM sources MFD mean that the seismic hazard of regions close to faults have a higher CoV and interquartile range than regions where

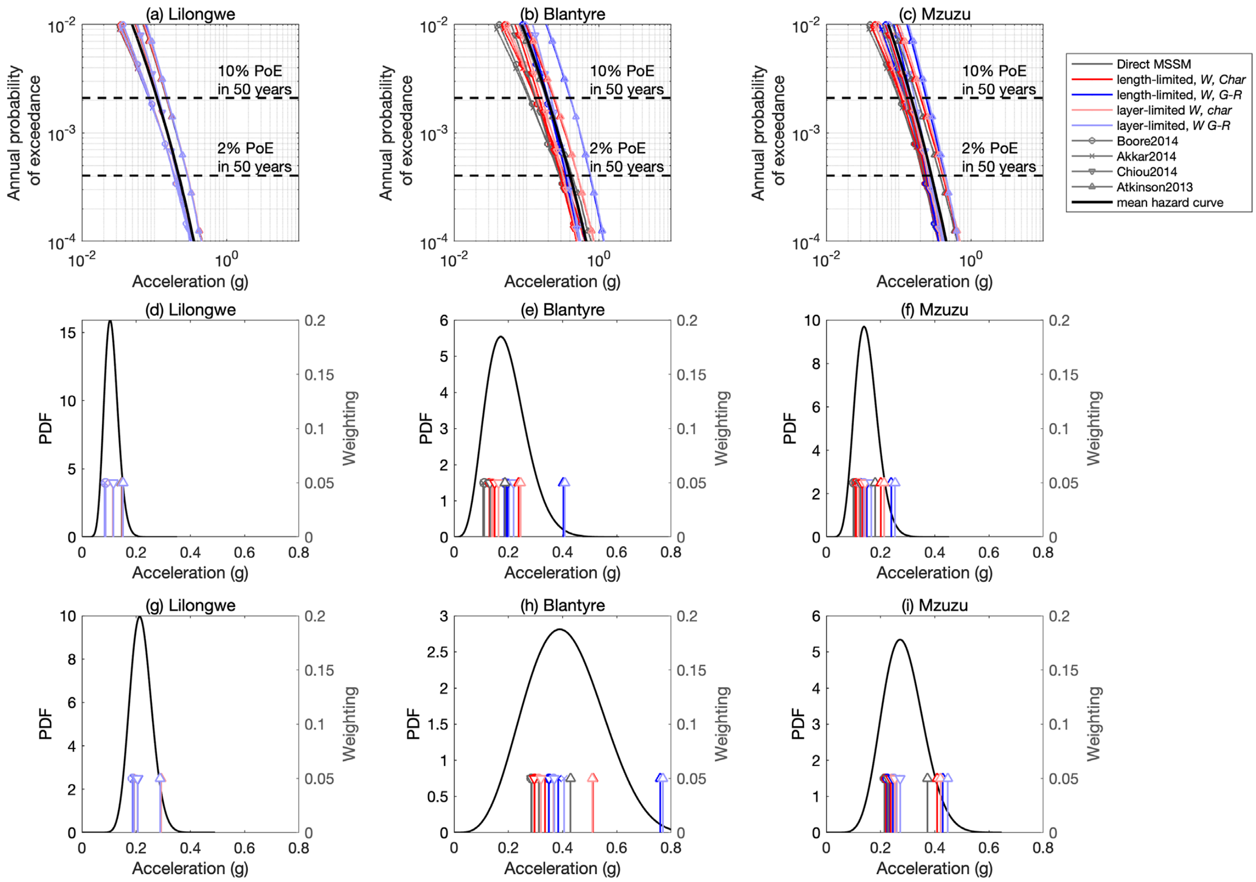

Figure 11. (a)–(c) Seismic hazard curves for each assessed site and all event catalog–GMM combinations. The mean hazard curve generated from these different catalog–GMM combinations is also shown. Horizontal lines show the annual probabilities that are equivalent to 2 per cent and 10 per cent PoE in 50 yr and the hazard levels at these rates for all 20 event catalog–GMM combinations are shown in (d)–(e) and (f)–(h), respectively. In addition, we show the mean value and Beta distribution fitted to these values. Line colors represent different event catalogs and symbols represent different GMMs. Analysis is for PGA and a V_{S30} condition of 760 m s^{-1}. An equivalent plot for 3 s spectral acceleration is shown in Fig. A10. Empirical cumulative distribution function (CFD) for these ground motion values and the Beta distribution CDF, are shown in Fig. A9.

the hazard is dominated by just the single areal source model we consider. By comparison, multiple areal and smoothed seismicity sources are considered in the Italian seismic hazard model and this means that regions far from faults have the highest CoV in hazard levels (Meletti *et al.* 2021). Regions peripheral to Malawi also have relatively high CoV (Fig. 15c), but this likely reflects their very low seismicity rate (Fig. 6) and not the underlying uncertainty in our analysis.

To quantify how the MSSM-Areal Combined map compares to seismic hazard maps previously developed for Malawi by Poggi *et al.* (2017) and Hodge *et al.* (2015), we find the closest sites within each map's respective grids and then subtract these hazard estimates from the MSSM-Areal Combined estimate using the reference V_{S30} value (760 m s^{-1}). This is the same V_{S30} condition used by Hodge *et al.* (2015), whereas Poggi *et al.* (2017) considered a slightly lower V_{S30} estimate (600 m s^{-1}). Poggi *et al.* (2017) also truncated the GMM sampling at ± 3 standard deviations (ϵ) whilst our sampling was unbounded (Section 5.1). Nevertheless, this different GMM sampling approach is unlikely to influence the hazard map comparisons, given that analysis of the disaggregation plots (Fig. 13) indicates that only ∼1–2 per cent of the probability mass were simulated when ϵ >3 (Fig. 13). We compare our hazard map to Hodge *et al.* (2015) for a 500 yr return period (equivalent to ∼9 per cent PoE in 50 yr), which was the minimum return period considered in their study.

For sites <40 km from the MSSM sources, our seismic hazard estimates for 10 per cent PoE in 50 yr level are up to 0.3 g higher than in the map from Poggi *et al.* (2017), with increases highest around the relatively high slip-rate border faults. The median difference between the Poggi *et al.* (2017) and MSSM-Areal combined maps is, however, only 0.01 g (Fig. A12a). This reflects that most sites in Malawi are sufficiently far from active faults (> 40 km), for areal sources to be the main contributor to hazard at high PoE. Indeed, at these sites > 40 km from active faults, near-identical hazard levels are expected because we incorporate off-fault seismicity using the areal sources developed by Poggi *et al.* (2017).

The MSSM-Areal Combined map indicates higher hazard levels than in Hodge *et al.* (2015), particularly at sites where new fault sources have been included (increases of 0.2–0.3 g; Fig. 16d–f). Locally, the MSSM-Areal combined map indicates lower hazard levels around the Bandawe and Mbamba faults (Fig. 16d). These faults were included as sources by Hodge *et al.* (2015) but not in the MSSM, as new seismic reflection data indicates that these are inactive faults (McCartney & Scholz 2016; Accardo *et al.* 2018; Scholz *et al.* 2020). Differences in GMM selection and fault and areal source modelling may have also affected comparisons between these two maps and we discuss this further in Section 7.1.

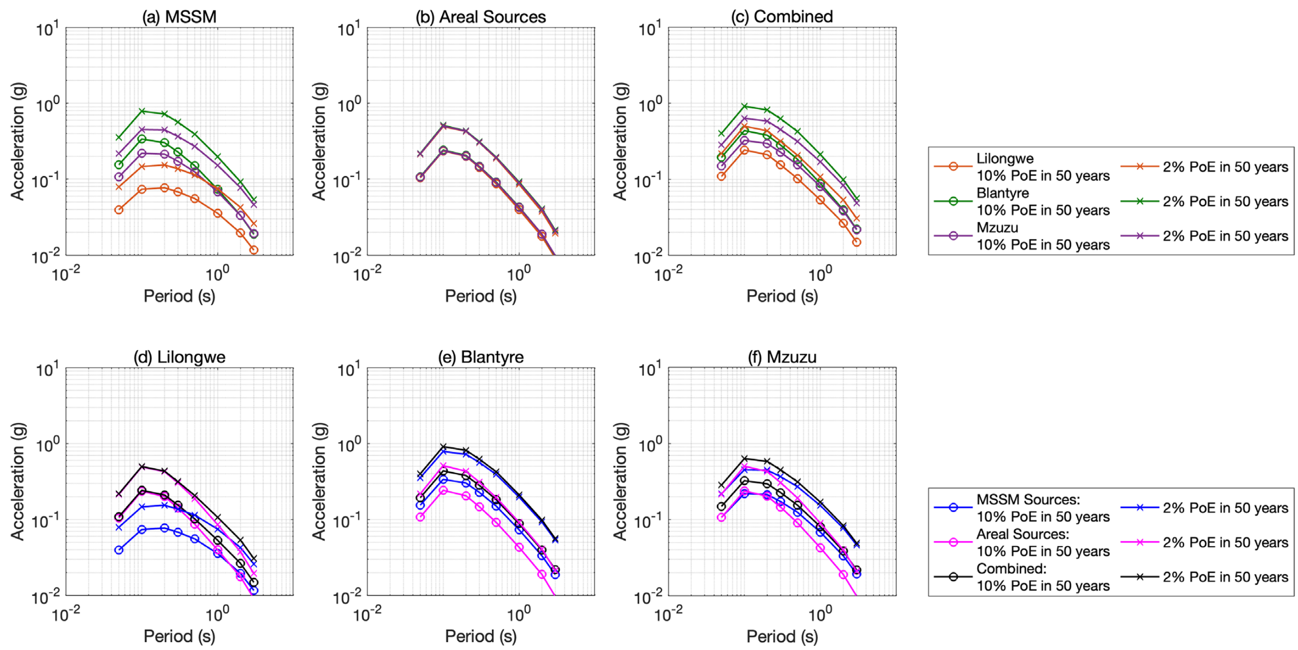

Figure 12. Uniform hazard spectra for selected sites in Malawi for 2 per cent and 10 per cent PoE in 50 yr, respectively and $V_{S30} = 760$ m s^{-1}. (a)–(c) Hazard spectra sorted by source type. (d)–(f) Hazard spectra sorted by site.

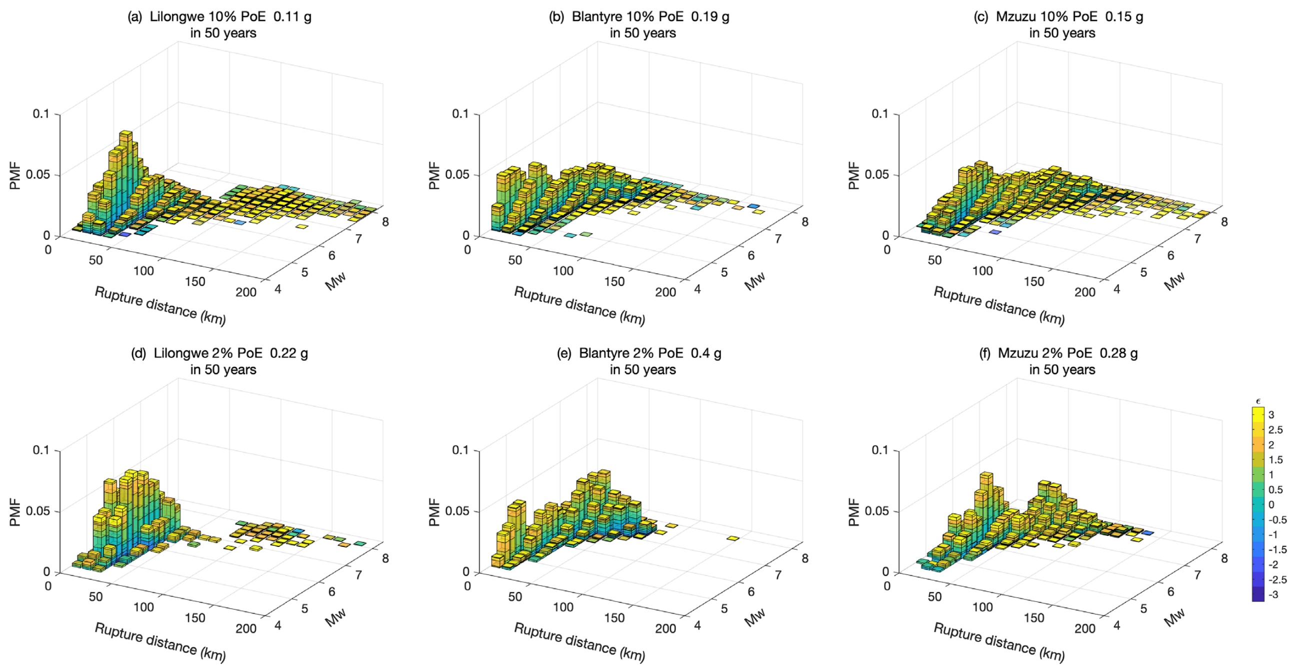

Figure 13. Seismic disaggregation plots for PGA for Lilongwe, Blantyre and Mzuzu and (a)–(c) 10 per cent and 2 per cent (d)–(f) PoE in 50 yr and $V_{S30} = 760$ m s^{-1}. ϵ; indicates the relative contribution to hazard from each standard deviation about the mean during ground motion modelling.

7 DISCUSSION

7.1 Implications for seismic hazard and risk in Malawi

The higher moment rate ($\dot{M}_0$) implied by the MSSM-based catalogs leads to elevated seismic hazard estimates in Malawi compared to previous instrumental-seismicity based PSHA (Fig. 16; Poggi *et al.* 2017). However, this increase is mainly observed for sites within 40 km of a MSSM source (Fig. 16a–c). This result demonstrates the importance of fault-based sources for understanding both the magnitude and spatial distribution of seismic hazard in Malawi.

Compared to the first generation of fault-based PSHA in Malawi (Hodge *et al.* 2015), the MSSM-Areal combined map indicates higher seismic hazard levels in the EAR valley (Fig. 16d–f). This reflects the incorporation of new fault sources in the MSSM (107 vs 7) and in particular intrarift faults, which have been highlighted as overlooked sources of seismic hazard in Malawi (Biggs *et al.* 2010; Shillington *et al.* 2020; Wedmore *et al.* 2020a). However, the Livingstone Fault is broadly coincident between the two maps and even though its slip rate estimate is lower in the MSSM (2.0 vs

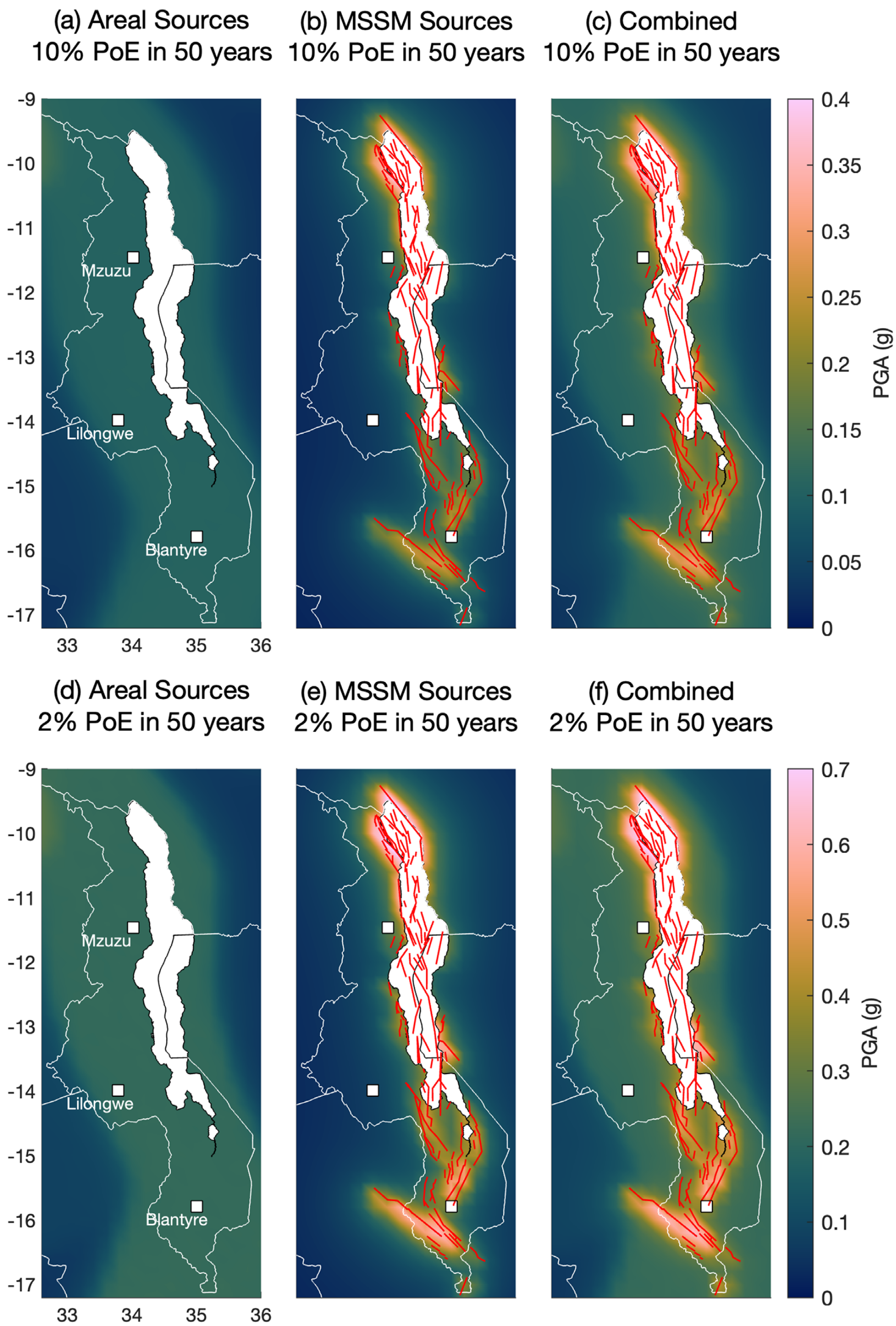

Figure 14. PGA seismic hazard maps for Malawi for (a)–(c) 10 per cent PoE in 50 yr and (d)–(f) 2 per cent PoE in 50 yr for reference V_{S30} value (760 m s^{-1}). Figure is arranged so each column represents a different catalog. Red lines depict the MSSM sources (Williams *et al.* 2022b). For equivalent maps for the slope-based USGS V_{S30} values (Wald & Allen 2007), see Fig. A11.

3.8 mm yr^{-1}), the MSSM-Areal combined map implies higher seismic hazard adjacent to it (Fig. 16d–f). This reflects a combination of: (1) our exploration of G–R on-fault MFD, which leads to higher hazard levels than the characteristic-only on-fault MFD considered by Hodge *et al.* (2015), (2) addition of nearby intrarift fault sources, (3) inclusion of a stable crust GMM and our increased estimates for (4) the base of the seismogenic layer (35 vs 30 km) and (5) the maximum background event magnitude (M_W 7 vs M_W 6.25–6.75).

For global context, with a 10 per cent PoE ∼ 0.2–0.4 g (PGA) in 50 yr close to MSSM sources and 10 per cent PoE ∼ 0.10–15 g PGA 50 yr in regions peripheral to these sources (Fig. 14), the seismic hazard in Malawi can be considered comparable to other regions with low slip rate normal faults, such as Italy (Meletti *et al.* 2021) and the Basin and Range Province in the USA (Petersen *et al.* 2015). Regional extension rates in Malawi are slightly lower than in these regions (0.5–1.5 mm yr^{-1} vs ∼3 mm yr^{-1}; D'Agostino *et al.* 2011; Hammond *et al.* 2014). However, this may be compensated for by Malawi's relatively thick seismogenic layer, which allows normal faults to reach larger lengths and widths (100–150-km long, 40-km wide) than in Italy (<60-km long, 15–20-km wide; Basili *et al.* 2008; Valentini *et al.* 2017) and although the Basin and Range Province's Wasatch Fault is 370-km long, its seismogenic width is

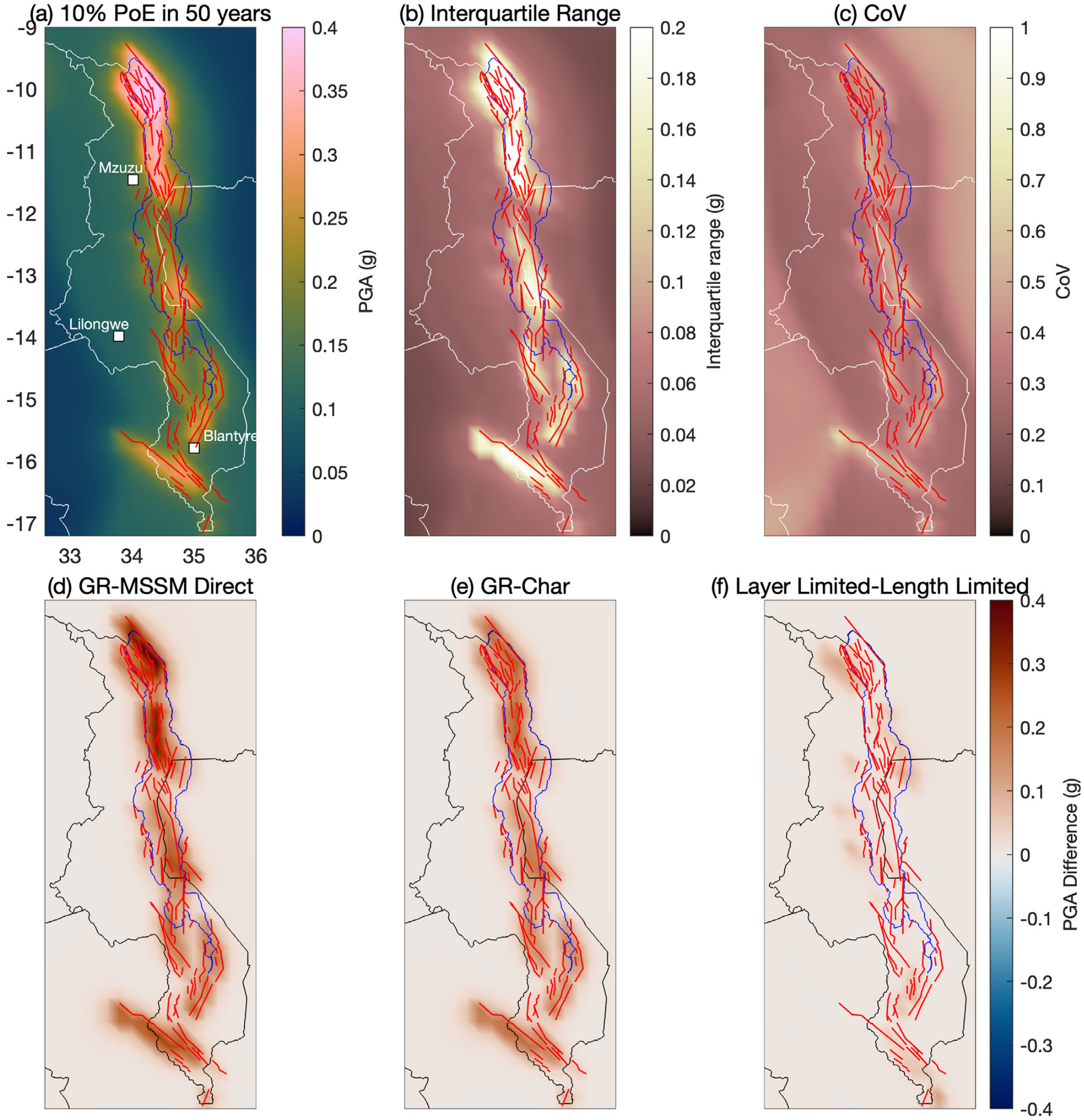

Figure 15. Sensitivity analysis for seismic hazard maps. (a) Combined 10 per cent PoE in 50 yr seismic hazard map as shown in Fig. 14(c), but with adjusted color axis. (b) Interquartile range and (c) Coefficient of Variation (CoV) of the 20 seismic hazard values calculated from each event catalog–GMM combination. (d)–(f) Maps showing how source modelling affects hazard uncertainty. (d) Difference in seismic hazard values for a G–R and MSSM Direct on-fault MFD, for the length-limited case. (e) Same as (d) but comparison is between a G–R and characteristic MFD. (f) Difference in seismic hazard values for layer- and length-limited source down dip extents for a G–R on-fault MFD. All maps are for 10 per cent PoE in 50 yr hazard level, PGA and the generic V_{S30} value (760 m s^{-1}). Comparison in (d)–(f) are for maps generated with the Boore *et al.* (2014) GMM. The area shown under Lake Malawi (blue outline) is included for the purpose of comparing hazard maps only.

assumed to be 20 km (Valentini *et al.* 2020) and paleoseismic data suggest most ruptures are 20–100-km long (DuRoss *et al.* 2016). In turn, Malawi's wider faults will have a disproportionately high $\dot{M}_0$ and can host larger magnitude earthquakes (Jackson & Blenkinsop 1997; Hodge *et al.* 2020).

To fully explore and quantify the implications of this study for seismic risk in Malawi, results should be combined with seismic vulnerability and exposure assessments (Goda *et al.* 2016, 2022; Ngoma *et al.* 2019; Kloukinas *et al.* 2020; Giordano *et al.* 2021; Novelli *et al.* 2021). Nevertheless, some implications of this PSHA to seismic risk are apparent. For example, given the low quality and high turnover of building stock in Malawi (Giordano *et al.* 2021), the results that are of most practical importance are for high PoE and in these instances the MSSM sources affect hazard levels only at long vibration periods and/or sites close (<40 km) to active faults (Fig. 12). Hence, off-fault areal sources are still important contributors to seismic risk in Malawi and future work should consider improving its seismic network so that future PSHA can use a more finely resolved off-fault source model.

Instances where the hazard estimates at low PoE are of importance in Malawi include hydro-electric dams in the Shire River valley in southern Malawi, which generates 80 per cent of Malawi's electricity (Taulo *et al.* 2015). The development of geothermal resources in Malawi, whose locations are inherently controlled by active faults (Dulanya *et al.* 2010; Gondwe 2015; Dávalos-Elizondo *et al.* 2021), should also consider local seismic hazard. PSHA only considers ground motions and other secondary seismic hazards in Malawi, such as liquefaction, fault displacement, landslides and seiches (Williams *et al.* 2022c), are not considered here.

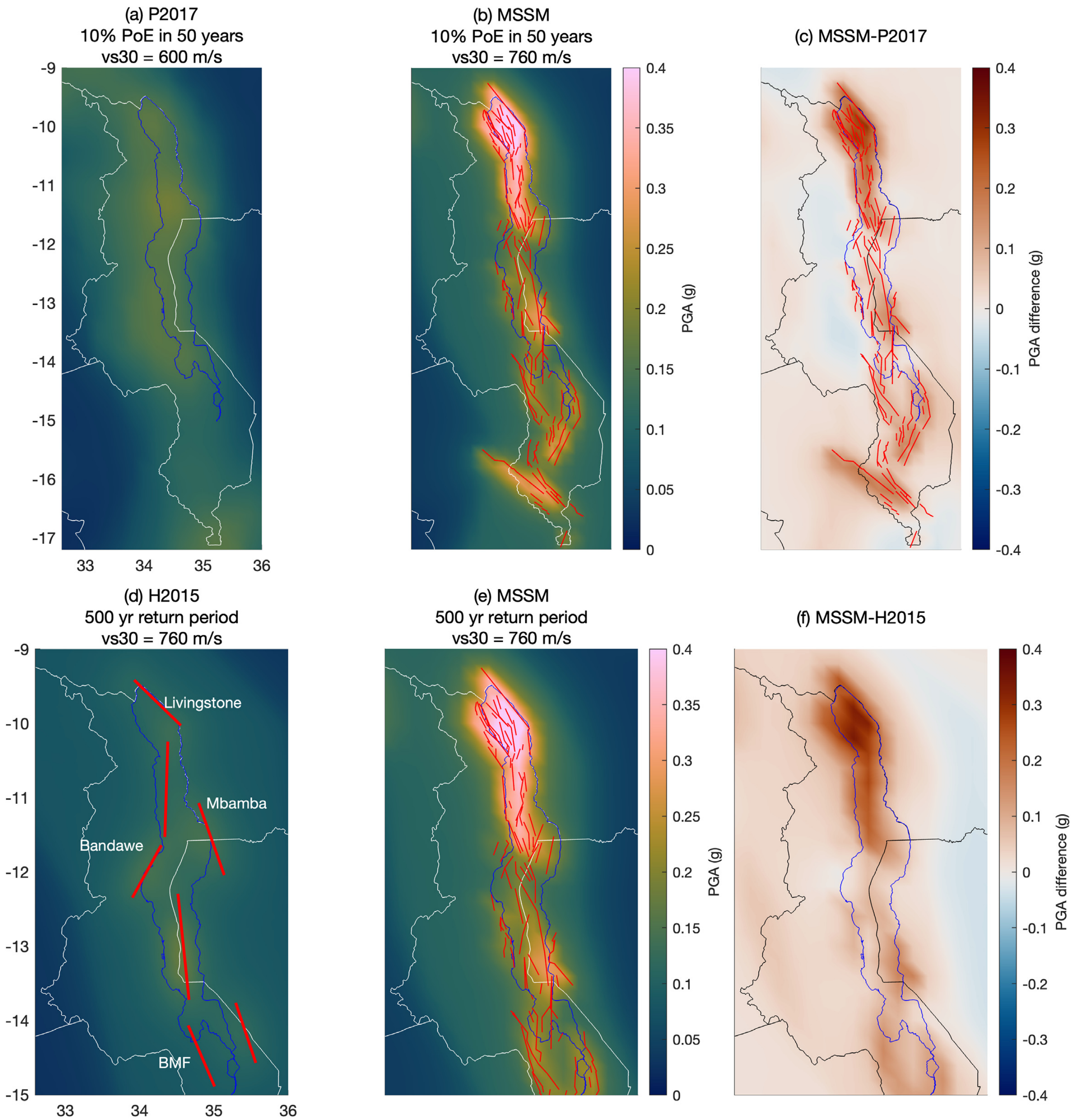

Figure 16. (a)–(c) Comparison of PGA seismic hazard maps previously generated for Malawi by Poggi *et al.* (2017) and in this study for 10 per cent PoE in 50 yr respectively. (d)–(f) Equivalent to (a)–(c), but comparisons of our map with the mixed rupture catalog (MRC) 2 per cent PoE in 50 yr seismic hazard map for Malawi from Hodge *et al.* (2015). The MRC catalog represents an equal combination of segmented and continuous ruptures along fault sources, except for the Livingstone and Bilila-Mtakataka faults, which host continuous ruptures only. Red lines in (d) indicate fault sources used in Hodge *et al.* (2015). This map is truncated at 15°S, as fault sources south of Lake Malawi were not considered by Hodge *et al.* (2015). As in Fig. 15, the area covered by Lake Malawi is shown to aid hazard map comparisons only.

7.2 Using fault-based sources for PSHA in Malawi and other regions with low strain rates and a thick seismogenic layer

Fault-based MSSM sources are incorporated into our PSHA of Malawi using stochastic event catalogs. Cumulatively, these catalogs explore five realisations of the MSSM (Fig. 2) with different on-fault MFD and down-dip extension of fault sources through Malawi's seismogenic layer (i.e. 'length' or 'layer' limited faults). We consider alternative down-dip extents as it is not clear how sources should be extrapolated through Malawi's ∼35-km thick seismogenic layer (see Section 4.2). The influence of this uncertainty is only significant in regions in Malawi with relatively short (<50 km) sources (Fig. 15f). Longer sources, which also tend to have the highest slip rates, are not sensitive to this uncertainty as they are expected to extend throughout the seismogenic layer (Fig. A7).

Three on-fault MFD are considered for MSSM sources during the PSHA: G–R, characteristic, or the 'Direct-MSSM' approach where sources may rupture in geometrically defined sections, faults, or multifault ruptures (Fig. 4). We find that for a 10 per cent PoE in 50 yr level, a G–R MFD implies higher hazard levels (Figs 11 and 15). This result can be understood in terms of the relatively frequent moderate magnitude seismicity (M_W 4.5–6.8; Fig. 7) that is inherent to G–R MFD and which in a low strain rate region is considerably more likely within a 50–500 yr time-frame than large magnitude characteristic events (Valentini *et al.* 2017; Goda & Sharipov 2021). Although the differences in hazard levels between G–R, characteristic and Direct MSSM MFD are reduced at lower PoE, they can still be significant for sites that are close to many long (<40 km) low slip rate (0.05–1 mm yr^{-1}) faults (e.g. Blantyre, Fig. 11).

In future, the on-fault MFD could be constrained by inversion-based source models (e.g. Field *et al.* 2021); however, there are currently considerable challenges to defining a regional MFD target for Malawi when developing these models (Section 4.6.2). In the meantime, we consider it prudent that multiple on-fault MFD cases should be explored during PSHA of regions like Malawi, with low strain rates and instrumental and historical records much shorter than the earthquake recurrence intervals of individual faults. Although a smaller source of uncertainty, our results also imply that alternative cases could be considered for source down-dip extrapolation in regions with an abnormally thick seismogenic layer (>20 km) and short (<50 km) faults.

The stochastic event catalogs used in this PSHA are simulated on the assumption that earthquakes in Malawi: (1) follow the Leonard (2010) scaling relations,(2) ruptures do not propagate below the presumed base of the seismogenic layer at 35 km and (3) earthquake inter-event times can be described by a time-independent Poisson process (Section 4.4). With so few well-instrumented $M_W>7$ continental normal fault earthquakes it is difficult to critically examine the first two assumptions (see also; Williams *et al.* 2022b). For the latter point, the 2009 Karonga earthquake sequence imply that fault interaction through static stress changes can lead to clustered non-Poisson seismicity in Malawi (Biggs *et al.* 2010; Fagereng 2013; Gaherty *et al.* 2019); indeed this is a widespread observation in low strain rate regions (e.g. Beanland & Berryman 1989; Wedmore *et al.* 2017; Griffin *et al.* 2020; Stevens & Avouac 2021; Iturrieta *et al.* 2022). In these cases, earthquake interevent times are more appropriately modelled using two-parameter time-dependent distributions such as Weibull or Brownian Passage Time (Matthews *et al.* 2002; Zöller & Hainzl 2007; Cowie *et al.* 2012). Seismic hazard assessment in Malawi should also recognize that previous large magnitude ($M_W>7$) earthquakes in the EAR were followed by long and damaging aftershock sequences (Ambraseys 1991; Ambraseys & Adams 1991; Gaulon *et al.* 1992; Lloyd *et al.* 2019). Future seismic hazard assessment in Malawi should consider these challenges when the appropriate paleoseismic and seismic records become available.

7.3 Application of GMM in Malawi

An ongoing challenge with PSHA in Malawi and elsewhere in the EAR, is the lack of geotechnical (i.e. V_{S30} measurements) and strong motion data (Midzi *et al.* 1999; Hodge *et al.* 2015; Poggi *et al.* 2017). This raises uncertainties when applying slope-based proxies for V_{S30} (Figs A6 and A11) and means our use of global GMMs implicitly assumes that the ground motion behaviour in Malawi will be similar to other regions (i.e. the 'ergodic assumption'; Anderson & Brune 1999). This could be addressed in the future by considering whether regional weak ground motion data in Malawi can be used to adjust GMMs (Yenier & Atkinson 2015). An additional problem is that EAR seismicity is characterised by deep moderate-large magnitude ($M_W>6$) normal fault earthquakes and it is difficult to calibrate GMMs for these events as so few of them have been recorded (Akkar *et al.* 2014; Boore *et al.* 2014).

The incorporation of a stable crust GMM into PSHA in Malawi raises further challenges. In particular, the near-field (<10 km) motions associated with events in stable crust are poorly understood. This could be addressed though incorporation of the Next Generation Attenuation East (NGA-East) GMM (Goulet *et al.* 2018) in East Africa and this would also allow R_{rup} to be considered in a stable crust GMMs. However, the NGA-East was developed for a reference V_{S30} condition of 3000 m s^{-1} and challenges remain in adapting the site amplification factors for lower V_{S30} values (Kolaj *et al.* 2019) that are likely in Malawi (200–800 m s^{-1}, Fig. A6).

7.4 Implications for seismic hazard elsewhere in the EAR

Our comparisons of PSHA maps for Malawi (Fig. 16a–c) highlight the limitations of using short historical and instrumental catalogs to assess seismic hazard in regions with low strain rates (Section 4.6.2). These challenges apply elsewhere in the EAR, where despite abundant evidence for late Quaternary faulting (e.g. Vittori *et al.* 1997; Lærdal & Talbot 2002; Wanke 2005; Kervyn *et al.* 2006; Zielke & Strecker 2009; Fontijn *et al.* 2010; Nicholas *et al.* 2016; Delvaux *et al.* 2012, 2017; Muirhead *et al.* 2016; Daly *et al.* 2020; Wedmore *et al.* 2022), no fault-based PSHA has been attempted outside Malawi. This partly reflects the lack of chronostratigraphic data needed to estimate fault slip rates in the EAR; however, this can be addressed to an extent by incorporating regional geodetic data using the MSSM systems-based approach (Williams *et al.* 2021a). Given the increasing levels of seismic risk (Goda *et al.* 2016; Meghraoui *et al.* 2016; Poggi *et al.* 2017; World-Bank 2019), we suggest there is a clear need to develop new fault-based PSHA maps elsewhere in the EAR.

8 CONCLUSIONS

We use the MSSM to develop a new fault-based PSHA in Malawi. We find that for sites close (<40 km) to these fault-based sources, seismic levels are higher than indicated by previous instrumental-based PSHA (Poggi *et al.* 2017). This replicates the findings of the first generation of fault-based PSHA in Malawi (Hodge *et al.* 2015). However, the incorporation of more fault sources in the MSSM (107 vs 7), source modelling and GMM selection, leads to a more complex seismic hazard pattern than Hodge *et al.* (2015). These results should motivate the development of more fault-based PSHA elsewhere in the EAR, as previous seismic hazard assessment has used the instrumental record of seismicity alone and in some situations, this may underestimate hazard levels.

The stochastic event catalogs we use to incorporate the MSSM into PSHA explore alternative hypotheses for on-fault MFD and the down-dip extension of fault-based sources through Malawi's 35-km thick seismogenic layer. We find that seismic hazard levels are only sensitive to the down-dip extension of relatively short sources (differences of ~0.1 g for 10 per cent PoE in 50 yr for regions with <50-km long sources), whilst the assumed MFD can influence the hazard estimates for all sources. In particular, we find that compared to a characteristic MFD or 'direct' implementation of the MSSM, a G–R MFD increases seismic hazard levels by up to 0.2 g for sites close to low slip rate sources (<1 mm yr^{-1}) and high PoE (10 per cent PoE in 50 yr).

Our new PSHA is also useful for highlighting sources of uncertainty that present key targets for future research in Malawi. In particular, (1) the uncertainty in fault slip rates, (2) the applicability of a Poisson model for earthquake recurrence, (3) refining off-fault sources and (4) the lack of local fault scaling and strong ground motion data to assess the applicability of global empirical scaling relations in Malawi. Nevertheless, we suggest our incorporation of a rich active fault and geodetic data set makes this the most robust assessment of seismic hazard currently available for Malawi and presents a framework for assessing seismic hazard in other low strain rate regions.

AUTHORS' CONTRIBUTIONS

Conceptualization: All authors. Methodology: All authors. Software: JW, KG and RD. Investigation: All authors. Writing – original draft preparation: JW. Writing – reviewing and editing: All authors. Data Curation: JW and LW. Funding acquisition: JB, AF, KG and MW.

ACKNOWLEDGMENTS

This study is funded by the EPSRC-Global Challenges Research Fund PREPARE (EP/P028233/1) and SAFER-PREPARED (part of the 'Innovative data services for aquaculture, seismic resilience and drought adaptation in East Africa' grant; EP/T015462/1) projects. Seismic hazard calculations were performed using the computational facilities of the Advanced Computing Research Centre, University of Bristol - http://www.bris.ac.uk/acrc/. Color maps in Figs 5, 14, 15, 16, A5 and A11 were produced following Crameri *et al.* (2020). We thank Vitor Silva (Global Earthquake Model Foundation) for providing the seismic hazard values from Poggi *et al.* (2017). This study benefited from constructive and detailed comments from Bruno Pace, Francesco Visini and an anonymous reviewer.

DATA AVAILABILITY

The Malawi Seismogenic Source Model v1.2 (MSSM; Williams *et al.* 2022a, b) can be accessed through Github at https://github.com/LukeWedmore/malawi_seismogenic_source_model/tree/v1.2 and through Zenodo at: https://doi.org/10.5281/zenodo.5599616. The Malawi Active Fault Database (MAFD; Williams *et al.* 2021b, 2022c) can be accessed at https://github.com/LukeWedmore/malawi_active_fault_database/tree/v1.0 and https://doi.org/10.5281/zenodo.5507189. The USGS V_{S30} database for Malawi is available from https://earthquake.usgs.gov/data/vs30/

MATLAB codes for the generation of the MSSM sources and the probabilistic seismic hazard analysis that is described in this study are available at: https://github.com/jack-williams1/Malawi_PSHA and version 1.0 is archived at https://doi.org/10.5281/zenodo.7265780.

REFERENCES

Accardo, N.J. *et al.*, 2018. Constraints on Rift Basin Structure and Border Fault Growth in the Northern Malawi Rift From 3-D Seismic Refraction Imaging, *J. Geophys. Res. Solid Earth,* **123**(11), 10,003–10,1025.

Accardo, N.J. *et al.*, 2020. Thermochemical Modification of the Upper Mantle Beneath the Northern Malawi Rift Constrained From Shear Velocity Imaging, *Geochem. Geophys. Geosyst.,* **21**(6), 1–19.

Agostini, A., Bonini, M., Corti, G., Sani, F. & Mazzarini, F., 2011. Fault architecture in the Main Ethiopian Rift and comparison with experimental models: Implications for rift evolution and Nubia-Somalia kinematics, *Earth Planet. Sci. Lett.,* **301**(3–4), 479–492.

Aki, K., 1965. Maximum likelihood estimate of b in the formula logN= a-bM and its confidence limits, *Bull. Earthquake Res. Inst. Univ. Tokyo,* **43,** 237–239.

Akkar, S., Sandıkkaya, M.A. & Bommer, J.J., 2014. Empirical ground-motion models for point- and extended-source crustal earthquake scenarios in Europe and the Middle East, *Bull. Earthq. Eng.,* **12**(1), 359–387.

Ambraseys, N.N., 1991. The Rukuwa Earthquake of 13 December 1910 In East-Africa, *Terra Nova,* **3**(2), 202–211.

Ambraseys, N.N. & Adams, R.D., 1991. Reappraisal of major African earthquakes, south of 20°N, 1900-1930, *Natural Hazards,* **4,** 389–419.

Anderson, J.G. & Brune, J.N., 1999. Probabilistic seismic hazard analysis without the ergodic assumption, *Seismol. Res. Lett.,* **70**(1), 19–28.

Atkinson, G.M. & Adams, J., 2013. Ground motion prediction equations for application to the 2015 Canadian national seismic hazard maps, *Can. J. Civil Eng.,* **40**(10), 988–998.

Atkinson, G.M. & Goda, K., 2013. Probabilistic seismic hazard analysis of civil infrastructure, In *Woodhead Publishing Series in Civil and Structural Engineering, Handbook of Seismic Risk analysis and Management of Civil Infrastructure Systems,* Woodhead Publishing, 3–28, Available at https://www.sciencedirect.com/science/article/pii/B9780857092687500013.

Ayele, A. & Kulhanek, O., 2000. *Reassessment of Source Parameters for Three Major Earthquakes in the East African Rift System from Historical Seismograms and Bulletins, Ann. Geofis.,* **43**(1), 81–94.

Basili, R., Valensise, G., Vannoli, P., Burrato, P., Fracassi, U., Mariano, S., Tiberti, M.M. & Boschi, E., 2008. The Database of Individual Seismogenic Sources (DISS), version 3: Summarizing 20 yr of research on Italy's earthquake geology, *Tectonophysics,* **453**(1–4), 20–43.

Beanland, S. & Berryman, K.R., 1989. Style and episodicity of late Quaternary activity on the Pisa-Grandview fault zone, Central Otago, New Zealand, *New Zealand J. Geol. Geophys.,* **32**(4), 451–461.

Ben-Zion, Y., 2008. Collective behavior of earthquakes and faults: Continuum-discrete transitions, progressive evolutionary changes and different dynamic regimes, *Rev. Geophys.,* **46**(4), RG4006, doi:10.1029/2008RG000260.

Biggs, J., Nissen, E., Craig, T., Jackson, J. & Robinson, D.P., 2010. Breaking up the hanging wall of a rift-border fault: The 2009 Karonga earthquakes, Malawi, *Geophys. Res. Lett.,* **37**(11), doi:10.1029/2010GL043179.

Billings, S.E. & Kattenhorn, S.A., 2005. The great thickness debate: Ice shell thickness models for Europa and comparisons with estimates based on flexure at ridges, *Icarus,* **177**(2), 397–412.

Bird, P. & Kreemer, C., 2015. Revised tectonic forecast of global shallow seismicity based on version 2.1 of the global strain rate map, *Bull. seism. Soc. Am.,* **105**(1), 152–166.

Bird, P. & Liu, Z., 2007. Seismic hazard inferred from tectonics: California, *Seismol. Res. Letters,* **78**(1), 37–48.

Boore, D.M., 2016. Determining generic velocity and density models for crustal amplification calculations, with an update of the Boore and Joyner (1997) generic site amplification for Vs(Z) = m/s, *Bull. seism. Soc. Am.,* **106**(1), 316–320.

Boore, D.M., Stewart, J.P., Seyhan, E. & Atkinson, G.M., 2014. NGA-West2 equations for predicting PGA, PGV and 5 shallow crustal earthquakes, *Earthquake Spectra,* **30**(3), 1057–1085.

Bwambale, B., Bagampadde, U., Gidudu, A. & Martini, F., 2016. Seismic Hazard Analysis for the Albertine Region, Uganda – A Probabilistic Approach, *South African J. Geology,* **118**(4), 411–424.

Carpenter, M. *et al.*, 2022. Comparing intrarift and border fault structure in the Malawi Rift: Implications for normal fault growth, *J. Struct. Geol.,* **165,** 104761, doi:10.1016/j.jsg.2022.104761.

Cassani, M., Pastore, M., Benedetto, F., Mpampatsikos, V., Librizzi, F., Vallone, P. & Fabbri, B., 2016. *Safer House Construction Guidelines,*

Tech. rep, Cecilia, Available at https://sheltercluster.org/malawi/documents/safer-housing-construction-guidelines.
Chapola, L.S. & Kaphwiyo, C.E., 1992. The Malawi rift: Geology, tectonics and seismicity, *Tectonophysics,* **209**(1–4), 159–164.
Chartier, T., Scotti, O. & Lyon-Caen, H., 2019. Sherifs: Open-source code for computing earthquake rates in fault systems and constructing hazard models, *Seismol. Res. Lett.,* **90**(4), 1678–1688.
Chiou, B. S.J. & Youngs, R.R., 2014. Update of the Chiou and Youngs NGA model for the average horizontal component of peak ground motion and response spectra, *Earthquake Spectra,* **30**(3), 1117–1153.
Chisenga, C., Dulanya, Z. & Jianguo, Y., 2019. The structural re-interpretation of the Lower Shire Basin in the Southern Malawi rift using gravity data, *J. African Earth Sci.,* **149**(September), 280–290.
Clark, D., McPherson, A. & Van Dissen, R., 2012. *Long-term Behaviour of Australian Stable Continental Region (SCR) Faults, Tectonophysics,* **566,** 1–30.
Convertito, V., Emolo, A. & Zollo, A., 2006. Seismic-hazard assessment for a characteristic earthquake scenario: An integrated probabilistic-deterministic method, *Bull. seism. Soc. Am.,* **96**(2), 377–391.
Copley, A., Hollingsworth, J. & Bergman, E., 2012. Constraints on fault and lithosphere rheology from the coseismic slip and postseismic afterslip of the 2006 Mw7.0 Mozambique earthquake, *J. Geophys. Res.: Solid Earth,* **117**(3), doi:10.1029/2011JB008580.
Cosentino, P., Ficarra, V. & Luzio, D., 1977. Truncated exponential frequency-magnitude relationship in earthquakes statistics, *Bull. seism. Soc. Am.,* **67**(6), 1615–1623.
Cowie, P.A., Roberts, G.P., Bull, J.M. & Visini, F., 2012. Relationships between fault geometry, slip rate variability and earthquake recurrence in extensional settings, *Geophys. J. Int.,* **189**(1), 143–160.
Cox, S.C., Stirling, M.W., Herman, F., Gerstenberger, M. & Ristau, J., 2012. Potentially active faults in the rapidly eroding landscape adjacent to the Alpine Fault, central Southern Alps, New Zealand, *Tectonics,* **31**(2), doi:10.1029/2011TC003038.
Craig, T.J. & Jackson, J.A., 2021. Variations in the Seismogenic Thickness of East Africa, *J. Geophys. Res.: Solid Earth,* **126**(3), 1–15.
Crameri, F., Shephard, G.E. & Heron, P.J., 2020. The misuse of colour in science communication, *Nature Commun.,* **11**(1), 1–10.
D'Agostino, N., Mantenuto, S., D'Anastasio, E., Giuliani, R., Mattone, M., Calcaterra, S., Gambino, P. & Bonci, L., 2011. Evidence for localized active extension in the central Apennines (Italy) from global positioning system observations, *Geology,* **39**(4), 291–294.
Daly, M.C., Green, P., Watts, A.B., Davies, O., Chibesakunda, F. & Walker, R., 2020. Tectonics and Landscape of the Central African Plateau and their Implications for a Propagating Southwestern Rift in Africa, *Geochem. Geophys. Geosyst.,* **21**(6), doi:10.1029/2019GC008746.
Dávalos-Elizondo, E., Atekwana, E.A., Atekwana, E.A., Tsokonombwe, G. & Laó-Dávila, D.A., 2021. Medium to low enthalpy geothermal reservoirs estimated from geothermometry and mixing models of hot springs along the Malawi Rift Zone, *Geothermics,* **89,** doi:10.1016/j.geothermics.2020.101963.
Delvaux, D. & Barth, A., 2010. African stress pattern from formal inversion of focal mechanism data, *Tectonophysics,* **482**(1–4), 105–128.
Delvaux, D., Kervyn, F., Macheyeki, A.S. & Temu, E.B., 2012. Geodynamic significance of the TRM segment in the East African Rift (W-Tanzania): Active tectonics and paleostress in the Ufipa plateau and Rukwa basin, *J. Struct. Geol.,* **37,** 161–180.
Delvaux, D., Mulumba, J.L., Sebagenzi, M. N.S., Bondo, S.F., Kervyn, F. & Havenith, H.B., 2017. Seismic hazard assessment of the Kivu rift segment based on a new seismotectonic zonation model (western branch, East African Rift system), *J. African Earth Sci.,* **134,** 831–855.
Déverchère, J., Petit, C., Gileva, N., Radziminovitch, N., Melnikova, V. & San'Kov, V., 2001. Depth distribution of earthquakes in the Baikal rift system and its implications for the rheology of the lithosphere, *Geophys. J. Int.,* **146**(3), 714–730.
Dixey, F., 1926. The Nyasaland section of the great rift valley, *Geogr. J.,* **68**(2), 117–137.
Dulanya, Z., 2017. *A Review of the Geomorphotectonic Evolution of the South Malawi Rift, Journal of African Earth Sciences,* **129,** 728–738, doi:10.1016/j.jafrearsci.2017.02.016.
Dulanya, Z., Morales-Simfors, N. & Sivertun, Å., 2010. Comparative study of the silica and cation geothermometry of the Malawi hot springs: Potential alternative energy source, *J. African Earth Sci.,* **57**(4), 321–327.
Dulanya, Z., Gallen, S.F., Kolawole, F., Williams, J.N., Wedmore, L.N., Biggs, J. & Fagereng, Å., 2022. Knickpoint morphotectonics of the Middle Shire River basin: Implications for the evolution of rift interaction zones, *Basin Res.,* doi:10.1111/bre.12687.
DuRoss, C.B., Personius, S.F., Crone, A.J., Olig, S.S., Hylland, M.D., Lund, W.R. & Schwartz, D.P., 2016. Fault segmentation: New concepts from the Wasatch Fault Zone, Utah, USA, *J. Geophys. Res.: Solid Earth,* **121**(2), 1131–1157.
Ebinger, C.J., Rosendahl, B.R. & Reynolds, D.J., 1987. Tectonic model of the Malaŵi rift, Africa, *Tectonophysics,* **141**(1–3), 215–235.
Ebinger, C.J. *et al.*, 2019. Kinematics of Active Deformation in the Malawi Rift and Rungwe Volcanic Province, Africa, *Geochem. Geophys. Geosyst.,* **20**(8), 3928–3951.
Ellis, S. *et al.*, 2021. *New Zealand Fault-Rupture Depth Model v1.0: A Provisional Estimate of the Maximum Depth of Seismic Rupture on New Zealand's Active Faults, GNS Science report,* GNS Science: Lower Hutt (NZ), 47 p., doi:10.21420/4Q75-HZ73.
Fagereng, Å., 2013. Fault segmentation, deep rift earthquakes and crustal rheology: Insights from the 2009 Karonga sequence and seismicity in the Rukwa–Malawi rift zone, *Tectonophysics,* **601,** 216–225.
Fenton, C.H. & Bommer, J.J., 2006. The Mw7 Machaze, Mozambique, earthquake of 23 February 2006, *Seismol. Res. Lett.,* **77**(4), 426–439.
Fenton, C.H., Adams, J. & Halchuk, S., 2006. Seismic hazards assessment for radioactive waste disposal sites in regions of low seismic activity, *Geotechnical Geological Eng.,* **24**(3), 579–592.
Field, E.H. *et al.*, 2014. Uniform California Earthquake Rupture Forecast, version 3 (UCERF3) -The time-independent model, *Bull. seism. Soc. Am.,* **104**(3), 1122–1180.
Field, E.H., Milner, K.R. & Page, M.T., 2021. Generalizing the inversion-based PSHA source model for an interconnected fault system, *Bull. seism. Soc. Am.,* **111**(1), 371–390.
Flannery, J.W. & Rosendahl, B.R., 1990. The seismic stratigraphy of Lake Malawi, Africa: implications for interpreting geological processes in lacustrine rifts, *J. African Earth Sci.,* **10**(3), 519–548.
Fontijn, K., Delvaux, D., Ernst, G. G.J., Kervyn, M., Mbede, E. & Jacobs, P., 2010. Tectonic control over active volcanism at a range of scales: Case of the Rungwe Volcanic Province, SW Tanzania; and hazard implications, *J. African Earth Sci.,* **58**(5), 764–777.
Frankel, A.D. *et al.*, 2000. USGS national seismic hazard maps, *Earthquake Spectra,* **16**(1), 1–19.
Fullgraf, T. *et al.*, 2017. *Geological Mapping and Mineral Assessment Project (GEMMAP) of Malawi. Report Inception Phase - February 2017,* available at: https://www.brgm.eu/project/ geological-mapping-mineral-inventory-malawi (last access: 17 February 2023).
Gaherty, J.B. *et al.*, 2019. Faulting processes during early-stage rifting: Seismic and geodetic analysis of the 2009-2010 Northern Malawi earthquake sequence, *Geophys. J. Int.,* **217**(3), 1767–1782.
Gaulon, R., Chorowicz, J., Vidal, G., Romanowicz, B. & Rouit, G., 1992. Regional geodynamic implications of the May-July 1990 earthquake sequence in southern Sudan, *Tectonophysics,* **209**(1–4), 87–103.
Geist, E.L. & Parsons, T., 2018. Determining on-fault earthquake magnitude distributions from integer programming, *Comput. Geosci.,* **111**(November 2017), 244–259.
Gerstenberger, M. *et al.*, 2022. *The Seismicity Rate Model for the 2022 New Zealand National Seismic Hazard Model MC,* Tech. rep., GNS Science. GNS Science report; 2022/47, Lower Hutt (NZ).
Giordano, N. *et al.*, 2021. Seismic fragility models for typical non-engineered URM residential buildings in Malawi, in *Structures,* Vol. **32,** pp. 2266–2278, doi:10.1016/j.istruc.2021.03.118.
Goda, K. & Sharipov, A., 2021. Fault-source-based probabilistic seismic hazard and risk analysis for victoria, british columbia, canada: A case of the

leech river valley fault and devil's mountain fault system, *Sustainability,* **13**(3), 1–36.

Goda, K., Gibson, E.D., Smith, H.R., Biggs, J. & Hodge, M., 2016. Seismic risk assessment of urban and rural settlements around lake malawi, *Frontiers Built Environ.,* **2**(30), doi:10.3389/fbuil.2016.00030.

Goda, K. *et al.*, 2022. Scenario-based earthquake risk assessment for central-southern Malawi: The case of the Bilila-Mtakataka Fault, *Int. J. Disaster Risk Reduct.,* **67,** 102655, doi:10.1016/j.ijdrr.2021.102655.

Goitom, B. *et al.*, 2017. Probabilistic seismic-hazard assessment for Eritrea, *Bull. seism. Soc. Am.,* **107**(3), 1478–1494.

Gómez-Novell, O., García-Mayordomo, J., Ortuño, M., Masana, E. & Chartier, T., 2020. Fault System-Based Probabilistic Seismic Hazard Assessment of a Moderate Seismicity Region: The Eastern Betics Shear Zone (SE Spain), *Frontiers Earth Sci.,* **8**(December), doi:10.3389/feart.2020.579398.

Gondwe, K.T., 2015. *Geothermal Energy Utilization Model for Nkhotakota Geothermal Springs in Malawi, United Nations University Geothermal Training Programme,* **12,** 181–219.

Goulet, C.A., Bozorgnia, Y., Abrahamson, N., Kuehn, N., Al Atik, L., Youngs, R., Graves, R. & Atkinson, G., 2018. *Central and Eastern North America Ground-Motion Characterization (NGA-East),* U.S. Department of Energy Office of Scientific and Technical Information, Technical Report, No. DOE-UC-08314, doi:10.2172/1593158.

Griffin, J.D., Stirling, M.W. & Wang, T., 2020. Periodicity and Clustering in the Long-Term Earthquake Record, *Geophys. Res. Lett.,* **47**(22), e2020GL089272, doi:10.1029/2020GL089272.

Gupta, H.K. & Malomo, S., 1995. The Malawi earthquake of March 10, 1989: A report of the macroseismic survey, *Seismol. Res. Lett.,* **66**(1), 20–27.

Hamiel, Y., Baer, G., Kalindekafe, L., Dombola, K. & Chindandali, P., 2012. Seismic and aseismic slip evolution and deformation associated with the 2009-2010 northern Malawi earthquake swarm, East African Rift, *Geophys. J. Int.,* **191**(3), 898–908.

Hammond, W.C., Blewitt, G. & Kreemer, C., 2014. Steady contemporary deformation of the central Basin and Range Province, western United States, *J. Geophys. Res.: Solid Earth,* **119,** 5235–5253.

Hanks, T.C. & Kanamori, H., 1979. A moment magnitude scale, *J. Geophys. Res. B: Solid Earth,* **84**(B5), 2348–2350.

Hellebrekers, N., Niemeijer, A.R., Fagereng, Å., Manda, B. & Mvula, R. L.S., 2019. Lower crustal earthquakes in the East African Rift System: Insights from frictional properties of rock samples from the Malawi rift, *Tectonophysics,* **767,** 228167, doi:10.1016/j.tecto.2019.228167.

Hodge, M., Biggs, J., Goda, K. & Aspinall, W., 2015. Assessing infrequent large earthquakes using geomorphology and geodesy: the Malawi Rift, *Natural Hazards,* **76**(3), 1781–1806.

Hodge, M., Biggs, J., Fagereng, A., Elliott, A., Mdala, H. & Mphepo, F., 2019. A semi-automated algorithm to quantify scarp morphology (SPARTA): Application to normal faults in southern Malawi, *Solid Earth,* **10**(1), 27–57.

Hodge, M., Biggs, J., Fagereng, Å., Mdala, H., Wedmore, L. & Williams, J., 2020. Evidence From High-Resolution Topography for Multiple Earthquakes on High Slip-to-Length Fault Scarps: The Bilila-Mtakataka Fault, Malawi, *Tectonics,* **39**(2), e2019TC005933, doi:10.1029/2019TC005933.

Hopper, E. *et al.*, 2020. Preferential localized thinning of lithospheric mantle in the melt-poor Malawi Rift, *Nature Geosci.,* **13**(8), 584–589.

Ishibe, T. & Shimazaki, K., 2012. Characteristic earthquake model and seismicity around late quaternary active faults in Japan, *Bull. seism. Soc. Am.,* **102**(3), 1041–1058.

Iturrieta, P., Gerstenberger, M., Rollins, C., van Dissen, R.J., Wang, T. & Schorlemmer, D., 2022. *Accounting for Earthquake Rates' Temporal and Spatial Variability Through Least-Information Uniform Rate Zone Forecasts,* Lower Hutt (NZ): GNS Science. 50 p., Tech. rep., GNS Science report 2022/14, doi:10.21420/HYDZ-8W17.

Jackson, J. & Blenkinsop, T., 1993. The Malaŵi Earthquake of March 10, 1989: Deep faulting within the East African Rift System, *Tectonics,* **12**(5), 1131–1139.

Jackson, J. & Blenkinsop, T., 1997. The Bilila-Mtakataka fault in Malawi: an active, 100-km long, normal fault segment in thick seismogenic crust, *Tectonics,* **16**(1), 137–150.

Jackson, J., McKenzie, D. & Priestley, K., 2021. Relations between earthquake distributions, geological history, tectonics and rheology on the continents, *Phil. Trans. R. Soc.,* **379**(2193), doi:10.1098/rsta.2019.0412.

Johnson, K., Wallace, L.M., Maurer, J., Hamling, I., Williams, C., Rollins, C., Gerstenberger, M. & Van Dissen, R., 2022. *Geodetic Deformation Model for the 2022 update of the New Zealand National Seismic Hazard Model,* Tech. rep., GNS Science, GNS Science report; 2021/37, Lower Hutt (NZ).

Kervyn, F., Ayub, S., Kajara, R., Kanza, E. & Temu, B., 2006. Evidence of recent faulting in the Rukwa rift (West Tanzania) based on radar interferometric DEMs, *J. African Earth Sci.,* **44**(2), 151–168.

Kloukinas, P., Novelli, V., Kafodya, I., Ngoma, I., Macdonald, J. & Goda, K., 2020. A building classification scheme of housing stock in Malawi for earthquake risk assessment, *J. Housing Built Environ.,* **35**(2), 507–537.

Kolaj, M., Allen, T., Mayfield, R., Adams, J. & Halchuk, S., 2019. Ground-motion models for the 6 th Generation Seismic Hazard Model of Canada, *12th Canadian Conference on Earthquake Engineering,* Quebec City.

Kolawole, F., Atekwana, E.A., Laó-Dávila, D.A., Abdelsalam, M.G., Chindandali, P.R., Salima, J. & Kalindekafe, L., 2018a. Active Deformation of Malawi Rift's North Basin Hinge Zone Modulated by Reactivation of Preexisting Precambrian Shear Zone Fabric, *Tectonics,* **37**(3), 683–704.

Kolawole, F., Atekwana, E.A., Laó-Dávila, D.A., Abdelsalam, M.G., Chindandali, P.R., Salima, J. & Kalindekafe, L., 2018b. High-resolution electrical resistivity and aeromagnetic imaging reveal the causative fault of the 2009 Mw 6.0 Karonga, Malawi earthquake, *Geophys. J. Int.,* **213**(2), 1412–1425.

Kolawole, F., Firkins, M.C., Al Wahaibi, T.S., Atekwana, E.A. & Soreghan, M.J., 2021. Rift interaction zones and the stages of rift linkage in active segmented continental rift systems, *Basin Res.,* **33**(6), 2984–3020.

Kreemer, C., Blewitt, G. & Klein, E.C., 2014. A geodetic plate motion and Global Strain Rate Model, *Geochem. Geophys. Geosyst.,* **15**(10), 3849–3889.

Lærdal, T. & Talbot, M.R., 2002. Basin neotectonics of lakes Edward and George, East African Rift, *Palaeogeography, Palaeoclimatology, Palaeoecology,* **187**(3–4), 213–232.

Lavayssière, A., Drooff, C., Ebinger, C., Gallacher, R., Illsley-Kemp, F., Oliva, S.J. & Keir, D., 2019. Depth extent and kinematics of faulting in the Southern Tanganyika Rift, Africa, *Tectonics,* **38**(3), 842–862.

Leonard, M., 2010. Earthquake fault scaling: Self-consistent relating of rupture length, width, average displacement and moment release, *Bull. seism. Soc. Am.,* **100**(5A), 1971–1988.

Lloyd, R., Biggs, J. & Copley, A., 2019. The decade-long Machaze-Zinave aftershock sequence in the slowly straining Mozambique Rift, *Geophys. J. Int.,* **217**(1), 504–531.

Lombardi, A.M. & Marzocchi, W., 2007. Evidence of clustering and nonstationarity in the time distribution of large worldwide earthquakes, *J. Geophys. Res.: Solid Earth,* **112**(2), doi:10.1029/2006JB004568.

McCartney, T. & Scholz, C.A., 2016. A 1.3 million year record of synchronous faulting in the hangingwall and border fault of a half-graben in the Malawi (Nyasa) Rift, *J. Struct. Geol.,* **91,** 114–129.

Macheyeki, A.S. *et al.*, 2015. Active fault mapping in Karonga-Malawi after the December 19, 2009 Ms 6.2 seismic event, *J. African Earth Sci.,* **102,** 233–246.

Malawi Bureau of Standards Board, 2014. *The Structural Use of Masonry-Code of Practice, Part 1: Unreinforced Masonry Walling,* MS791-1., Tech. rep., Government of Malawi.

Marzocchi, W., Taroni, M. & Selva, J., 2015. Accounting for epistemic uncertainty in PSHA: Logic tree and ensemble modeling, *Bull. seism. Soc. Am.,* **105**(4), 2151–2159.

Matthews, M.V., Ellsworth, W.L. & Reasenberg, P.A., 2002. A Brownian model for recurrent earthquakes, *Bull. seism. Soc. Am.,* **92**(6), 2233–2250.

Meghraoui, M. *et al.*, 2016. The seismotectonic map of Africa, *Episodes,* **39**(1), 9–18.

Meletti, C. *et al.*, 2021. The new Italian seismic hazard model (MPS19), *Ann. Geophys.,* **64**(1), 1–29.

Midzi, V., Hlatywayo, D.J., Chapola, L.S., Kebede, F., Atakan, K., Lombe, D.K., Turyomurugyendo, G. & Tugume, F.A., 1999. *Seismic Hazard Assessment in Eastern and Southern Africa, Annali di Geofisica,* **42**(3), 1067–1083.

Msabi, M.M. & Ferdinand, R.W., 2021. Probabilistic seismic hazard analysis for Northern Tanzania Divergence Region and the adjoining areas, *Tanzania J. Sci.,* **47**(2), 862–876.

Muirhead, J.D. *et al.*, 2016. Evolution of upper crustal faulting assisted by magmatic volatile release during early-stage continental rift development in the East African Rift, *Geosphere,* **12**(6), 1670–1700.

Muirhead, J.D., Wright, L. J.M. & Scholz, C.A., 2019. Rift evolution in regions of low magma input in East Africa, *Earth planet. Sci. Lett.,* **506,** 332–346.

Musson, R. M.W., 1999. Determination of design earthquakes in seismic hazard analysis through monte carlo simulation, *J. Earthquake Eng.,* **3**(4), 463–474.

Ngoma, I. *et al.*, 2019. Building classification and seismic vulnerability of current housing construction in Malawi, *Malawi J. Sci. Technol.,* **11**(1), 57–72.

Nicholas, C.J., Newth, I.R., Abeinomugisha, D., Tumushabe, W.M. & Twinomujuni, L., 2016. Geology and stratigraphy of the south-eastern Lake Edward basin (Petroleum Exploration Area 4B), Albertine Rift Valley, Uganda, *J. Maps,* **12**(2), 237–248.

Njinju, E.A., Kolawole, F., Atekwana, E.A., Stamps, D.S., Atekwana, E.A., Abdelsalam, M.G. & Mickus, K.L., 2019. Terrestrial heat flow in the Malawi Rifted Zone, East Africa: Implications for tectono-thermal inheritance in continental rift basins, *J. Volcanol. Geotherm. Res.,* **387,** doi:10.1016/j.jvolgeores.2019.07.023.

Novelli, V.I., De Risi, R., Ngoma, I., Kafodya, I., Kloukinas, P., Macdonald, J. & Goda, K., 2021. Fragility curves for non-engineered masonry buildings in developing countries derived from real data based on structural surveys and laboratory tests, *Soft Computing,* **25**(8), 6113–6138.

Nyblade, A.A. & Langston, C.A., 1995. East African earthquakes below 20 km depth and their implications for crustal structure, *Geophys. J. Int.,* **121**(1), 49–62.

Pace, B., Visini, F. & Peruzza, L., 2016. FiSH : MATLAB tools to turn fault data into seismic-hazard models, *Seismol. Res. Lett.,* **87**(2A), 374–386.

Page, M. & Felzer, K., 2015. Southern San Andreas fault seismicity is consistent with the Gutenberg–Richter magnitude-frequency distribution, *Bull. seism. Soc. Am.,* **105**(4), 2070–2080.

Petersen, M.D. *et al.*, 2015. The 2014 United States National Seismic Hazard Model, *Earthquake Spectra,* **31,** S1—–S30.

Philippon, M., Willingshofer, E., Sokoutis, D., Corti, G., Sani, F., Bonini, M. & Cloetingh, S., 2015. Slip re-orientation in oblique rifts, *Geology,* **43**(2), 147–150.

Poggi, V., Durrheim, R., Tuluka, G.M., Weatherill, G., Gee, R., Pagani, M., Nyblade, A. & Delvaux, D., 2017. Assessing seismic hazard of the East African Rift: a pilot study from GEM and AfricaArray, *Bull. Earthquake Eng.,* **15**(11), 4499–4529.

Powers, P.M. & Field, E.H., 2013. Appendix O: Gridded seismicity sources, *US Geol. Surv. Open-File Rept. 2013-1165-O and California Geol. Surv. Special Rept. 228-O*.

Saria, E., Calais, E., Stamps, D.S., Delvaux, D. & Hartnady, C. J.H., 2014. Present-day kinematics of the East African Rift, *J. Geophys. Res.: Solid Earth,* **119**(4), 3584–3600.

Scholz, C.H. & Contreras, J.C., 1998. Mechanics of continental rift architecture, *Geology,* **26**(11), 967–970.

Scholz, C.A., Shillington, D.J., Wright, L. J.M., Accardo, N., Gaherty, J.B. & Chindandali, P., 2020. Intrarift fault fabric, segmentation and basin evolution of the Lake Malawi (Nyasa) Rift, East Africa, *Geosphere,* **16**(5), 1293–1311.

Schwartz, D.P. & Coppersmith, K.J., 1984. Fault behavior and characteristic earthquakes: Examples from the Wasatch and San Andreas Fault Zones, *J. Geophys. Res.: Solid Earth,* **89**(B7), 5681–5698.

Shaw, B.E., 2013. Earthquake surface slip-length data is fit by constant stress drop and is useful for seismic hazard analysis, *Bull. seism. Soc. Am.,* **103**(2A), 876–893.

Shillington, D.J. *et al.*, 2016. Acquisition of a unique onshore/offshore geophysica l and geochemical dataset in the northern Malawi (Nyasa) rift, *Seismol. Res. Lett.,* **87**(6), 1406–1416.

Shillington, D.J. *et al.*, 2020. Controls on Rift Faulting in the North Basin of the Malawi (Nyasa) Rift, East Africa, *Tectonics,* **39**(3), e2019TC005633, doi:10.1029/2019TC005633.

Specht, T.D. & Rosendahl, B.R., 1989. Architecture of the Lake Malawi Rift, East Africa, *J. African Earth Sci.,* **8**(2–4), 355–382.

Stamps, D.S., Calais, E., Saria, E., Hartnady, C., Nocquet, J.M., Ebinger, C.J. & Fernandes, R.M., 2008. A kinematic model for the East African Rift, *Geophys. Res. Lett.,* **35**(5), doi:10.1029/2007GL032781.

Stamps, D.S., Saria, E. & Kreemer, C., 2018. A Geodetic Strain Rate Model for the East African Rift System, *Sci. Rep.,* **8**(1), doi:10.1038/s41598-017-19097-w.

Stamps, D.S., Kreemer, C., Fernandes, R., Rajaonarison, T.A. & Rambolamanana, G., 2021. Redefining East African Rift System kinematics, *Geology,* **49**(2), 150–155.

Stevens, V.L. & Avouac, J.P., 2021. On the relationship between strain rate and seismicity in the India-Asia collision zone: Implications for probabilistic seismic hazard, *Geophys. J. Int.,* **226**(1), 220–245.

Stevens, V.L., Sloan, R.A., Chindandali, P.R., Wedmore, L. N.J., Salomon, G.W. & Muir, R.A., 2021. The Entire Crust can be Seismogenic: Evidence from Southern Malawi, *Tectonics,* **40**(6), e2020TC006654, doi:10.1029/2020tc006654.

Stirling, M. & Gerstenberger, M., 2018. Applicability of the Gutenberg–Richter relation for major active faults in New Zealand, *Bull. seism. Soc. Am.,* **108**(2), 718–728.

Stirling, M. *et al.*, 2012. National seismic hazard model for New Zealand: 2010 update, *Bull. seism. Soc. Am.,* **102**(4), 1514–1542.

Taulo, J.L., Gondwe, K.J. & Sebitosi, A.B., 2015. Energy supply in Malawi: Options and issues, *J. Energy Southern Africa,* **26**(2), 19–32.

Tinti, S. & Mulargia, F., 1987. Confidence intervals of b values for grouped magnitudes, *Bull. seism. Soc. Am.,* **77**(6), 2125–2134.

Tuluka, G.M., Lukindula, J. & Durrheim, R.J., 2020. Seismic Hazard Assessment of the Democratic Republic of Congo and Environs Based on the GEM–SSA Catalogue and a New Seismic Source Model, *Pure Appl. Geophys.,* **177**(1), 195–214.

Turcotte, D.L. & Schubert, G., 1982. *Geodynamics: Applications of Continuum Physics to Geological Problems,* p. 450, ISBN 10 0471060186.

Twiss, R.J. & Unruh, J.R., 1998. Analysis of fault slip inversions: Do they constrain stress or strain rate?, *J. Geophys. Res.: Solid Earth,* **103**(B6), 12205–12222.

Valentini, A., Visini, F. & Pace, B., 2017. Integrating faults and past earthquakes into a probabilistic seismic hazard model for peninsular Italy, *Natural Hazards Earth Syst. Sci.,* **17**(11), 2017–2039.

Valentini, A., DuRoss, C.B., Field, E.H., Gold, R.D., Briggs, R.W., Visini, F. & Pace, B., 2020. Relaxing Segmentation on the Wasatch Fault Zone: Impact on Seismic Hazard, *Bull. seism. Soc. Am.,* **110**(1), 83–109.

Vallage, A. & Bollinger, L., 2020. Testing Fault Models in Intraplate Settings: A Potential for Challenging the Seismic Hazard Assessment Inputs and Hypothesis?, *Pure Appl. Geophys.,* **177**(5), 1879–1889.

Visini, F., Valentini, A., Chartier, T., Scotti, O. & Pace, B., 2020. Computational Tools for Relaxing the Fault Segmentation in Probabilistic Seismic Hazard Modelling in Complex Fault Systems, *Pure Appl. Geophys.,* **177**(5), 1855–1877.

Vittori, E., Delvaux, D. & Kervyn, F., 1997. Kanda fault: A major seismogenic element west of the Rukwa Rift (Tanzania, East Africa), *J. Geodynamics,* **24**(1–4), 139–153.

Wald, D.J. & Allen, T.I., 2007. Topographic slope as a proxy for seismic site conditions and amplification, *Bull. seism. Soc. Am.,* **97**(5), 1379–1395.

Wallace, R.E., 1970. Earthquake recurrence intervals on the San Andreas fault, *Bull. Geological Soc. America,* **81**(10), 2875–2890.

Wang, S., Werner, M.J. & Yu, R., 2021. How Well Does Poissonian Probabilistic Seismic Hazard Assessment (PSHA) Approximate the Simulated Hazard of Epidemic-Type Earthquake Sequences?, *Bull. seism. Soc. Am.,* **112**(1), 508–526.

Wang, Y.J., Chan, C.H., Lee, Y.T., Ma, K.F., Shyu, J.B.H., Rau, R.J. & Cheng, C.T., 2016. Probabilistic seismic hazard assessment for Taiwan, *Terr. Atmos. Oceanic Sci.,* **27**(3), 325–340.

Wanke, H., 2005. The namibian Eiseb Graben as an extension of the east African Rift: Evidence from Landsat TM 5 imagery, *South African J. Geol.,* **108**(4), 541–546.

Wedmore, L., Faure Walker, J.P., Roberts, G.P., Sammonds, P.R., McCaffrey, K. J.W. & Cowie, P.A., 2017. A 667 year record of coseismic and interseismic Coulomb stress changes in central Italy reveals the role of fault interaction in controlling irregular earthquake recurrence intervals, *J. Geophys. Res.: Solid Earth,* **122**(7), 5691–5711.

Wedmore, L., Biggs, J., Williams, J., Fagereng, Å., Dulanya, Z., Mphepo, F. & Mdala, H., 2020a. Active Fault Scarps in Southern Malawi and Their Implications for the Distribution of Strain in Incipient Continental Rifts, *Tectonics,* **39**(3), e2019TC005834, doi:10.1029/2019TC005834.

Wedmore, L. *et al.*, 2020b. Structural inheritance and border fault reactivation during active early-stage rifting along the Thyolo fault, Malawi, *J. Struct. Geol.,* **139,** 104097, doi:10.1016/j.jsg.2020.104097.

Wedmore, L., Biggs, J., Floyd, M., Fagereng, Mdala, H., Chindandali, P., Williams, J.N. & Mphepo, F., 2021. Geodetic Constraints on Cratonic Microplates and Broad Strain During Rifting of Thick Southern African Lithosphere, *Geophys. Res. Lett.,* **48**(17), doi:10.1029/2021GL093785.

Wedmore, L., Turner, T., Biggs, J., Williams, J.N., Sichingabula, H.M., Kabumbu, C. & Banda, K., 2022. The Luangwa Rift Active Fault Database and fault reactivation along the southwestern branch of the East African Rift, *Solid Earth,* **13**(11), 1731–1753.

Wesnousky, S.G., Scholz, C.H., Shimazaki, K. & Matsuda, T., 1983. Earthquake frequency distribution and the mechanics of faulting, *J. Geophys. Res.,* **88**(B11), 9331–9340.

Williams, J.N., Fagereng, Å., Wedmore, L., Biggs, J., Mphepo, F., Dulanya, Z., Mdala, H. & Blenkinsop, T., 2019. How Do Variably Striking Faults Reactivate During Rifting? Insights From Southern Malawi, *Geochem. Geophys. Geosyst.,* **20**(7), 3588–3607.

Williams, J.N., Mdala, H., Fagereng, Å., Wedmore, L., Biggs, J., Dulanya, Z., Chindandali, P. & Mphepo, F., 2021a. A systems-based approach to parameterise seismic hazard in regions with little historical or instrumental seismicity: Active fault and seismogenic source databases for southern Malawi, *Solid Earth,* **12**(1), 187–217.

Williams, J.N. *et al.*, 2021b. *Malawi Active Fault Database (v1.0) [Data set],* doi:10.5281/ZENODO.5507189.

Williams, J.N. *et al.*, 2022a. *Malawi Seismogenic Source Model (v1.2) [Data set],* doi:10.5281/zenodo.5599616.

Williams, J.N. *et al.*, 2022b. Geologic and geodetic constraints on the magnitude and frequency of earthquakes along Malawi's active faults: the Malawi Seismogenic Source Model (MSSM), *Natural Hazards Earth Syst. Sci.,* **22**(11), 3607–3639.

Williams, J.N. *et al.*, 2022c. The Malawi Active Fault Database: an onshore-offshore database for regional assessment of seismic hazard and tectonic evolution, *Geochem. Geophys. Geosyst.,* **23**(5), e2022GC010425, doi:10.1029/2022gc010425.

Williams, J.N., Fagereng, Å., Wedmore, L.N., Biggs, J., Mdala, H., Mphepo, F. & Hodge, M., 2022d. Low Dissipation of Earthquake Energy Where a Fault Follows Pre-Existing Weaknesses: Field and Microstructural Observations of Malawi's Bilila-Mtakataka Fault, *Geophys. Res. Lett.,* **49**(8), e2021GL095286, doi:10.1029/2021GL095286.

Woessner, J. *et al.*, 2015. The 2013 European Seismic Hazard Model: key components and results, *Bull. Earthquake Eng.,* **13**(12), 3553–3596.

World-Bank, 2019. *Tectonic Shift : Rift 2018 - Regional Seismic Risk and Resilience Workshop (English),* Tech. rep., World Bank Group, Washington, D.C.

Wright, L. J.M., Muirhead, J.D. & Scholz, C.A., 2020. Spatiotemporal Variations in Upper Crustal Extension Across the Different Basement Terranes of the Lake Tanganyika Rift, East Africa, *Tectonics,* **39**(3), doi:10.1029/2019TC006019.

Wu, W.N., Yen, Y.T., Hsu, Y.J., Wu, Y.M., Lin, J.Y. & Hsu, S.K., 2017. Spatial variation of seismogenic depths of crustal earthquakes in the Taiwan region: Implications for seismic hazard assessment, *Tectonophysics,* **708,** 81–95.

Yenier, E. & Atkinson, G.M., 2015. Regionally adjustable generic ground-motion prediction equation based on equivalent point-source simulations: Application to central and eastern North America, *Bull. seism. Soc. Am.,* **105**(4), 1989–2009.

Youngs, R.R. & Coppersmith, K.J., 1985. Implications of fault slip rates and earthquake recurrence models to probabilistic seismic hazard estimates, *Bull. seism. Soc. Am.,* **75**(4), 939–964.

Zahran, H.M., Sokolov, V., Youssef, S. E.H. & Alraddadi, W.W., 2015. Preliminary probabilistic seismic hazard assessment for the Kingdom of Saudi Arabia based on combined areal source model: Monte Carlo approach and sensitivity analyses, *Soil Dyn. Earthquake Eng.,* **77,** 453–468.

Zheng, W., Oliva, S.J., Ebinger, C. & Pritchard, M.E., 2020. Aseismic Deformation During the 2014 Mw 5.2 Karonga Earthquake, Malawi, From Satellite Interferometry and Earthquake Source Mechanisms, *Geophys. Res. Lett.,* **47**(22), doi:10.1029/2020GL090930.

Zhuang, J., Werner, M.J., Harte, D., Hainzl, S. & Zhou, S., 2012. Basic models of seismicity, Community Online Resource for Statistical Seismicity Analysis, pp. 2–41, doi:10.5078/corssa-79905851.

Zielke, O. & Strecker, M.R., 2009. Recurrence of large earthquakes in magmatic continental rifts: Insights from a paleoseismic study along the Laikipia-Marmanet fault, Subukia Valley, Kenya rift, *Bull. seism. Soc. Am.,* **99**(1), 61–70.

Zöller, G. & Hainzl, S., 2007. Recurrence time distributions of large earthquakes in a stochastic model for coupled fault systems: The role of fault interaction, *Bull. seism. Soc. Am.,* **97**(5), 1679–1687.

APPENDIX A: STOCHASTIC EVENT CATALOG TESTS

Herein, we provide further descriptions of the internal and external tests performed on the stochastic catalog that were used in our probabilistic seismic hazard analysis (PSHA) of Malawi: (1) how different weightings of section, fault and multifault Malawi Seismogenic Source Model (MSSM) sources can be fitted to the regional *b*-value in the Direct MSSM catalog, (2) if the Adapted MSSM catalogs replicate the seismicity implied by the Youngs & Coppersmith (1985) recurrence models (Appendix A2), (3) in Appendix A3, if the moment rate ($\dot{M}_0$) of the areal sources in the catalog match the $\dot{M}_0$ derived analytically from their G–R relation (Poggi *et al.* 2017), (4) an examination of combining MSSM and areal source seismicity in Malawi (Appendix A4) and (5) in Appendix A5, if the Combined Catalog matches independent estimates of the geodetic $\dot{M}_0$ in Malawi (Kreemer *et al.* 2014; Stamps *et al.* 2018). Results from this testing are also presented in Section 4.6 in the main article.

A1 Weighting sources in the Direct MSSM catalog

For a MSSM fault source that is divided along-strike into smaller section sources and/or combined with closely spaced faults into a multifault source, the frequency of one type of source event will impact the frequency of other source types (Williams *et al.* 2022b); simply assuming that events along these different source types are independent of each other will lead to double counting of the fault's seismicity. As is common in PSHA, combining these different MSSM source types can be achieved through a logic tree approach, with weightings assigned to each branch to describe their relative likelihood.

Section sources imply relatively frequent moderate magnitude seismicity, whilst multifault sources are indicative of rarer larger magnitude events (Williams *et al.* 2022b). Therefore, the gradient

Table A1. The *b*-value that is derived from generating stochastic event catalogs that consider all 36 weighting combinations of fault, section and multifault MSSM sources. The target *b*-value (1.02). See also Fig. 8.

Fault	Section	Multifault	*b*-value	Moment rate (Nm yr^{-1})
0.1	0.1	0.8	0.98	1.44E+18
0.1	0.2	0.7	0.97	1.32E+18
0.1	0.3	0.6	0.96	1.27E+18
0.1	0.4	0.5	0.95	1.23E+18
0.1	0.5	0.4	0.95	1.16E+18
0.1	0.6	0.3	0.94	1.09E+18
0.1	0.7	0.2	0.94	1.07E+18
0.1	0.8	0.1	0.93	1.03E+18
0.2	0.1	0.7	1.00	1.50E+18
0.2	0.2	0.6	0.97	1.43E+18
0.2	0.3	0.5	0.96	1.32E+18
0.2	0.4	0.4	0.96	1.26E+18
0.2	0.5	0.3	0.95	1.22E+18
0.2	0.6	0.2	0.94	1.17E+18
0.2	0.7	0.1	0.93	1.11E+18
0.3	0.1	0.6	1.00	1.52E+18
0.3	0.2	0.5	0.98	1.42E+18
0.3	0.3	0.4	0.96	1.39E+18
0.3	0.4	0.3	0.95	1.29E+18
0.3	0.5	0.2	0.95	1.22E+18
0.3	0.6	0.1	0.94	1.20E+18
0.4	0.1	0.5	1.00	1.55E+18
0.4	0.2	0.4	0.98	1.45E+18
0.4	0.3	0.3	0.96	1.37E+18
0.4	0.4	0.2	0.95	1.31E+18
0.4	0.5	0.1	0.94	1.30E+18
0.5	0.1	0.4	0.99	1.53E+18
0.5	0.2	0.3	0.97	1.46E+18
0.5	0.3	0.2	0.96	1.38E+18
0.5	0.4	0.1	0.95	1.31E+18
0.6	0.1	0.3	0.98	1.56E+18
0.6	0.2	0.2	0.97	1.47E+18
0.6	0.3	0.1	0.96	1.41E+18
0.7	0.1	0.2	0.98	1.52E+18
0.7	0.2	0.1	0.97	1.46E+18
0.8	0.1	0.1	0.98	1.55E+18

of the the Direct MSSM stochastic event catalogs MFD (i.e. *b*-value) will be sensitive to the weighting of these sources types. A convenient way of weighting these sources is therefore to find the catalog, which when combined with areal source events, has a *b*-value closest to the regional estimate (1.02; Hodge *et al.* 2015; Poggi *et al.* 2017).

To perform this analysis, we generate two million 1-yr long event catalogs for all possible source type weighting combinations at intervals of 0.1 with the limitation that the weighting of any source type ≥ 0.1 ($n = 36$, Table A1). In cases where a fault source is not divided into section sources and/or combined into a multifault source types, its weighting is accordingly re-adjusted. For example, in the case of 0.4–0.4–0.2 weighting for section, fault and multifault sources respectively and for a fault that contains section sources but is not part of a multifault source, the re-adjusted weightings are 0.5–0.5. In this respect, seismicity along fault sources that do not have corresponding section or multifault sources follows the characteristic earthquake model (Schwartz & Coppersmith 1984). Alternative hypotheses must also be considered for where the MSSM sources splay in map view (Williams *et al.* 2022b). In these cases, an equal weighting is applied for which branch will rupture. All of these Direct MSSM catalogs are then combined with the areal source catalog for events in the assessed region (Fig. 6).

We use the maximum-likelihood indicator to derive the *b*-value of each catalog (Aki 1965) over the magnitude range M_W 4.5–7.6. At greater magnitudes, the MFD is non G–R (Fig. 8). From this, we find the optimal source type weighting is 0.3–0.1–0.6 for fault, section and multifault MSSM sources respectively (*b*-value = 0.998; Fig. 8, Table A1). No catalog can directly replicate the estimated *b*-value of 1.02 in Malawi (Table A1). However, the *b*-value for the optimal source type weighting is within the *b*-value measurement uncertainty (∼0.95–1.05; Hodge *et al.* 2015). The low weighting assigned to MSSM section sources in this approach reflects that much of the moderate magnitude seismicity they produce is instead incorporated into the areal source events; hence to maintain a *b*-value ∼1, the MSSM sources should be dominated by larger fault and multifault events.

This MSSM source type weighting analysis does not explicitly consider the earthquake rates produced by each weighting combination ($\dot{M}_0$, Table A1). These variations are a consequence of the Leonard (2010) scaling relationships, which disproportionately increase the $\dot{M}_0$ of longer (and wider) sources. Since the $\dot{M}_0$ inferred from recorded seismicity in Malawi is poorly constrained (Section 4.6.2; Hodge *et al.* 2015; Ebinger *et al.* 2019), we did not consider this a useful constraint when selecting the source type weighting combination.

A2 Adapted MSSM sources

In the Adapted MSSM approach, we distribute a source's $\dot{M}_0$ (eq. 2) across either a G–R or characteristic MFD (Section 4.2, Fig. 4). In this section, we first provide the equations given by Youngs & Coppersmith (1985) and Convertito *et al.* (2006) that were used to develop these sources and then examine if the stochastic event catalogs reproduce the seismicity anticipated by these recurrence models.

For a G–R distribution, the probability density function $f_M(m)$ for magnitude m is given by

$$f_M(m) = \frac{\beta e^{(-\beta(m-M_{min}))}}{1-e^{(-\beta(M_{Max}-M_{min}))}}, \text{ for } M_{min} \leq m \leq M_{Max} \tag{A1}$$

where $\beta = b \ln 10$ and $M_{\min}$ and M_{Max} describe the range of event magnitudes that are assessed for each source. For a characteristic recurrence model, $f_M(m)$ is given by

$$f_M(m) = \begin{cases} \frac{\beta e^{(-\beta(m-M_{min}))}}{(1+C)(1-e^{(-\beta(M_{Max}-M_{min}-\Delta m_2))})}, & \text{for } M_{min} \leq m \leq M_c \\ \frac{\beta e^{(-\beta(M_{Max}-M_{min}-\Delta m_1-\Delta m_2))}}{(1+C)(1-e^{(-\beta(M_{Max}-M_{min}-\Delta m_2))})}, & \text{for } M_c \leq m \leq M_{Max} \end{cases} \tag{A2}$$

where Δm_1 is the magnitude range across which the G–R portion of the source's MFD that has a recurrence rate lower than the characteristic portion, Δm_2 is the magnitude range over which characteristic earthquakes occur and which is bounded by the minimum characteristic earthquake magnitude (M_c) and M_{Max} (Fig. 4a; Youngs & Coppersmith 1985; Convertito *et al.* 2006). The constant C is

$$C = \frac{\beta e^{-(M_{Max}-M_{min}-\Delta m_1-\Delta m_2)}}{1-e^{(-\beta(M_{Max}-M_{min}-\Delta m_2))}}\Delta m_2 \tag{A3}$$

The annual frequency, or 'activity rate,' for events with $m \geq M_{\min}$ for a G–R magnitude frequency relationship (α_{GR}) is

$$\alpha_{GR} = \frac{\dot{M}_0(c-b)(1-e^{(-\beta(M_{Max}-M_{min}))})}{b M_0^{Max} e^{-\beta(M_{Max}-M_{min})}} \tag{A4}$$

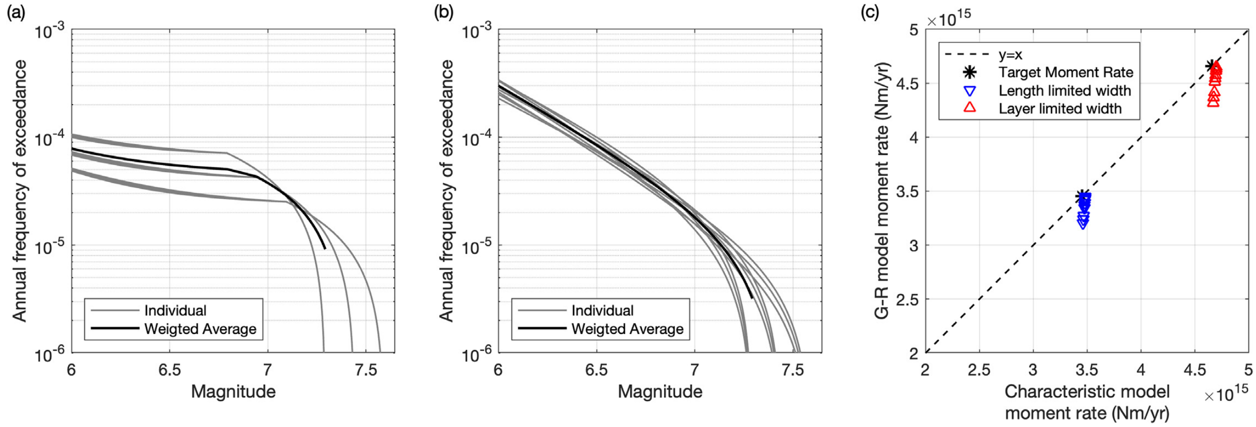

Figure A1. Nine MFD for the Chingale Step Fault for (a) characteristic and (b) G–R type seismicity in the MSSM-adapted approach (Youngs & Coppersmith 1985; Convertito *et al.* 2006). Each MFD considers a different b-value and M_{Max} combination and is assigned a weighting as described in Fig. 2. (c) Comparison of these MFD $\dot{M}_0$ for a given fault width, b-value and M_{Max} case. The target $\dot{M}_0$ indicates the $\dot{M}_0$ as calculated from eq. (2). Results for the length-limited case and are also shown in Table A1.

Table A2. Comparisons of the Chingale Step Fault $\dot{M}_0$ that are produced by a characteristic and G–R models in the Adapted MSSM approach. In this approach, nine recurrence models are generated for each MFD, which cumulatively explore uncertainty in the b-value and M_{Max}. These are are then randomly sampled in the event catalogs using the weightings in Fig. 2. Analysis for the length-limited case. $\dot{M}_0$ ratio is the ratio of the recurrence model's $\dot{M}_0$ to the Chingale Step Fault's $\dot{M}_0$ as calculated from eq. (2) (3.47×10^{15} Nm yr^{-1}). Results also shown in Fig. A2.

b-value	M_{Max} shift	Weighting	Characteristic $\dot{M}_0$ (Nm yr^{-1})	Char $\dot{M}_0$ ratio	G–R $\dot{M}_0$ (Nm yr^{-1})	G–R $\dot{M}_0$ ratio
1.12	−0.15	0.048	3.39×10^{15}	97.7 per cent	3.14×10^{15}	90.5 per cent
1.12	0	0.096	3.40×10^{15}	98.9 per cent	3.18×10^{15}	91.7 per cent
1.12	+0.15	0.016	3.40×10^{15}	98.0 per cent	3.21×10^{15}	92.5 per cent
1.02	−0.15	0.204	3.40×10^{15}	98.0 per cent	3.28×10^{15}	94.6 per cent
1.02	0	0.408	3.41×10^{15}	98.3 per cent	3.30×10^{15}	95.1 per cent
1.02	+0.15	0.068	3.41×10^{15}	98.3 per cent	3.32×10^{15}	95.7 per cent
0.92	−0.15	0.048	3.41×10^{15}	98.3 per cent	3.35×10^{15}	96.6 per cent
0.92	0	0.096	3.41×10^{15}	98.3 per cent	3.37×10^{15}	97.1 per cent
0.92	+0.15	0.016	3.41×10^{15}	98.3 per cent	3.38×10^{15}	97.4 per cent

Table A3. Comparison of total $\dot{M}_0$ from all MSSM Sources as derived by their slip rate and area (Target $\dot{M}_0$) and as replicated in the stochastic event catalogs (Catalog $\dot{M}_0$). For the Adapted MSSM sources, a comparison is to the total $\dot{M}_0$ derived from eqs (A1) and (A7) (Source model $\dot{M}_0$).

Catalog	Target $\dot{M}_0$ (Nm yr^{-1})	Source Models $\dot{M}_0$ (Nm yr^{-1})	Catalog $\dot{M}_0$ (Nm yr^{-1})
Direct MSSM	1.48×10^{18}	N/A	1.52×10^{18}
Length-limited, char	1.61×10^{18}	1.58×10^{18}	1.63×10^{18}
Length-limited, G–R	1.61×10^{18}	1.53×10^{18}	1.48×10^{18}
Layer-limited, char	1.80×10^{18}	1.78×10^{18}	1.78×10^{18}
Layer-limited, G–R	1.80×10^{18}	1.71×10^{18}	1.65×10^{18}

Table A4. G–R relationships and moment rate ($\dot{M}_0$) for areal source zones located within the region assessed during PSHA (Fig. 6).

Source ID (Poggi *et al.* 2017)	Source zone	a-value	b-value	M_{Max}	Discretized $\dot{M}_0$ (Nm yr^{-1})	Catalog $\dot{M}_0$ (Nm yr^{-1})
8	Tanganynika	2.9	1.02	7.9	1.2×10^{16}	1.3×10^{16}
9	Rukwa–Malawi	4.7	1.02	7.9	7.3×10^{17}	7.4×10^{17}
13	Kariba-Okavango	2.8	0.99	6.9	4.3×10^{15}	4.5×10^{15}
20	Rovuma Basin	2.6	1.02	6.9	1.8×10^{15}	1.8×10^{15}
N/A	Nyanga	0.4	0.8	7.0	2.6×10^{14}	3.0×10^{14}
N/A	Northeast Mozambique	0.1	0.8	7.0	1.3×10^{14}	1.7×10^{14}
				Total	7.45×10^{17}	7.62×10^{17}

In this analysis, the a-value has been scaled from Table 2 given the overlap between the source zone and assessed region and events $M_W > 7$ have been removed from the event catalogs.

where M_0^{Max} is the seismic moment for M_{Max} and c is the parameter from the relation $\log M_0 = cm + d$ and equals 1.5 (Hanks & Kanamori 1979). For characteristic earthquakes, the activity rate

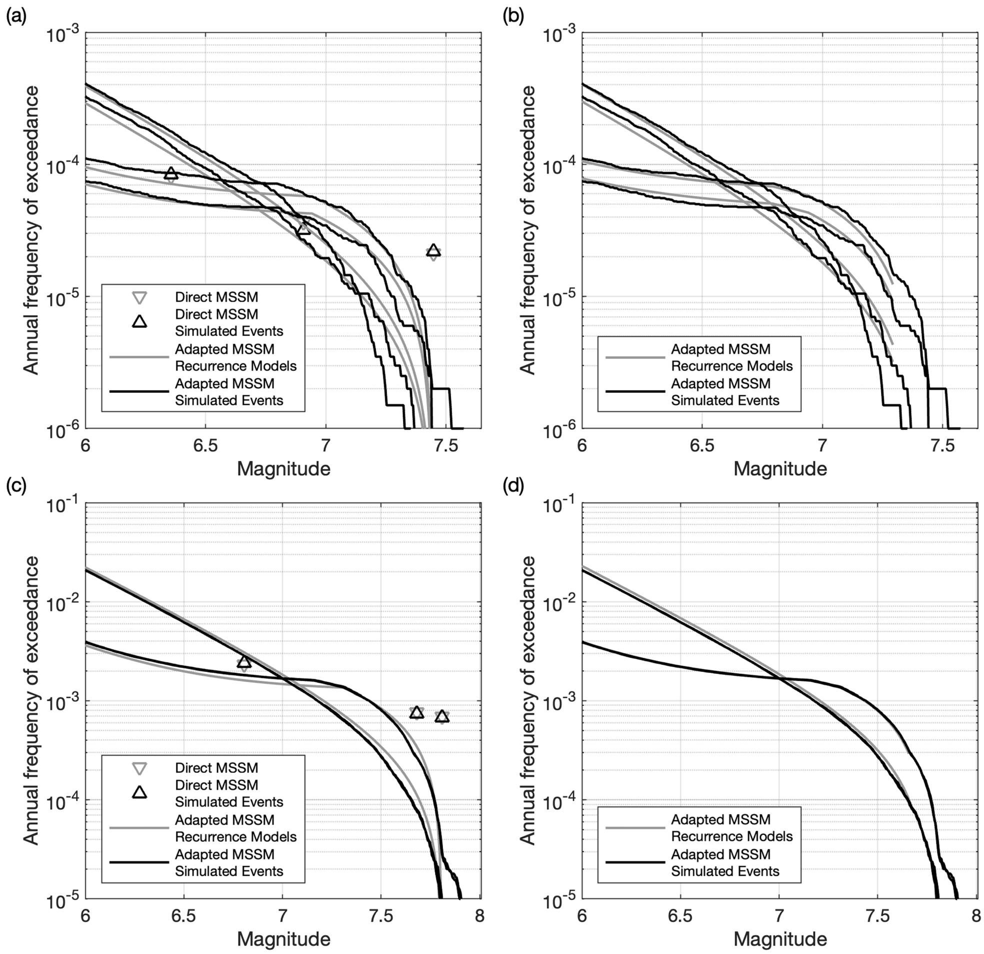

Figure A2. The (a) median and (b) weighted average of the nine MFD curves for the Chingale Step Fault (slip rate ~0.04 mm yr^{-1}) derived from all possible variations in the *b*-value and $M_{\max}$ in the adapted moment rate balancing approach (see also Fig. 2 and A1). These are then plotted with respect to the MFD of the Chingale Step Fault in the stochastic event catalogs. In (a) a comparison is also made for how the occurrence rate of the Chingale Step Fault in the Direct MSSM approach is replicated in the catalogs. (c) and (d) Equivalent to (a) and (b), but for the Livingstone Fault (slip rate 2.1 mm yr^{-1}).

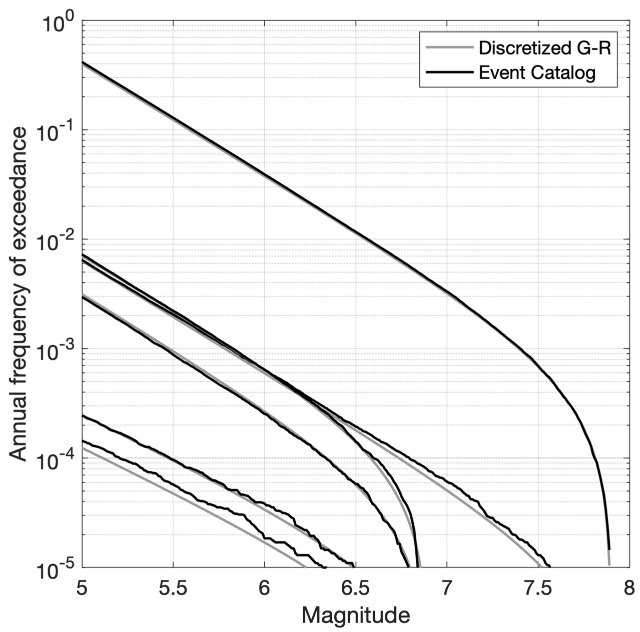

Figure A3. Discretized and event catalog MFD for the six areal sources from Poggi *et al.* (2017) that lie within the region assessed for PSHA (Fig. 6).

(α_C) is

$$\alpha_C = \alpha_{NC} \frac{\beta \Delta m_2 e^{-\beta(M_{Max} - M_{min} - \Delta m_1 - \Delta m_2)}}{1 - e^{-\beta(M_{Max} - M_{min} - \Delta m_2)}} \tag{A5}$$

where α_{NC} represents the activity rate of the non-characteristic magnitude range (i.e. for $M_{\min} \leq m \leq M_c$, Fig. 4a) and is given by

$$\alpha_{NC} = \frac{\dot{M}_0(1 - e^{-\beta(M_{Max} - M_{min} - \Delta m_2)})}{K M_0^{Max} e^{-\beta(M_{Max} - M_{min} - \Delta m_2)}} \tag{A6}$$

where the constant K is defined by

$$K = \frac{b 10^{-c\Delta m_2}}{c - b} + \frac{b e^{\beta \Delta m_1}(1 - 10^{-c\Delta m_2})}{c} \tag{A7}$$

β in eqs (A1)–(A7) is taken from the regional *b*-value in Malawi (1.02; Poggi *et al.* 2017). The Leonard (2010) area-magnitude scaling relationships are used to derive $M_{\rm Max}$ for each source and hence it is equivalent to the magnitude estimate m_s used in the Direct MSSM approach (Section 4.1). The uncertainty in these parameters is explored by converting them to discrete variables, with the *b*-value shifted by ± 0.1 with weightings of 0.16 for lower and upper cases and $M_{\rm Max}$ shifted ± 0.15 with weightings of 0.3 and 0.1 for lower and upper cases, respectively (Fig. 2 and A1, Table A2). These weightings are based on expert opinion and follow that of Goda & Sharipov (2021). Nine source-specific recurrence models

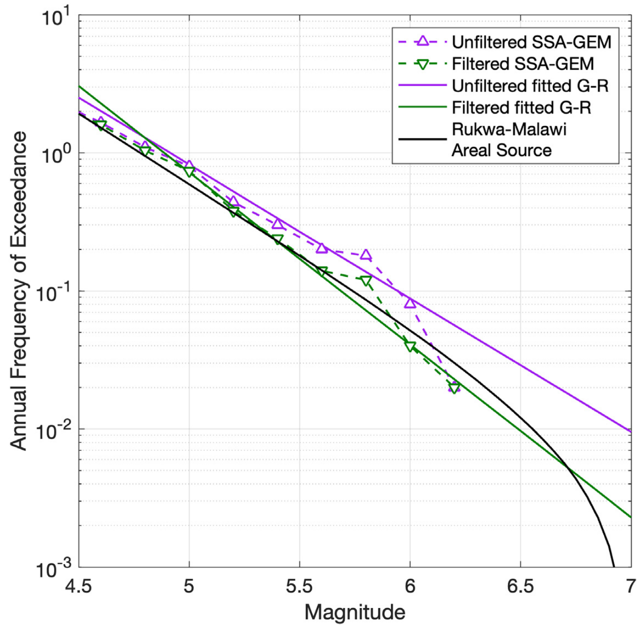

Figure A4. MFD for all events in the Rukwa–Malawi areal source zone between 1965–2015 in the SSA-GEM catalog ('Unfiltered') and the MFD after removing the four largest events in the 2009 Karonga earthquake sequence ('Filtered'). Also shown are the G–R distributions that can be fitted these filtered and unfiltered catalogs (Tinti & Mulargia 1987) and the Rukwa–Malawi source zone stochastic event catalog. and the MFD for the Rukwa–Malawi source zone stochastic event catalog. For a description of the SSA-GEM catalog and Rukwa–Malawi source zone, see Poggi *et al.* (2017).

can therefore be generated from sampling different combinations of these parameters, with these models more sensitive to variations in M_{Max} than the b-value (Fig. A1 and Table A2.).

M_{min} typically represents the smallest sized event that can still produce damaging ground motions (Youngs & Coppersmith 1985). Seismic fragility curves indicate that buildings in Malawi are vulnerable to ground motions as low as 0.1 g (Novelli *et al.* 2021; Giordano *et al.* 2021) and so we adopt a relatively conservative value for M_{min} of 4.5. Following Youngs & Coppersmith (1985), Δm_1 and Δm_2 are 1.0 and 0.5, respectively. By defining a lower magnitude cutoff with M_{min}, it is implicit that not all of a source's $\dot{M}_0$, as defined by eq. (2), will be included in these recurrence models (Fig. A1c). However, 90-98 per cent of a source's $\dot{M}_0$ is still retained depending on the logic tree branch (Table A2). Branches that consider a G–R MFD, high b-value and low M_{Max} will experience the highest $\dot{M}_0$ loss, as they imply the highest amount of seismicity at $M_W < 4.5$ (Fig. A1, Table A2).

The Adapted MSSM stochastic event catalogs assign magnitudes to source events by sampling the probability distribution functions given by eqs (A1) and (A2) (Section 4.4). Given a sufficient catalog duration, the catalog MFD shape and $\dot{M}_0$ for each source should match those derived by these equations. For the event catalogs generated here, this is true for high slip rates sources and characteristic MFD (Fig. A2c and d; Table A3). However, the catalogs do not replicate infrequent (annual rates <0.001) high magnitude events along low slip rate sources with a G–R MFD (Fig. A2b) leading to further discrepancies between the theoretical $\dot{M}_0$ of the MSSM sources and their $\dot{M}_0$ in the event catalogs (Table A3).

This $\dot{M}_0$ discrepancy could be resolved by running more simulation cycles (i.e. generating a catalog with a longer duration). We highlight, however, that these $\dot{M}_0$ comparisons can sometimes be misleading since large magnitudes have a disproportionately high impact on $\dot{M}_0$; for each increase in M_W unit and for a b-value ∼1, the seismic moment will increase ∼30 times, whilst the rate will only reduce by a tenth. If we instead consider the MFD shape at moderate magnitudes for low slip rate sources, it can be observed the catalog corresponds with the recurrence model (Fig. A2b). This is important as it is these moderate magnitude events that are the main contributors to hazard for a G–R MFD (Section 7.2).

A3 Areal source catalog validation

To consider whether the stochastic event catalog $\dot{M}_0$ of the six areal sources that lie within the region assessed during the PSHA (Fig. 6) matches their $\dot{M}_0$ as derived from their a- and b-value, we first adjust the a-value so that it is consistent with the size of the overlap between the assessed region and the areal source (Table A4). We then discretize this G–R relationship into magnitude bins of 0.01 and calculate the $\dot{M}_0$ of each bin and for consistency with the event catalogs (Section 4.3), by assuming the magnitude probability distribution follows a truncated exponential relationship (Cosentino *et al.* 1977). In this $\dot{M}_0$ comparison, events in the areal source catalog with $m > M_{Max}$ (i.e. 7.0) were not removed as they are for the PSHA (Section 4.3).

For most source zones, the catalog's $\dot{M}_0$ and MFD matches that expected from discretizing their G–R relationship (Table A4 and Fig. A3). Discrepancies do exist for the Nyanga and Northeast Mozambique sources. However, as these sources have very low rates of seismicity (annual probability of $M_W > 5$ events is <0.001), they are only minor contributors to Malawi's seismic hazard. We therefore conclude that the two million simulations in the areal source catalogs are of sufficient duration to characterise off-fault seismicity for the PSHA. Notably, the $\dot{M}_0$ implied by these areal sources for Malawi (7.45×10^{17} Nm yr^{-1}; Table A4) is lower than that derived in in the MSSM-based catalogs (1.89×10^{18} Nm yr^{-1}, Fig. 7). We discuss this further in Section 4.6.2.

A4 Combining MSSM and areal sources in stochastic event catalogs

The historical and instrumental record of seismicity in Malawi comprises events on known mapped active faults that are included in the MSSM and on hitherto unknown faults (i.e. 'off-fault' or 'background' earthquakes). In theory, distinguishing whether these earthquakes are on- or off-fault can be determined by resolving whether their locations fall within km-scale 3D buffer zones around known faults (Powers & Field 2013; Gerstenberger *et al.* 2022). However, this type of analysis is challenging in Malawi due to high location uncertainties (5–20 km; Jackson & Blenkinsop 1993; Gaherty *et al.* 2019), such that the 2009 Karonga earthquakes are the only events in the SSA-GEM catalog that can be confidently placed on a known active fault (Biggs *et al.* 2010; Macheyeki *et al.* 2015). In using the SSA-GEM catalog to fit G–R relationships to areal sources (Table 2; Poggi *et al.* 2017) and estimating that the largest areal source event, M_{Max}, is M_W 7, our PSHA implies all SSA-GEM catalog events $M_W < 7$ are off-fault. This is not true and hence raises the risk that between M_W 4.5–7, we are double-counting recorded seismicity as both areal source and fault-based source events. To investigate how this simplification impacts our PSHA, we examine: (1) if the areal source seismicity is still consistent with the SSA-GEM catalog after removing the 2009 Karonga earthquakes and (2) the physical basis of areal source events in the context of the MSSM's development.

For the first test, we consider all earthquakes in the SSA-GEM catalog between 1965–2015 that fall within the Rukwa–Malawi

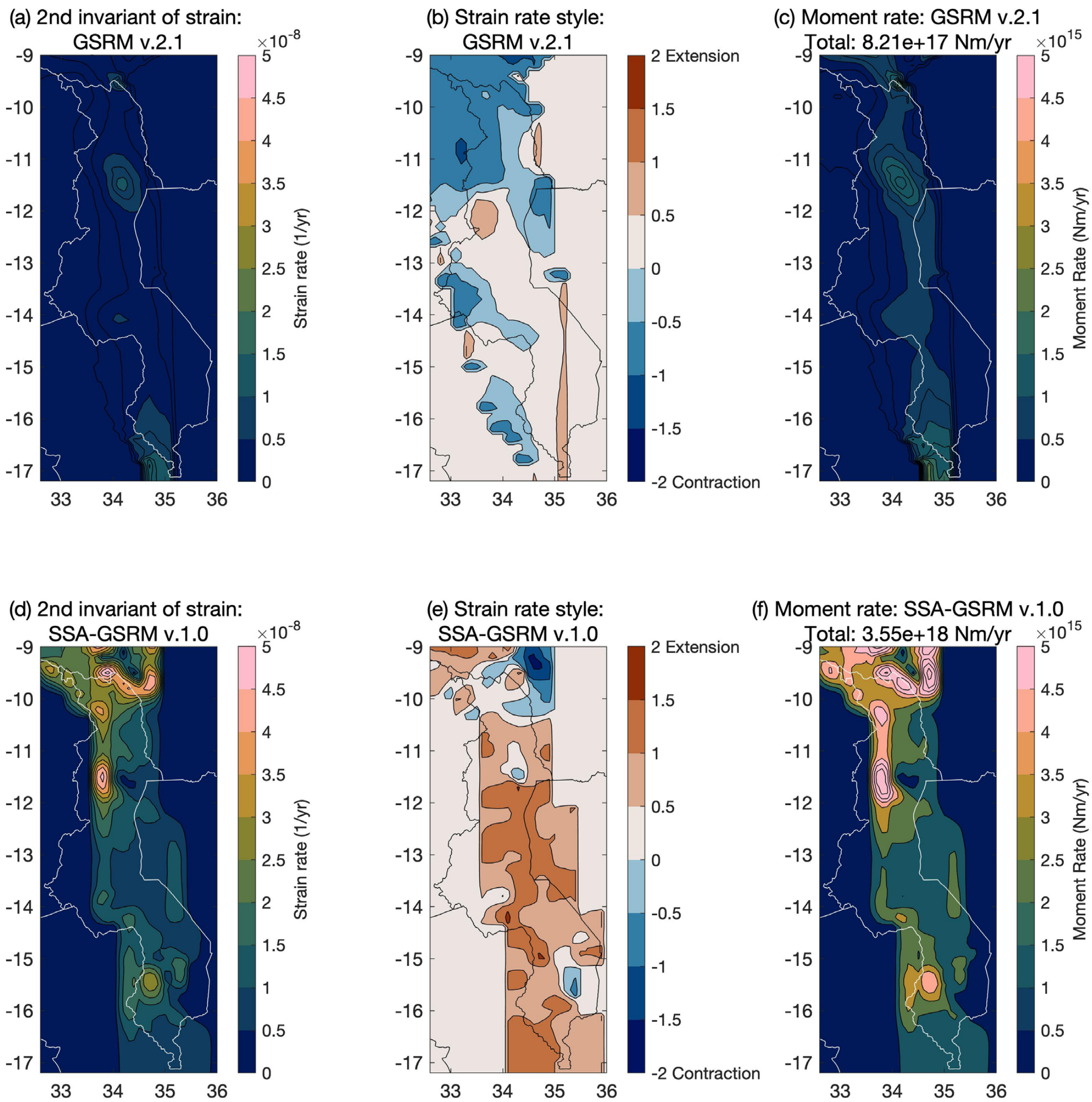

Figure A5. Analysis of the Global Strain Rate Model (GSRM v.2.1; Kreemer *et al.* 2014) and and the Sub-Saharan African Geodetic Strain Rate Model (SSA-GSRM v.1.0; Stamps *et al.* 2018) within the region assessed in the PSHA. Equations for the 2nd invariant of strain, strain rate style and Moment Rate ($\dot{M}_0$) are given in the text. Total $\dot{M}_0$ refers to the sum of the $\dot{M}_0$ from all $0.1^\circ \times 0.1^\circ$ grids that were assessed.

source zone of Poggi *et al.* (2017), which is the principal areal source in our PSHA (Section 6.2). We then plot the MFD: (1) for all events in this area in this period, (2) all events after removing the four principal ($M_W \geq 5.5$) earthquakes in the 2009 Karonga sequence (Biggs *et al.* 2010), (3) the G–R relationships that can be fitted to the filtered and unfiltered catalogs (Tinti & Mulargia 1987) and (4) the stochastic event catalog for this source zone (Fig. A4).

This analysis indicates that the Rukwa–Malawi areal source stochastic event catalog actually corresponds most closely to the SSA-GEM catalog once it has been filted for the Karonga earthquakes (Fig. A4). This result can be explained by: (1) when deriving the *b*-value for areal sources in East Africa, (Poggi *et al.* 2017) grouped some sources together and so the *b*-value assigned to the Rukwa–Malawi source is relatively independent of whether the Karonga earthquakes are included, (2) some events in this earthquake sequence may have been removed during catalog declustering prior to fitting G–R relationships to the sources (Poggi *et al.* 2017). In either case, the areal sources used in our PSHA for Malawi are not impacted by the (incorrect) inclusion of the 2009 Karonga earthquakes when defining their G–R parameters. Nevertheless, there are likely other 'on-fault' earthquakes in the SSA-GEM catalog that we cannot resolve due to their large location uncertainties and so the possibility remains that combining the areal sources in Table 2 with the MSSM sources in the stochastic event catalogs leads to an overestimate of the $\dot{M}_0$ in Malawi. We discuss this further below.

The MSSM assigns most fault slip rates by partitioning regional geodetically derived extension rates across all known mapped faults (Williams *et al.* 2022b). This systems-based approach is therefore subtly different from traditional methods of obtaining slip rates in

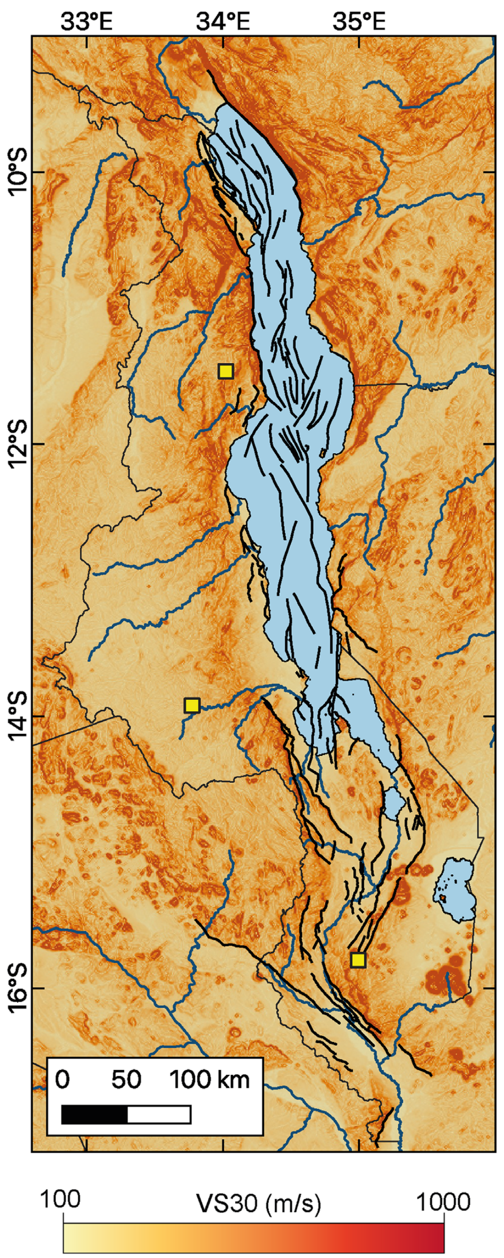

Figure A6. V_{S30} values in Malawi derived from using a slope-based proxy (Wald & Allen 2007) and used in the USGS V_{S30} database (https://earthquake.usgs.gov/data/vs30/). Black lines depict the MAFD (Williams *et al.* 2022c) and yellow squares depict the locations for the site-specific PSHA.

which each fault is considered individually using on-fault paleoseismic or geomorphic constraints. Significantly, it is implicit in the systems-based approach that not all of the geodetically derived extension rate is converted to fault slip, as a correction is made for the obliquity of faults to the regional extension direction (Williams *et al.* 2021a). In this context, areal source events could represent the seismic moment that is lost from projecting the fault dip direction through the regional extension azimuth.

To quantify this, we define the obliquity factor (*OF*) of MSSM source *i*, as the ratio of the source's $\dot{M}_0$ relative to its $\dot{M}_0$ if it was optimally oriented to the regional extension direction,

$$OF_i = cos(\theta_i - \phi) \tag{A8}$$

where θ_i is the source's strike and ϕ is the regional extension it is projected through. In some of the MSSM-based catalogs, a source's down-dip is not necessarily extrapolated through the full width of the seismogenic layer, which also implies that the geodetic $\dot{M}_0$ is not all converted to seismic $\dot{M}_0$ (Section 4.2). To account for these two effects, we calculated the total $\dot{M}_0$ from all MSSM fault sources on the basis that they were all optimally oriented to the regional extension direction (i.e. $OF = 1$) and that they extend through the full width of Malawi's 35-km thick seismogenic layer (Ebinger *et al.* 2019; Stevens *et al.* 2021). The latter correction was not made for the MSSM sources whose down-dip extrapolation implies they intersect with another fault (Section 4.5) and neither correction was made for MSSM sources whose slip rate was estimated independently from offset of the 75 ka seismic reflection (Shillington *et al.* 2020; Williams *et al.* 2022b).

The total $\dot{M}_0$ of all MSSM fault sources, given the corrections for fault obliquity and down-dip extent is 1.88×10^{18} Nm yr^{-1}. By comparison, the combined catalog $\dot{M}_0$ is 1.89×10^{18} Nm yr^{-1} and so implies that the inclusion of areal sources developed from the SSA-GEM catalog (Poggi *et al.* 2017) essentially compensates for the geodetic $\dot{M}_0$ that is lost due to normal fault obliquity and limited down-dip extent. Hence, although the Combined Catalog represents an oversimplified combination of areal and MSSM sources, this does not lead to an overestimate the $\dot{M}_0$ in Malawi compared to that inferred from geodesy and optimally oriented faults. This comparison does not, however, consider the possibility of aseismic moment release in Malawi (Section 4.6.2; Zheng *et al.* 2020).

As a final comparison, of the Combined Catalog's 1.88×10^{18} Nm yr^{-1} $\dot{M}_0$, areal sources in Malawi contribute 2.8×10^{17} Nm yr^{-1} and MSSM sources contribute 1.61×10^{18} Nm yr^{-1}. Our PSHA therefore implies that ~15 per cent of seismicity in Malawi is 'off-fault.' Caution should be applied when comparing this value to other seismic hazard models due to differences in how on- and off-fault sources are developed. Nevertheless, this proportion of off-fault seismicity is lower than estimated in other seismic hazard models (20–50 per cent; Field *et al.* 2014; Johnson *et al.* 2022)

A5 Analysis of independent geodetic models of Malawi

To derive independent estimates of the geodetic $\dot{M}_0$ in Malawi, we consider the Global Strain Rate Model (GSRM v.2.1; Kreemer *et al.* 2014) and the Sub-Saharan African Geodetic Strain Rate Model (SSA-GSRM v.1.0; Stamps *et al.* 2018). Both models are thus distinct from the geodetic constraints used to generate the MSSM-based stochastic event catalogs (Wedmore *et al.* 2021). We first divide the assessed region shown in Fig. 6 into a grid with intervals of 0.1° × 0.1° longitude and latitude. These grid sizes do not necessarily reflect the true spatial resolution of these geodetic models; however, the spatial variations in strain rate in regions with few stations are minimized (Stamps *et al.* 2018). For both models, within each grid *i*, we first calculate: (1) the second invariant of strain: $(\dot{\epsilon}_{1hi}^2 + \dot{\epsilon}_{2hi}^2)^{0.5}$, where $\dot{\epsilon}_{1hi}$ and $\dot{\epsilon}_{2hi}$ are the two principal strain rates in the horizontal plane of grid *i* and (2) the strain rate style: $(\dot{\epsilon}_{1hi} + \dot{\epsilon}_{2hi})/\max(|\dot{\epsilon}_{1hi}|, |\dot{\epsilon}_{2h}|)$ where a positive style indicates extension and vice versa (Kreemer *et al.* 2014). We then calculate the moment rate of each grid ($\dot{M}_{0(i)}$) through

$$\dot{M}_{0(i)} = A_i z \mu \begin{cases} \frac{1}{sin\theta}\dot{\epsilon}_{3i}, & \text{if } \dot{\epsilon}_{2i} < 0 \\ \frac{-1}{sin\theta}\dot{\epsilon}_{1i}, & \text{if } \dot{\epsilon}_{2i} \geq 0 \end{cases} \tag{A9}$$

where A_i is the area of each grid, *z* is the thickness of the seismogenic crust (35 km; Ebinger *et al.* 2019; Stevens *et al.* 2021), μ represents

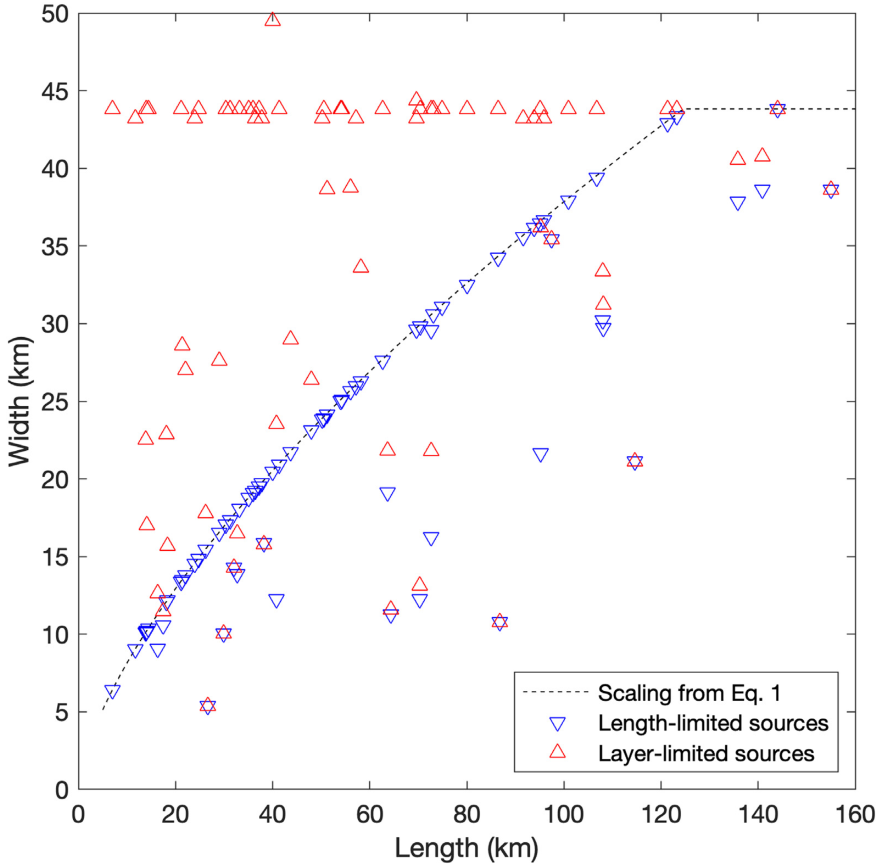

Figure A7. Comparison for the length-width scaling for the length- and layer-limited Adapted MSSM sources. Length-limited source widths follow eq. (1), in which they follow the Leonard (2010) scaling up to a width at which they will exceed the 35-km thick seismogenic layer in Malawi (dashed line indicates scaling for a 53° dipping fault). Layer-limited sources are extrapolated down-dip to a depth of 35 km (Section 4.2). Exceptions to these scalings occur when the down-dip extent of MSSM sources are presumed to intersect and cut each other off (Williams *et al.* 2022b). The layer-limited source with a width >45 km is the St Mary Fault, which has a relatively low dip (45°; Biggs *et al.* 2010; Kolawole *et al.* 2018a).

the shear modulus (33 GPa for consistency with; Leonard 2010), θ is fault dip (53°, section 4.5) and the three principal strain rates of each grid ($\dot{\epsilon}_{1i} \leq \dot{\epsilon}_{2i} \leq \dot{\epsilon}_{3i}$,) are derived by invoking that the vertical strain rate ($\dot{\epsilon}_{rri}$) is a principal strain rate and that to maintain incompressibility, $\dot{\epsilon}_{1hi} + \dot{\epsilon}_{2hi} + \dot{\epsilon}_{rri} = 0$ (Bird & Liu 2007; Bird & Kreemer 2015). Eq. (A9) is therefore similar to the $\dot{M}_0$ calculation in the SHIFT model (Bird & Liu 2007; Bird & Kreemer 2015); however, we consider the seismic coupling factor (c) = 1 (Section 4.6.2) and the assumed 53° dip of faults mean they do not satisfy the criteria that $1/sin(\theta) = 2$. To derive the total geodetic $\dot{M}_0$ across the assessed region, we sum the $\dot{M}_{0(i)}$ from each 0.1° × 0.1° grid.

Malawi can be considered as a region of low magnitude extensional deformation in both of the assessed geodetic models (Fig. A5), which is consistent with the model developed by Wedmore *et al.* (2021) and observations from seismicity (Ebinger *et al.* 2019; Williams *et al.* 2019; Stevens *et al.* 2021). The SSA-GSRM v.1.0 implies greater spatial variability in the magnitude and style of strain in Malawi than the GSRM v.2.1 model. This likely reflects the more comprehensive suite of geodetic data used to develop the SSA-GSRM v.1.0 and although it indicates strike-slip and even contraction, in regions that have experienced normal fault earthquakes (Biggs *et al.* 2010; Ebinger *et al.* 2019), such discrepancies may be reconciled by local strain rotations at the scale of individual faults (Twiss & Unruh 1998; Philippon *et al.* 2015; Williams *et al.* 2019). The MSSM based Combined Catalog $\dot{M}_0$ (1.89×10^{18} Nm yr^{-1}; Fig. 7) is approximately intermediate between the total estimates of $\dot{M}_0$ derived from these geodetic models (8.2×10^{17} and 3.5×10^{18} Nm yr^{-1} respectively; Fig. A5). This is discussed further in Section 4.6.2.

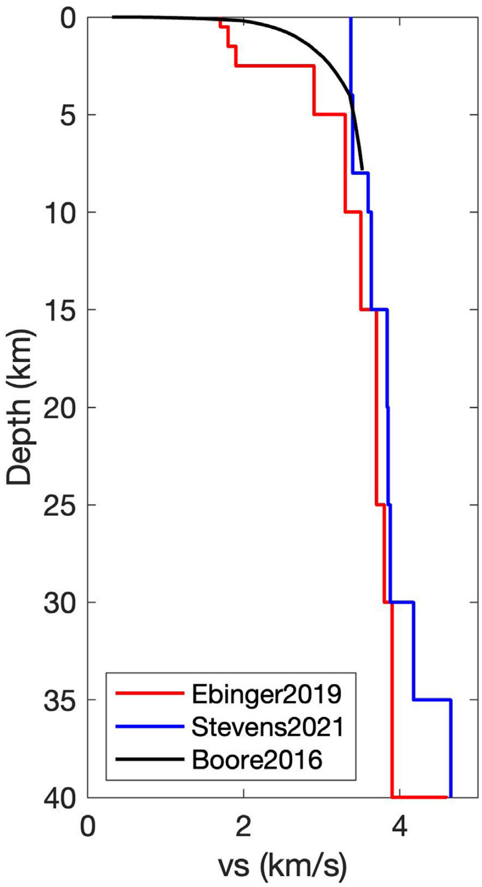

Figure A8. 1D seismic velocity models previously derived in northern (Ebinger *et al.* 2019) and southern (Stevens *et al.* 2021) Malawi from short-term seismic deployments. For context the velocity model for the generic rock site from Boore (2016) is also shown for depths 0–8 km.

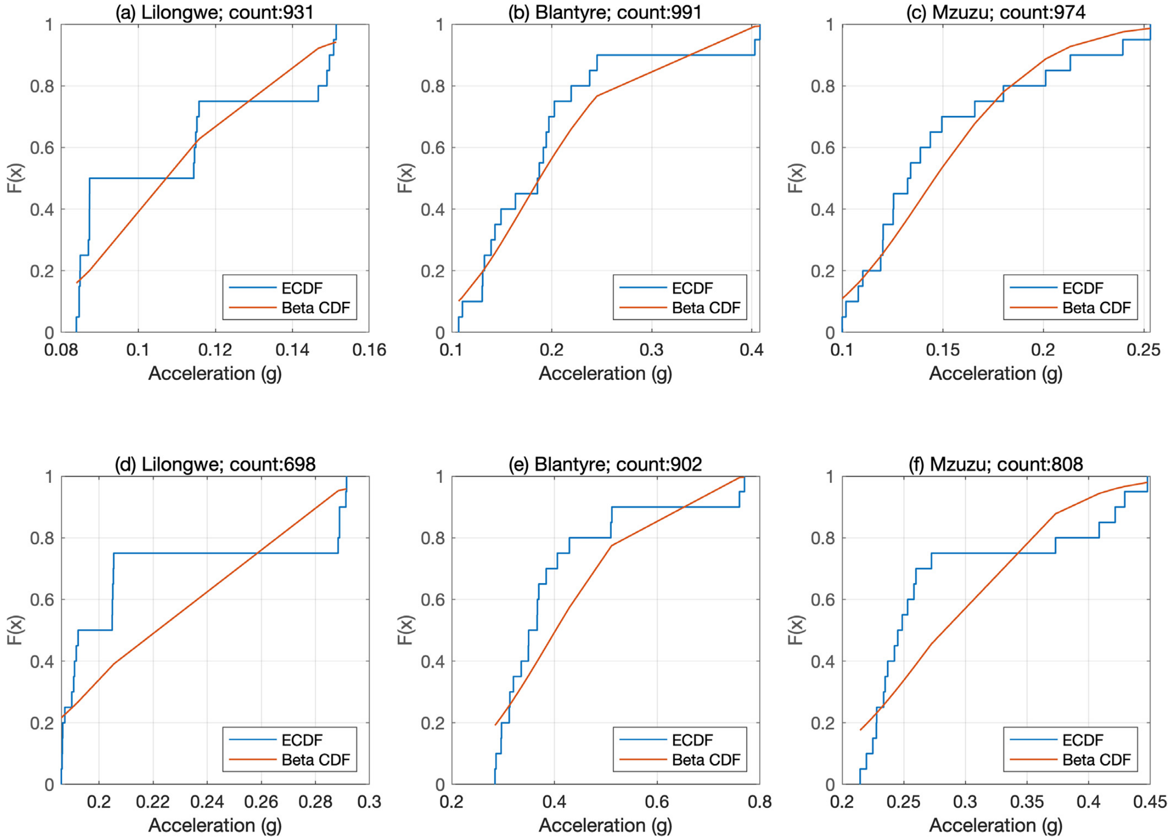

Figure A9. Empirical cumulative distribution functions for the 20 ground motions intensity values derived for each site for PGA and for (a)–(c) 10 per cent PoE in 50 yr and (d)–(f) 2 per cent PoE in 50 yr. For comparison, the cumulative distribution functions for the beta distribution that is fitted to these 20 values in Fig. 11 is also shown. In addition, we randomly take 20 samples from these beta distribution and then perform a two sample Kolmogrov-Smirnov test for the null hypothesis that these random samples come from the same continuous distribution as the 20 calculated ground motion values. We repeat this test 1000 times and the number of times where the null hypothesis is not rejected (at a 5 per cent significance level) is reported in the title of each plot.

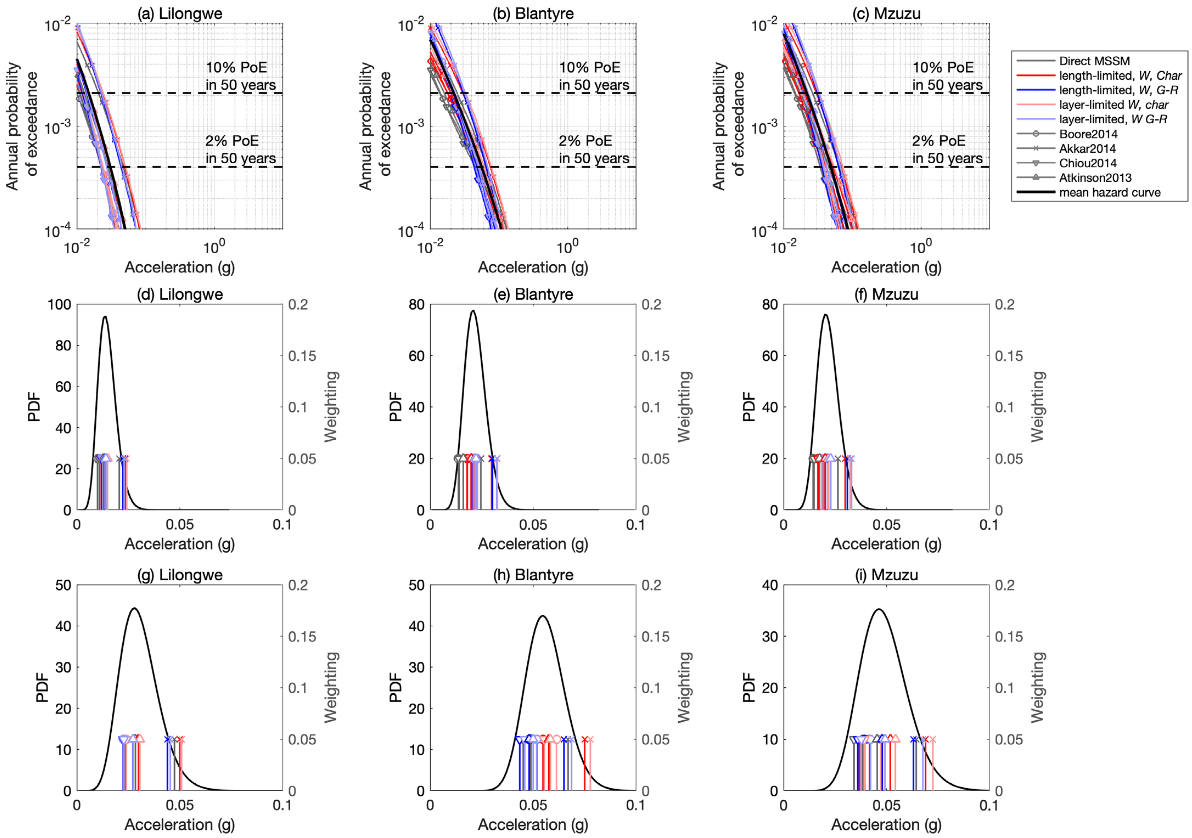

Figure A10. (a)–(c) Seismic hazard curves as shown in Fig. 11 but for a 3 s spectral acceleration. In addition, we show the mean value and Beta distribution that may be fitted to these values for (d)–(f) 10 per cent PoE in 50 yr and (g)–(i) 2 per cent PoE in 50 yr. Line colors represent different event catalogs and symbols represent different GMMs. For V_{S30} value of 760 m s^{-1}.

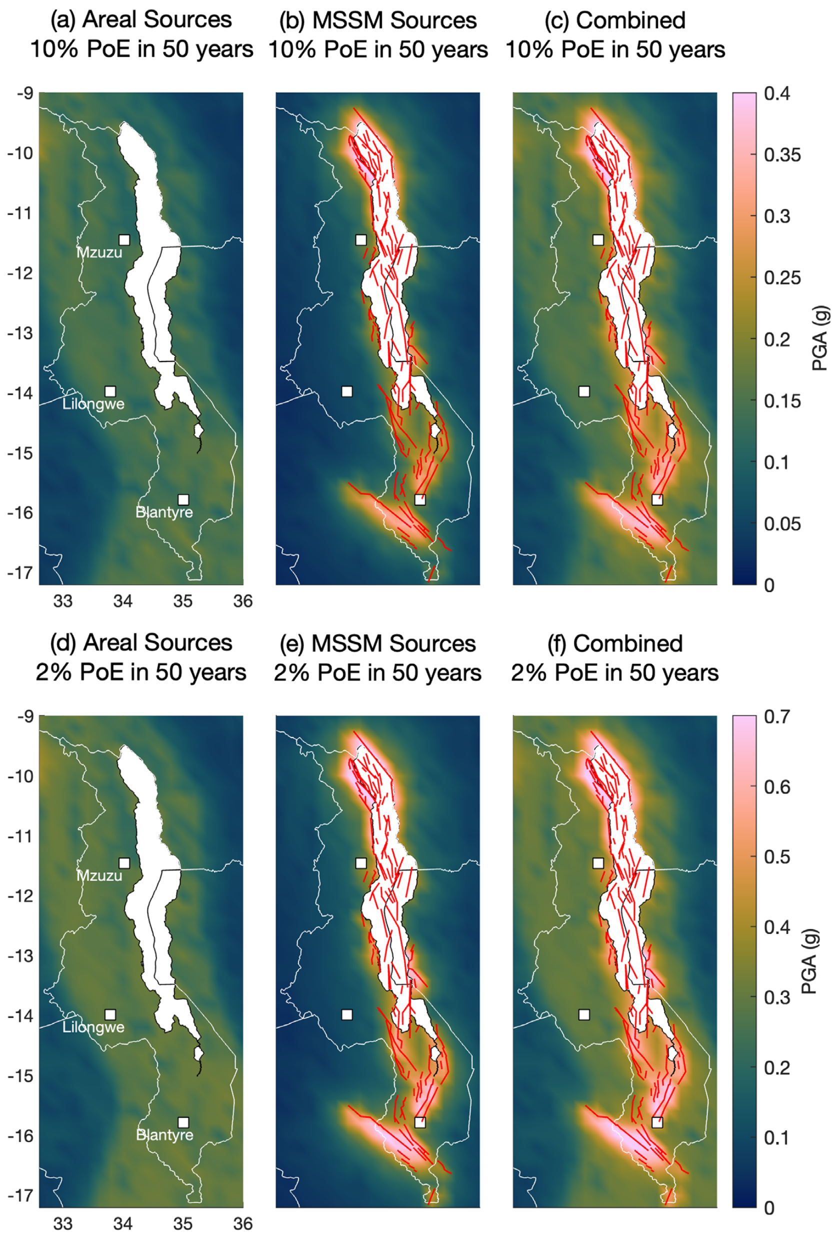

Figure A11. Equivalent to Fig. 14 with PGA seismic hazard maps for Malawi, but using the USGS V_{S30} values (Fig. A6; Wald & Allen 2007). Maps (a)–(c) are for 10 per cent PoE in 50 yr and (d)–(f) 2 per cent PoE in 50 yr. Figure is arranged so each column represents a different catalog. Red lines depict the MSSM fault sources (Williams *et al.* 2022b).

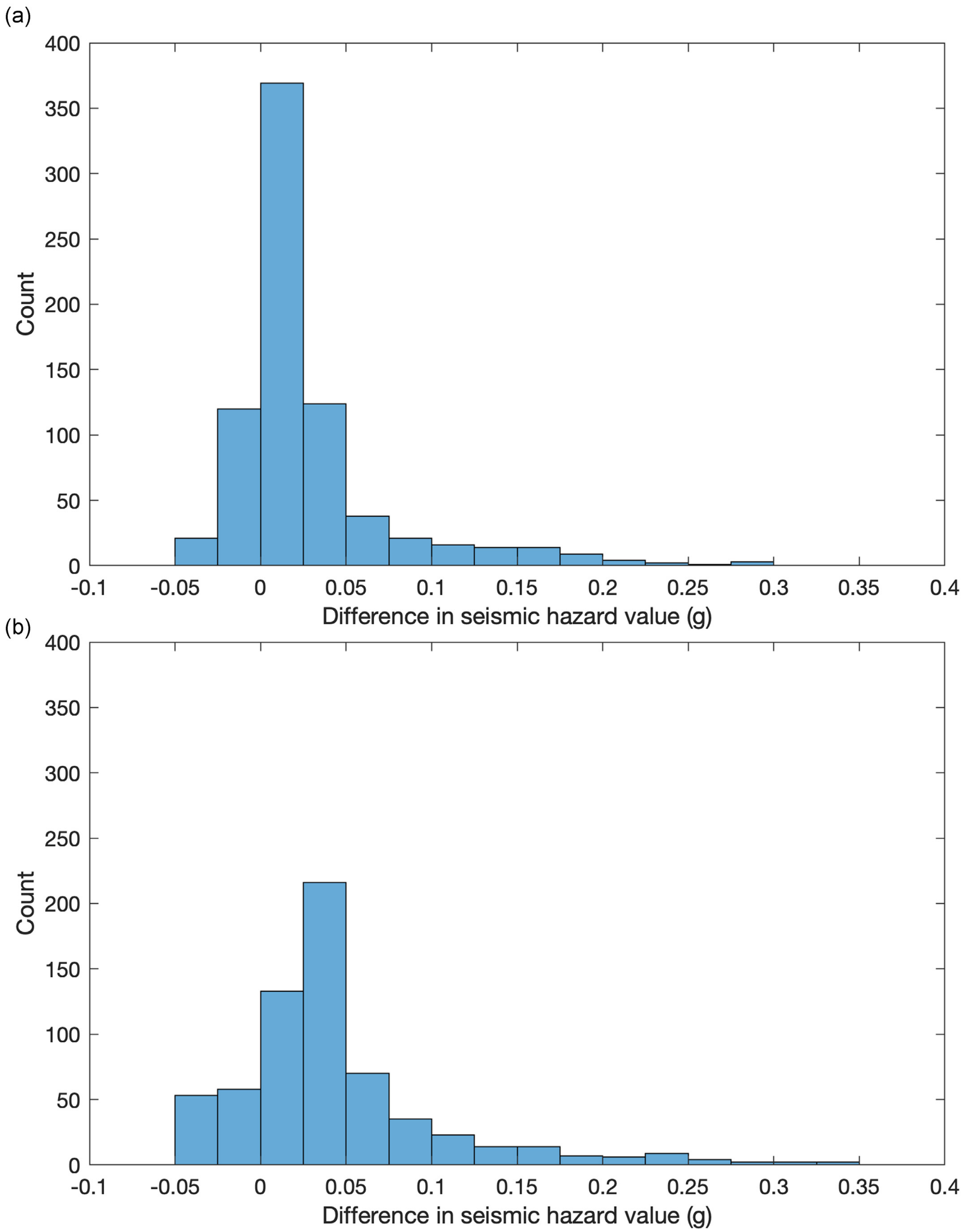

Figure A12. Histogram for the differences in seismic hazard levels in Malawi between the maps presented in this study and from (a) Poggi *et al.* (2017) for 10 per cent PoE in 50 yr and (b) from the mixed rupture catalog of Hodge *et al.* (2015) for a 500 yr return period (see also Fig. 16). Histogram considers the difference in hazard levels for each point in a 0.2° × 0.2° latitude and longitude grid across Malawi ($n = 756$).